

---

[All ETDs from UAB](#)

[UAB Theses & Dissertations](#)

---

2022

## Spectrum-Efficient High-Density Data Communication for Wireless Sensor Networks

Md. Kamal Hossain  
*University Of Alabama At Birmingham*

Follow this and additional works at: <https://digitalcommons.library.uab.edu/etd-collection>



Part of the [Engineering Commons](#)

---

### Recommended Citation

Hossain, Md. Kamal, "Spectrum-Efficient High-Density Data Communication for Wireless Sensor Networks" (2022). *All ETDs from UAB*. 196.

<https://digitalcommons.library.uab.edu/etd-collection/196>

This content has been accepted for inclusion by an authorized administrator of the UAB Digital Commons, and is provided as a free open access item. All inquiries regarding this item or the UAB Digital Commons should be directed to the [UAB Libraries Office of Scholarly Communication](#).

SPECTRUM-EFFICIENT HIGH-DENSITY DATA COMMUNICATION FOR  
WIRELESS SENSOR NETWORKS

by

MD. KAMAL HOSSAIN

MOHAMMAD R. HAIDER, COMMITTEE CHAIR  
LEON JOLOLIAN  
KARTHIKEYAN LINGASUBRAMANIAN  
ALEKSANDAR MILENKOVIC  
S. ABDOLLAH MIRBOZORGI  
NASIM UDDIN

A DISSERTATION

Submitted to the graduate faculty of The University of Alabama at Birmingham,  
in partial fulfillment of the requirements for the degree of  
Doctor of Philosophy

BIRMINGHAM, ALABAMA

2022



# SPECTRUM-EFFICIENT HIGH-DENSITY DATA COMMUNICATION FOR WIRELESS SENSOR NETWORKS

MD. KAMAL HOSSAIN

COMPUTER ENGINEERING

## ABSTRACT

Spectrum-efficient data telemetry is critically important in high-density wireless sensor networks. The rapid expansion of the sensor network has generated a large volume of data on the limited bandwidth and brought new challenges, including transmission bottlenecks, latency, and congestion. The existing wireless technologies cannot support the proliferation of sensor devices for the limitations of spectrum and resources, including computational power, memory, and feature size that hinder the deployment of sophisticated signal processing. To overcome these limitations, orthogonal pulse-based telemetry provides an excellent alternative with reduced complexity, data compression, and efficient transmission. However, the number of data channels also limits the single pulse system to support high-density IoT networks.

This dissertation work proposes two innovative encoding schemes to address the above challenges. The first scheme encodes multi-bit data using index randomization, where a single-order pulse carries multi-bit data. The second scheme encodes individual data channels by a distinct pulse-sequence (PS) instead of a single pulse, where the permutation of a group of higher-order pulses in adjacent time slots creates a series of PSs. The superposition of the PSs creates a unified composite sequence and a compressed data representation of the encoded channels. At the receiver end, a cyclic pulse elimination algorithm decodes individual pulses from the combined signal. This dissertation also presents orthogonal PS generation to simplify the pulse decoding

scheme for finding the missing channel. Finally, a prototype test platform is configured to validate the proposed scheme's performance, feasibility, and compatibility using the channel effect investigations, existing bandwidth, communication architecture, and network protocol.

Simulation results show that index randomization increases the data compression ratio, improves processing time, and adds an extra level of physical layer security. Test results show that the BER satisfies the lower bound for wireless telemetry and increases data transmission speed by supporting large number of channels. The proposed scheme is also different than the IFFT-based Walsh-Hadamard orthogonal code generation for wireless communication. In addition, the orthogonal pulse-based compression is free from sophisticated signal processing. The simplicity and efficacy show enormous potentials to meet the demand for next-generation high-density IoT networks using existing bandwidth and communication architecture.

**Keywords:** Analog orthogonal pulse, multi-bit encoding, pulse-sequence based data compression, spectrum-sharing, prototype development, and IoT networks.

## DEDICATION

I would like to dedicate this work to my beloved parents, who always support me, has faith in my life, and believe in my ability to be successful in the academic arena. My parents' belief on me has made possible this long Ph.D. journey smoothly. I also thank my beloved wife, Kaniz Fatema Mim, for her continuous support. This Ph.D. dissertation work would not be possible to complete without their strong support and encouragement.

## ACKNOWLEDGMENTS

This dissertation would not be possible without the help and support of the Electrical and Computer Engineering (ECE) faculty members and staffs at the University of Alabama at Birmingham (UAB), my lab fellows, family and relatives, colleagues, and friends. I want to thank all the people for their continuous support.

First, I would like to express my sincerest gratitude to my academic adviser and Ph.D. committee chair, **Dr. Mohammad R. Haider**, Associate Professor and Director of Bio-inspired Integrated Circuit Design Laboratory, Department of ECE, UAB, for his proper supervision, guidance, and encouragement. Dr. Haider has been a great mentor throughout the Ph.D. journey by helping me to establish a fruitful research direction, constructive feedback, kind support, and valuable advice. I am happy to get such a dynamic adviser and mentor. Thank you very much to Dr. Haider. I appreciate your valuable time, proper guidance, and supervision of my Ph.D. dissertation. His extensive knowledge, inspiration, and hard-working will be a lifetime motivation for my career.

I want to thank the rest of dissertation committee members, Dr. Leon Jololian, Dr. Kartik Lingasubramanian, Dr. S. Abdollah Mirbozorgi, Dr. Nasim Uddin, and Dr. Aleksandar Milenkovic for serving on my Ph.D. committee and their fruitful suggestions that enriched the dissertation work higher than my expectation. I appreciate Dr. Leon's valuable time for meeting with me in several times to discuss my research and career objectives. I owe thanks to Dr. Karthik, who is also the instructor of one of my graduate-level courses. I am also grateful to Dr. Tauhidur Rahman for his fruitful suggestions and

expertise that expedite my dissertation work. I am also pleased to Dr. S. Abdollah Mirbozorgi and Dr. Aleksandar Milenkovic for agreeing to serve on my dissertation committee with their valuable suggestions and expertise.

I am also grateful to the BIC design team's past and current lab members for their continued support. In particular, the Ph.D. students Steven D. Gardner and Mohammad Masud Rana helped me greatly in my experimental test and data collection as a team member. I would like to thank former students and my other lab fellows, including Shang-Kai Wei, Hanzhi Teng, Md. Toriqul Islam, Ting Zhang, and Ruikuan Lu for their collaboration work, group discussion, and research direction, which inspired my work.

I wish to thank the ECE department, the BIC design research laboratory, and the National Science Foundation (NSF) award no. ECCS-1813949, CNS-1645863, and ECCS-2201447 successfully finish the dissertation work for their assistance and financial support. **Finally**, I wish to extend my special thanks to my beloved wife, Kaniz Fatema Mim, for her tremendous support, motivation, and encouragement to complete my Ph.D. degree. I am highly grateful to Mim for her help and patience.



## TABLE OF CONTENTS

	Page
ABSTRACT .....	iii
DEDICATION .....	v
ACKNOWLEDGMENTS .....	vi
LIST OF TABLES .....	xii
LIST OF FIGURES .....	xiii
LIST OF ABBREVIATIONS .....	xvii
CHAPTER	
I. INTRODUCTION .....	1
1.1 Introduction .....	1
1.2 The Internet-of-Things Markets .....	1
1.3 Architecture of IoT Systems .....	3
1.3.1 The IoT Device .....	3
1.3.2 IoT Gateway .....	4
1.3.3 Data Center/Cloud Based Data Processing Unit .....	5
1.4 Wireless Data Telemetry System .....	5
1.4.1 Digital Data Telemetry Platform .....	8
1.4.2 Analog Pulse Based Data Telemetry .....	9
1.5 Standard Communication Technology for IoT Telemetry .....	10
1.6 Literature Survey .....	12
1.7 Problems Identification .....	16
1.8 Proposed Solutions .....	18
1.9 Research Impact on Society and Economic .....	19
1.10 Dissertation Outlines .....	20
2. ANALOG ORTHOGONAL PULSE GENERATION AND TELEMETRY .....	23
2.1 Introduction .....	23
2.2 Analog Pulse-Based Data Telemetry .....	23
2.2.1 Analog Pulse-Based RF Transmitter .....	24

2.2.2 Correlator Based Pulse Decoding Receiver .....	24
2.2.3 Communication Channel .....	25
2.3 Conventional Pulse Generation Scheme .....	26
2.4 Analog Orthogonal Pulse Set Generation .....	27
2.4.1 Mathematical Model .....	28
2.4.2 MATLAB Simulink Model.....	28
2.4.3 Signal Orthogonality .....	29
2.4.4 Pulse Signal Strength .....	31
2.4.5 Orthogonal Shifted Pulse Generation .....	33
2.5 Proposed Data Encoding Schemes.....	34
2.5.1 Single Pulse Based Multi-bit Encoding .....	34
2.5.2 Pulse Sequence Based Data Channel Encoding.....	36
2.6 Conclusion .....	38
3. ANALOG PULSE BASED MULTI-BIT DATA TELEMETRY .....	39
3.1 Introduction.....	39
3.2 Pulse Index Encoding for Multi-bit Data Telemetry .....	39
3.3 Architecture of Proposed Pulse Index Encoding .....	41
3.4 Pulse Randomization Techniques .....	44
3.5 Security Analysis .....	45
3.5.1 Threat Model.....	45
3.5.2 Exhaustive Key-searching .....	46
3.5.3 Time Interval and Amplitude.....	47
3.6 Simulation Results .....	48
3.7 Significant Improvements of the PI Encoding.....	50
3.7.1 Architectural Simplicity.....	50
3.7.2 Level of Data Compression Improvement.....	51
3.7.3 Data Transmission Rate Improvement.....	52
3.7.4 Data Accuracy Comparison .....	52
3.8 Conclusion .....	54
4. PULSE SEQUENCE BASED ENCODING AND DATA COMPRESSION.....	55
4.1 Introduction.....	55
4.2 Pulse Sequence Based Data Encoding and Compression .....	55
4.2.1 Pulse Sequence Generation.....	56
4.2.2 Pulse Sequence Based Channel Encoding .....	58
4.2.3 Pulse Sequence Based High-Volume Data Compression.....	58
4.3 Cyclic Pulse Elimination Based Data Decompression .....	60
4.4 Orthogonal Pulse Sequence Generation and Channel Coding.....	63
4.5 Orthogonal Pulse Sequence Decoding Scheme .....	65
4.6 Simulation Results .....	66
4.6.1 Permutation Technique .....	66
4.6.2 Gold Sequence .....	71
4.7 Significant Improvements.....	74

4.8 Conclusion .....	75
5. CHANNEL EFFECT ON ANALOG PULSES AND OBJECT SENSING.....	76
5.1 Introduction.....	76
5.2 Communication Channel Characterizations .....	77
5.3 Measurement Setup and Configuration .....	78
5.4 Signal Processing in Time-Frequency Analysis .....	80
5.5 Measurement Results and Channel Effects.....	81
5.5.1 Variation of Antenna Positions in Between Tx-Rx Separation .....	82
5.5.1(a) Middle in the Tx-Rx Separation .....	83
5.5.1(b) Nearest to the Tx antenna .....	83
5.5.1(c) Nearest to the Rx antenna .....	84
5.5.2 Variation of Channel Obstacle Combinations .....	84
5.5.3 Variation of Channel Obstacle Size .....	85
5.5.4 Measurements at Different Locations .....	86
5.5.5 Room to Room Measurements at Different locations .....	87
5.6 Modification of the Receiver Architecture .....	88
5.6.1 Automatic Gain Control .....	88
5.6.2 Threshold Level Selection for Pulse Elimination .....	89
5.6.3 Pulse Elimination Results .....	89
5.7 Conclusion .....	91
6. PROTOTYPE DEVELOPMENT AND TEST RESULTS .....	92
6.1 Introduction.....	92
6.2 Arduino Implementation.....	92
6.3 Configuring Communication Architecture .....	94
6.4 design and Implementation of Driver and LPF circuits.....	96
6.4.1 Driver Circuit Design for RF Mixer Module.....	96
6.4.2 Low Pass Filter Design .....	97
6.4.3 Experimental Test Results .....	98
6.5 Prototype Test Platform .....	107
6.5.1 Test Results for Multi-bit Encoding .....	108
6.5.2 BER and PER Investigation for PI Encoding Scheme.....	109
6.5.3 Test Results for Pulse Sequence Based Encoding .....	110
6.5.4 Test Results for Orthogonal Pulse Sequence Based Encoding.....	115
6.6 Conclusion .....	120
7. CONCLUSION AND FUTURE RESEARCH.....	122
7.1 Introduction.....	122
7.2 Summary and Potential Research Impacts.....	122
7.3 Future Works .....	127
LIST OF REFERENCES .....	130

## APPENDICES

A	LIST OF PUBLICATIONS .....	137
B	CORRELATION PEAK TABLE.....	140
C	PSEUDO CODE FOR ALGORITHM DESIGN .....	143

## LIST OF TABLES

<i>Tables</i>	<i>Page</i>
1.1 List of existing communication standards for WSNs .....	11
2.1 Correlation coefficient peak table for individual AOPs .....	31
2.2 The half-power (3-dB) bandwidth for multi-order analog pulses.....	32
2.3 PS generation and channel encoding template for 4-pulse systems .....	36
3.1 Average time required for exhaustive key searching.....	46
3.2 Data compression and latency improvement compared to Huffman coding .....	52
4.1 Correlation between composite pulses with distinct AOPs .....	70
4.2 Test validation for CPE based channel decoding .....	71
4.3 Significant improvements of the proposed PS-based data channel encoding.....	74
5.1 List of different size of communication channel blockages .....	86
6.1 Technical specifications of MKR1010 microcontroller board .....	93
6.2 Selected customize mini-circuits RF modules for transceiver configuration .....	94
6.3 Correlation peak table for entire OPSs eliminated from composite signal.....	116
6.4 Test validation of orthogonal pulse sequence based wireless data telemetry .....	119
7.1 Comparison results with the existing works. ....	126

## LIST OF FIGURES

<i>Figure</i>	<i>Page</i>
1.1 Explosive growth of IoT devices for the future world (adopted from [3]).	2
1.2 Overview block architecture of a generic IoT system.	3
1.3 Conceptual overview of high-density wireless telemetry for IoT applications.	6
1.4 Block diagram of the conventional wireless communication systems.	7
1.5 Generic data encoding scheme and carrier modulation (a) digital pulse format, (b) BPSK modulation, (c) analog pulse format, and (d) carrier modulation.	9
2.1 The AOP-based transceiver architecture (a) transmitter and (b) receiver.	24
2.2 Simulink model of MHP-based multi-order analog pulse generator.	29
2.3 Different order AOP signal in (a) time domain and (b) frequency domain.	30
2.4 Power spectral density of MHPs at 500 MHz carrier frequency.	32
2.5 Multi-order analog pulses and their time-shifted pulse signals.	33
2.6 Analog pulse-based encoding using multi-order and their shifted pulses.	35
2.7 Data compression in PS-based encoding using original and shifted AOPs.	37
3.1 Transceiver block diagram of PI encoding (a) transmitter and (b) receiver	40
3.2 Data modulation (a) PI encoding architecture, (b) conventional single pulse system, and (c) k-bit encoding ( $k = 3$ ).	42
3.3 Index randomization architecture (i) initial pulse dictionary, (ii) index randomization at $T_h$ sec, and (iii) randomization dictionary at $n * T_h$ sec.	44
3.4 Simulation results of error vs. SNR at different (a) number of pulse transmission and (b) k-bit encoding for proposed PI encoding.	49
3.5 Comparison between k-bit encoding and Huffman coding in terms of BER investigation	53

4.1	Distinct PS generation using switch matrix algorithm using AOP set. ....	57
4.2	Data modulation scheme (a) single pulse and (b) PS-based compression.....	59
4.3	Data decoding architecture using cyclic pulse elimination algorithm. ....	61
4.4	Flow chart of proposed CPE algorithm for single time slot. ....	62
4.5	Flow chart of orthogonal pulse sequence generation.....	64
4.6	Correlation peak based OPS decoding scheme for finding missing channels. ....	65
4.7	PS-based encoding channels and corresponding UCP signal. ....	67
4.8	Simulation results for PS and UCP signals for original and shifted AOPs. ....	67
4.9	Power spectral density of individual pulses and their UCP signals.....	68
4.10	Simulation results of UCP (a) without AWGN and (b) with AWGN signal.....	69
4.11	Simulation results (a) decoded pulses and (b) residual signal. ....	70
4.12	Composite UCP signal corresponding to each time slot.....	71
4.13	Simulation results of distinct OPS generation using Gold code method. ....	72
4.14	Simulation results for BER investigation for OPS-based encoding. ....	73
5.1	Indoor S-parameter measurements (a) floor map and (b) test setup. ....	79
5.2	Signal processing steps for numerical simulation using S-parameter. ....	80
5.3	Measurement results (a) S-parameters and (b) numerical simulation. ....	81
5.4	Numerical simulated results for channel obstructions (a) concrete & foam and (b) wood and metal in the middle of the Tx-Rx position.....	82
5.5	Numerical simulated results for channel obstructions (a) concrete and foam and (b) wood and metal in the nearest to the Tx antenna. ....	83
5.6	Numerical simulated results for channel obstructions (a) concrete and foam and (b) wood and metal in the nearest to the Rx antenna. ....	84
5.7	Numerical simulated results for different cases (a) object size, (b) different Indoor locations, and (c) object combinations.....	85
5.8	Simulated results for (a) room to room and (b) corridor communication.....	87
5.9	Simulation results (a) encoded and decoded pulses and (b) BER. ....	90

6.1	Configuring transceiver architecture using RF modules (a) Tx and (b) Rx. ....	95
6.2	Design and implementation of (a) low-power driver circuit and (b) LPF. ....	97
6.3	Prototype design (a) driver circuit, (b) evaluation board, and (c) LPF. ....	98
6.4	Driver circuit testing (a) known sync and (b) proposed analog pulse signal. ....	100
6.5	Amplitude modulated of multi-order AOPs by 1.0 MHz carrier frequency. ....	100
6.6	Test results for the (a) MHP <sub>0</sub> (b) MHP <sub>1</sub> , (c) MHP <sub>2</sub> , and (d) MHP <sub>3</sub> . ....	101
6.7	Test results (a) frequency spectrum and (b) spectrogram of AOP signal. ....	102
6.8	Test results (a) without LPF and (b) with LPF to remove noise signal. ....	103
6.9	Test results for different order AOPs in short-range wireless telemetry. ....	104
6.10	Test results for composite signal (a) driver circuit and (b) frequency spectrum. ....	105
6.11	Test results for composite signal (a) without LPF and (b) with LPF. ....	106
6.12	Prototype test platform development using customize RF modules. ....	107
6.13	Test results of pulse train (a) transmitted, (b) received, and (c) modulated signal at 500 MHz. ....	109
6.14	Test results (a) PER and (b) BER for multi-bit data transmission. ....	110
6.15	Test results of distinct PS generation using AOPs of 8.0 $\mu$ s width. ....	111
6.16	Composite UCP signal corresponding to each time slot of 8.0 $\mu$ s. ....	112
6.17	Test results (a) all the PSs are present and (b) PS 3 and 5 are absent in the UCP signal. ....	113
6.18	Test results of pulse elimination from the composite signal by CPE. ....	114
6.19	Template signal of distinct orthogonal pulse sequences. ....	116
6.20	Composite signal for OPSs (a) simulation results, (b) experimental results where all the sequences are present, and (c) 3 and 5 PSs are absent. ....	117
6.21	Test results for data decompression scheme (a) eliminated OPSs in each iteration and (b) residual signal after eliminating OPSs sequentially. ....	118
6.22	Test results at two test condition, where column represent (a) MATLAB <sup>®</sup>	



simulation, experimental results (b) transmitted signal before carrier multiplication, and (c) received signal at baseband frequency after carrier removing.....120

## LIST OF ABBREVIATIONS

AOP	analog orthogonal pulse
ASK	amplitude shift keying
AGC	automatic gain control
BLE	bluetooth lower energy
BAN	body area network
BER	bit-error-rate
BPSK	binary phase shift keying
BIC	bio-inspired integrated circuit
CPU	central processing unit
CPE	cyclic pulse elimination
CDMA	code division multiplexing
DUT	device under test
DSSS	direct sequence spread spectrum
DSP	digital signal processing
DoD	department of energy
EIRP	equivalent isotopically radiated power
EE	energy efficient
FSK	frequency shift keying
FPGA	field-programmable gate array

FFT	first Fourier transform
FCC	Federal Communication Commission
IFFT	inverse first Fourier transform
FSIM	frequency shape modulation
GCI-SM	generalized code index-spatial modulation
GDP	gross domestic product
HG	Hermite-Gaussian
IM	index modulation
ISI	inter-symbol-interference
ICI	inter-carrier-interference
IoT	internet-of-things
LNA	low noise amplifier
LPF	low pass filter
LTE	long term evolution
LOS	line-of-sight
MHP	modified Hermite polynomial
NB	narrow band
OPS	orthogonal pulse sequence
OOK	on-off keying
OFDM	orthogonal frequency division multiplexing
OFDMA	orthogonal frequency division multiplexing
PI	pulse index
PSD	power spectral density

PER	pulse-error-rate
PCM	permutation channel modulation
PSM	pulse shape modulation
PAM	pulse amplitude modulation
PWM	pulse width modulation
PPM	pulse position modulation
PSK	phase shift keying
PA	power amplifier
PIM	pulse index modulation
PIR	pulse index randomization
PS	pulse sequence
QPSK	quadrature phase shift keying
QAM	quadrature amplitude modulation
RFID	radio frequency identification
SPM	spatial permutation modulation
SE	spectrum-efficient
TS	time slot
TFDM	time frequency division multiplexing
UWB	ultra-wideband
U.S.	United States
VNA	vector network analyzer
WSNs	wireless sensor networks

## CHAPTER 1

### INTRODUCTION

#### **1.1 Introduction**

Spectrum-efficient (SE) wireless data telemetry is an emerging field in WSNs. It dramatically impacts modern IoT technology to support high-volume data and transmits it effectively by utilizing a limited spectrum. The frequency spectrum is a prime natural resource that is available to use by citizens all over the world. The demand to access many segments of spectrum increases as new technologies allow a variety of applications. It also makes the importance of efficient applications to support the growing demand of new devices. Currently, a broader range of frequency band is used by mutual interference between two or more radio transmissions simultaneously. This dissertation introduces the necessity of SE wireless telemetry with more details on benefits and proposes innovative solutions to meet the demand for next-generation high-density IoT networks.

#### **1.2 The Internet-of-Things Markets**

In recent years, the IoT market has gained a lot of attraction from researchers, scientists, and engineers of tech industries with technological innovation in wireless data transmission. The demand for IoT devices also has gradually increased as the globe moves towards urbanization, modernization, and government investment in digital networks. The exponential growth in wireless technology has benefited society in many sectors, including

health, transportation, commerce, science, and defense. IoT promises to play a pivotal role in the WSNs and linking the physical world to the virtual variety. Fig. 1.1 shows the rising trends of IoT devices in the future world. This figure is redrawn by adopting data from the open source available in online [3]. IoT technology will travel a high-growth track over the next few years using mobile networks for device connectivity. The statistical data of the IoT market shows that in 2021 there were over 10 billion sensor devices worldwide in WSNs. It also claims that every second, one hundred and twenty-seven new devices are hooked up to the internet for the first time [1]. IoT extensive data statistics also show that North America remains the largest market for consumer sensor devices and has the potential to generate \$11.0 trillion in economic value by 2025 [2]. They also predicted the number of IoT devices will surpass 25.4 billion by 2030. A report by Forbes shows that everything will be connected under the same network [2]. Forbes report also shows that the North America IoT market used 646 million devices in hospitals and medical offices in 2020. It is expected to be worth more than \$534.3 billion by the end of 2025 [1].

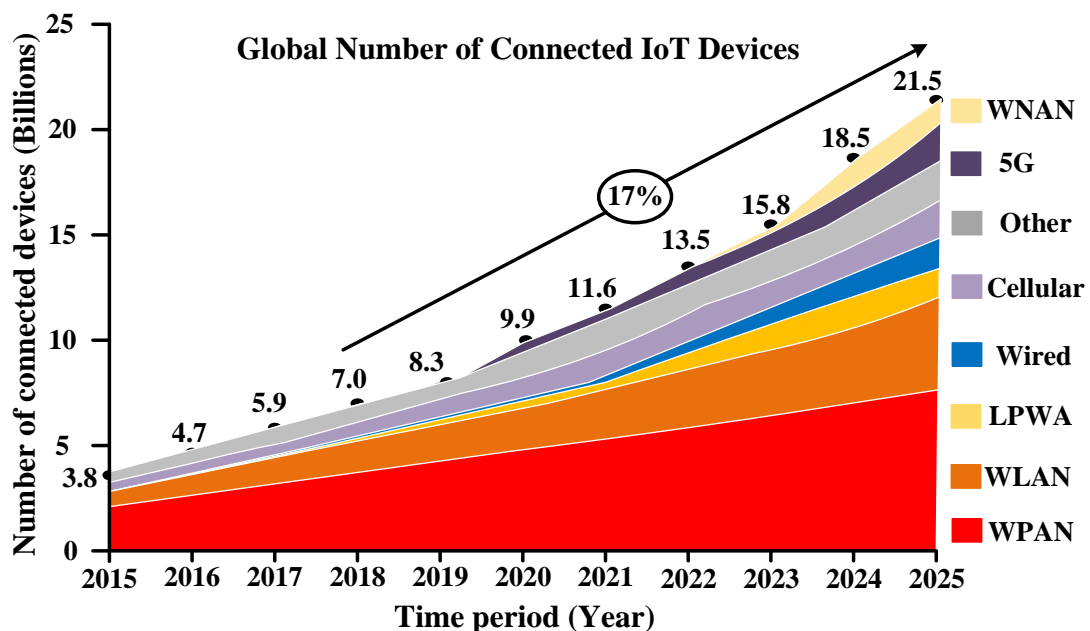


**Figure 1.1:** Explosive growth of IoT devices in the future world (adopted from [3]).

### 1.3 Architecture of IoT Systems

IoT is a system of interrelated computing devices which are connected under an internet connection. It can transfer data over a network without human-to-human or human-to-computer interconnections. The IoT devices exchange information between the devices themselves and with the data center. The devices communicate with local nodes depending on how the link can be merged with the devices and increased the sensing, processing, and communication capabilities. It has a vision in the future internet where different objects from consumer electronics to bicycles, autonomous vehicles to utility devices, etc., will be connected under the same network and controlled through an internet connection. These devices can exchange information among themselves and their surroundings through wireless connection. Fig. 1.2 shows the generic architecture of an IoT system. The IoT node consists of the IoT devices and the IoT gateway. The system involves with IoT nodes and the cloud based data center that allows IoT devices to communicate with each other.

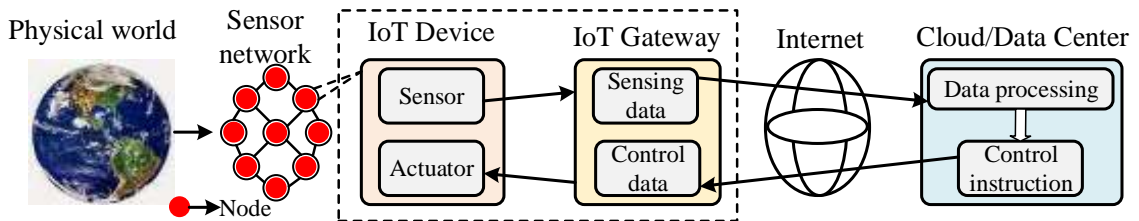


**Figure 1.2:** Overview block architecture of a generic IoT system.

#### 1.3.1 The IoT Device

IoT devices are pieces of hardware, including sensors and actuators, which are programmed for specific applications. It can range from small ordinary household cooking appliances to sophisticated industrial tools. Typically, the sensor in an IoT device collects data from the physical world and transmits it over the internet or other networks. The sensor could be anything to sense the physical phenomena, including temperature, humidity,

motion, accelerator, gas, voice signal, video signal, or any objects. Many types of IoT devices are used based on their applications. The most common IoT devices are consumer IoT, commercial IoT, industrial IoT, and infrastructure IoT. The IoT device has made it possible for the physical world to meet the digital world and cooperate with each other. IoT devices have different functions, but almost all IoT devices have similarities regarding their working principle. First, IoT devices are physical objects that sense things happening in the physical world. Then, the sensing data is passed to the IoT gateway for transmitting via the internet to the cloud or data processing center for further actions. IoT device contains an integrated CPU and network adapter and connects to a dynamic host configuration protocol server. It also requires an IP address to function over the network. However, the hardware resource limitations of IoT devices pose critical problems of limited speed, memory, feature size, etc., and hamper high-volume data telemetry using the existing frequency spectrum.

### ***1.3.2 IoT Gateway***

An IoT gateway is a centralized hub that connects IoT devices and sensors to cloud-based data computing and processing. It could be a physical device or software program serving as the connection point between the cloud, controllers, sensors, and intelligent devices. All the physical object sensing data passes through an IoT gateway for transferring between IoT devices and the data center. It works as a network router for routing data between IoT devices and the center. Most of the gateway devices only send traffic in one direction from IoT devices to the data center, but the modern gateway can support bidirectional data transmission. Recent IoT gateways also preprocess data locally by routing traffic at the edge before sending it through the internet. The IoT gateway devices



summarize or aggregate data to reduce the high volume of data that can affect response times and network transmission costs. Another benefit of an IoT gateway is to provide additional security for the IoT devices. The organization can secure its IoT ecosystem by adopting an IoT gateway explicitly designed with some features, including tamper detection, data encryption, random number generators, and crypto engines. The above features with the standard network security protocol can help to secure data transmission.

### ***1.3.3 Data Center/Cloud Based Data Processing Unit***

A data processing center or data center is a place, where various electronic equipment, including high-processor computers, telecommunication equipment, and other infrastructure are available to process the received data from IoT devices. The primary purpose of a data processing center is to run applications that process the essential functioning of a society. The requirements for data management are to design and develop these applications internally and serve primarily to process the information necessary for a specific business. The main elements of a data center are the facility, core components, and support infrastructure. It is commonly used to fill a critical mission for computing and telematics, including environmental monitoring, physical object sensing, real-time data gathering, and controlling. After receiving the physical world data and processing, it sends a controlling signal or instruction to IoT devices.

## **1.4 Wireless Data Telemetry System**

Telemetry is read-only data about the environment or physical world and is usually collected through sensors from remote places for analysis and other purposes. Each source of telemetry result is a data channel. Wireless data telemetry is becoming increasingly

pervasive for monitoring a wide range of physical phenomena occurring in different sectors of human life. Fig. 1.3 depicts the conceptual diagram of an IoT telemetry with wireless connectivity and its applications in diverse fields. Smart and intelligent devices are widely used in indoor automation, including enterprise or industrial, hospital, school, business offices, and outdoor applications, such as intelligent agriculture, environment monitoring, and intelligent city development [5-10]. In above applications, the IoT devices act as the bridge for wireless telemetry for information collection, monitoring, assessment, and controlling. Typically, the high-density data is collected and compressed from several sensor devices and sent it to the cloud-based data center for further processing, management, and sending controlling instructions to control IoT devices.

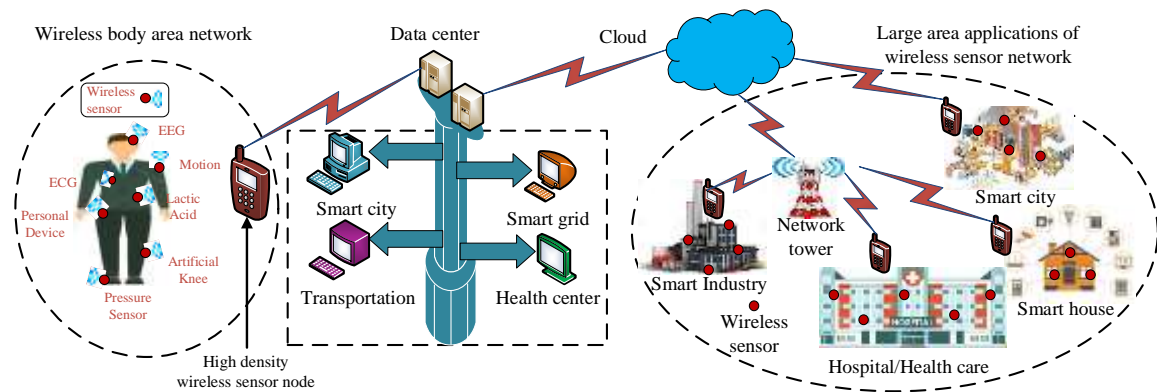


**Figure 1.3:** Conceptual overview of high-density wireless telemetry for IoT applications.

Wireless data telemetry transfers the data from transmitter to receiver with the help of either an analog pulse or digital pulse signal. Any information, including voice, sound, and image signals, can be transferred into binary data bits by signal processing with the help of a transducer and transmitted through the communication channel. Fig. 1.4 shows the block diagram of a conventional wireless communication system. It manifests sensor transmitters, receivers, and a display system. It easily replaces the wired systems to reduce

installation and maintenance costs. The sensor unit senses the physical phenomena, converts to binary data, encodes the data bits to either digital/analog pulse format, and transmits by RF antenna.

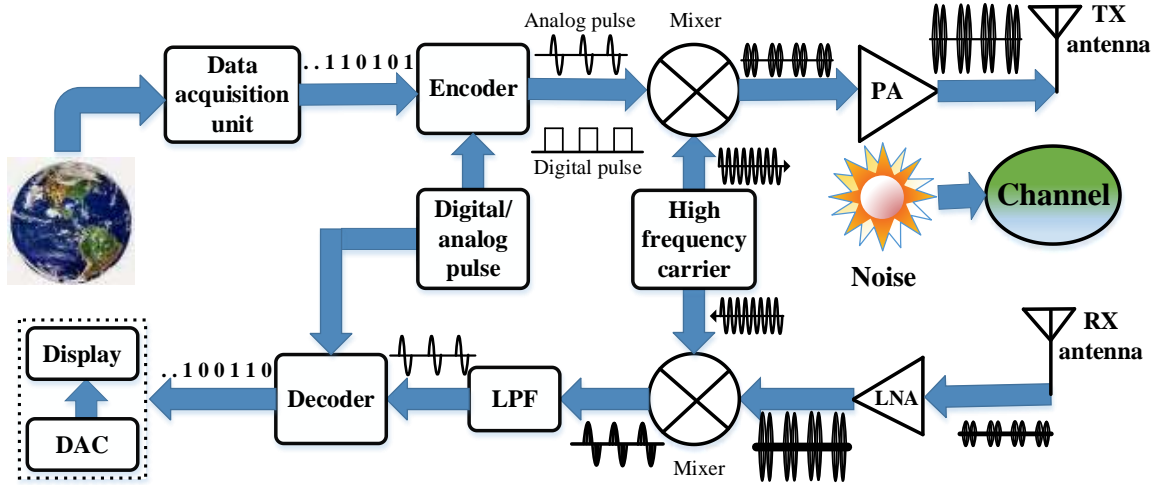


**Figure 1.4:** Block diagram of the conventional wireless communication system.

The low-frequency baseband signal is translated to high-frequency by carrier multiplication. An analog pulse communication is appropriate for short-range transmission, but it can also be used for long-distance transmission with the help of carrier modulation. Usually, the electromagnetic energy is transmitted at radio frequencies that carries the information bits. The carrier-modulated high-frequency signal is amplified by PA before transmission by the RF antenna and propagation through the communication channel. The transmitted RF signal is captured by the receiving RF antenna. The received signal strength is first increased by low-noise antenna (LNA) then demodulated and down-converted the high frequency into baseband frequency by same carrier multiplication. Therefore, one carrier modulator is required at the transmitter and one demodulator is connected at the receiver to retrieve the baseband transmitted signal. The low-pass filter (LPF) removed the unwanted noise signal from the baseband frequency. Finally, the

received signal is converted to binary data bits by utilizing the encoding template and recovered the transmitted original message information.

The frequency spectrum is limited. It requires appropriately sharing among all wireless systems and applications, including active and passive users. A recent report shows that in the U.S., spectrum utilization ranges from **15%** to **85%** under the fixed spectrum allocation policy [11]. Therefore, modern IoT networks must increase spectral efficiency and sharing capacity among many users. The **main requirements of 5G technology** are higher frequency spectrum, higher data transmission speed to enable high-definition video signal, high-volume data transmission, simultaneous IoT connectivity of  $1 \times 10^6$  connections per  $1.0 \text{ km}^2$  area, data reliability and security of the connection, and latency below 1.0 milli-second [12-13]. In addition, the next-generation technology also demands more and better functionality for developing new schemes, lower transmitting power, network architecture, and spectrum sharing to maximize the network capacity.

#### ***1.4.1 Digital Data Telemetry Platform***

The digital pulse signal is used to encode and transmit information bits in digital communication. Typically, the square wave pulse is used in most of the existing data communication technology. The common modulation techniques are including amplitude shift-keying (ASK), frequency shift-keying (FSK), phase shift-keying (PSK), binary phase shift-keying (BPSK), quadrature phase shift-keying (QPSK), M-ary encoding, quadrature amplitude modulation (QAM), and different pulse shaping techniques. Each modulation techniques have some pros and cons. The PSK technique is widely used for wireless LANs, bio-metric, contactless operations, RFID, and Bluetooth communications. Figs. 1.5 (a) and (b) shows the data encoding using digital pulse signal, and BPSK modulation using carrier

multiplication, respectively. The spread-spectrum modulation is a common technique in digital data communication to prevent interference. Since multiple users can share the spread spectrum bandwidth; therefore, it is also known as multiple access techniques. Frequency hopping and DSSS are mainly used as two standard modulation techniques in wireless mobile communication. In frequency hopping, multiple frequencies are used in a specified time interval, while a secret code, called a chipping code, is used for a single frequency in DSSS modulation. The CDMA wireless technology is based on DSSS modulation. The main benefits of digital pulse platform are noise immunity and simple hardware. But, it requires higher bandwidth and involves computational complexity.

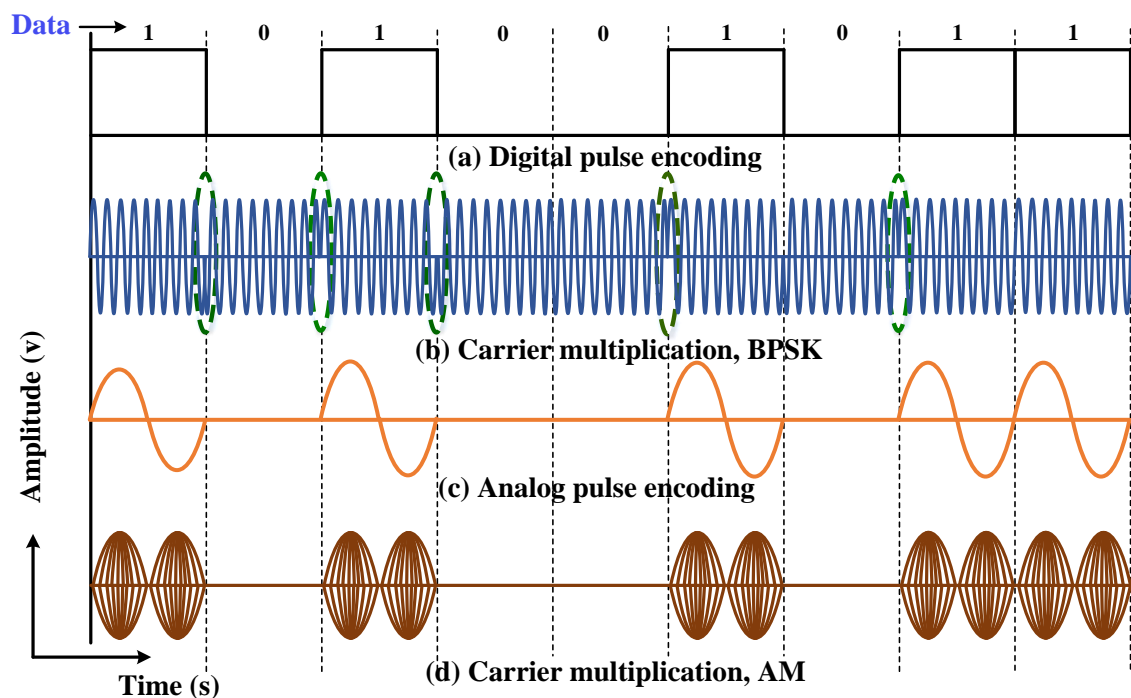


**Figure 1.5:** Generic data encoding scheme and carrier modulation (a) digital pulse format, (b) BPSK modulation, (c) analog pulse format, and (d) carrier multiplication.

#### 1.4.2 Analog Pulse Based Data Telemetry

An analog communication is a data transmission system where the information bits are transmitted in an analog pulse format. Analog signals are commonly used in

communication systems to convey voice, data, image, or video information using a continuous signal. An analog pulse signal is used instead of a square wave in analog pulse communication. Figs. 1.5(c) and (d) show the analog pulse-based data bit encoding and carrier multiplication for analog pulse communication, respectively. It is called analog modulation, if the amplitude, pulse duration, or pulse position are varied under instantaneous values of the baseband modulating signal. The standard analog modulation schemes are pulse amplitude modulation (PAM), pulse width modulation (PWM), and pulse position modulation (PPM). The main advantages of analog pulse include less bandwidth requirements, suitable for audio/video transmission, and spectrum sharing capability. However, the primary difficulties are undesirable signal distortion in the long-distance data transmission, prone to pulse generation loss, noise and distortion, and suffering from low-quality signals than digital signals. The analog orthogonal pulse (AOP) signal also supports efficient wireless data telemetry. It doesn't require any spread-spectrum technique or first Fourier transform (FFT) and inverse-IFFT computation like digital communication for multi-user applications to support high-density IoT networks.

### **1.5 Standard Communication Technology for IoT Telemetry**

Several wireless communication technologies have been developed in recent years to support WSNs in building IoT systems. However, the features vary in their different matrices, such as capacity, power consumption, and security protocol. Table 1.1 represents the feature list of existing standard wireless technology. Most of the technologies are used digital pulse format and digital modulation that involves with digital signal processing (DSP) computation. In addition, the state-of-the-art wireless technology is also limited and

incompatible with resource-constraint IoT devices to support high-density sensor networks. SigFox is a wireless cellular network that connects sensors directly to support a low-power and low-throughput wide-area network. This technology can support many sensor devices in the mid-range coverage and make them suitable for IoT solutions. The end devices used BPSK modulation using a standard digital pulse to connect to the base stations. SigFox technology enables IoT telemetry over distances and transmits with minimal base stations. It also has a higher network capacity to scale up to billions of sensor devices; however, the main drawbacks are lower data rates and higher power consumption for long-distance transmission within sensor networks [15].

**Table 1.1:** List of existing communication standards for WSNs [6, 15].

Technology name	Data rate (Mbps)	Power consumption (mW)	Channel numbers	Modulation scheme
SigFox	0.0006	122	360	BPSK
Z-wave	0.0096	35	232	FSK
LoRa	0.050	100	71	Chirp SS
Zigbee	0.250	36.9	16	DSSS
Bluetooth	25	10	40-79	FHSS

Z-wave wireless protocol is specially designed for innovative home applications for short-range, low-energy communications with a data speed of up to 40 kbps. It can support a maximum of 232 devices with a data speed from 9.6 kbps to 40 kbps and consume low power compared to the SigFox protocol [6]. The LoRa is a low-power long-distance technology and it is suitable for indoor IoT networks. The chirp spread spectrum encoding technique is used in LoRa technology for data modulation in long-range, low-power, and less interference. However, the lower data transmission rates ranging from 300 bps to 50 kbps is the main hindrance to the success of the IoT objectives' [6]. ZigBee technology is also developed for low-cost, low-power, and lower bandwidth requirement applications

within a single network. It uses the direct sequence spread spectrum (DSSS) modulation using a digital pulse signal and supports up to 16 distinct data channels. Though, we consider it one of the best candidates for IoT; however, it operates at lower data rates up to 250.0 kbps, supports maximum 16 sensor devices, and requires 5.0 MHz for channel bandwidth [6]. Bluetooth 4.0 is a short-range wireless data communication within 10.0 m distance and transmits data over ultra-high frequency radio signals. It leverages the *IEEE 802.11* standard for the fastest transfers and uses a frequency hopping spread-spectrum (FHSS) technology for multiple devices for different frequencies to limit interference. The BLE is another low-power wireless telemetry protocol with data rates at 25.0 Mbps [6]; however, it requires higher computation for spreading the digital pulse and it is more vulnerable to secure data transmission in wireless sensor networks.

## 1.6 Literature Survey

The explosion of mobile communication and sensor applications in recent years necessitate to development of new technique and adaptive, flexible, and efficient radio access technologies. The SE technique has been extensively searched in the last decade for wireless data communications to meet the advanced technological requirements. This broad interest is primarily because of spectrum sharing with other applications and spectrum allocation for multi-user transmission by sensing, adopting new modulation, and encoding techniques. The success of IoT system requires reliable, EE, SE, and scalable for sharing and transferring information from device to device or device to data center [13]. It is also essential to support high-density data and manage the spectrum for higher data rate.



The narrowband (NB)-IoT is one of the most efficient technologies among low-power wide-area networks that use NB frequency to support numerous IoT devices. However, it has a bandwidth of 180 kHz with a 3.75 kHz sub-carrier spacing, and it has allocated each to a different user for a 32.0 ms gap [16]. Specifically, the standard has been designed to support many data users, but each has a lower transmission rate [17]. Moreover, the design of NB-IoT is limited by a modulation scheme such as BPSK and QPSK to improve the EE system for data rate-sensitive applications [18]. Recently, many modulations technique have emerged, including EE, SE, and index modulation (IM) for WSNs to solve some of the existing challenges [19-22]. Like LTE technology, the NB-IoT system also uses orthogonal frequency division multiplexing (OFDM) and single-carrier division multiple access at the physical layer [23]. Its advantages include higher spectral efficiency, lower complexity, and immunity to inter-symbol interference, and it doesn't possess any immunity against channel fading for wireless data telemetry.

Recently, the emerging IM has arisen as a promising technique to meet the demands of high-volume data transmission for next-generation IoT networks [24]. The IM techniques rely on physical resources, including antenna, frequency sub-carrier, or virtual building blocks, such as signal constellation, antenna activation order, and space-time matrix [24]. The OFDM-IM has proposed by utilizing a higher-order modulation technique. The OFDM-IM moves the symbols in active sub-carriers to support higher SE telemetry with improved performance compared to the classical OFDM technique [25]. The code division multiplexing (CDMA) technology also uses IM technique by generating orthogonal code for EE and SE wireless transmission with better error performances [26-27]. The IM is utilized for OFDM and CDMA communication for SE wideband

transmission with higher throughput and better bit error rate (BER), but the system complexities are relatively high. A novel spatial pulse modulation (SPM) has been developed to modulate data bits by a permutation vector and activate the antenna at a successive time instants [28]. The SPM technique performs better in fast-fading than in slow-fading channels, but it increases the system complexity.

The generalized code index (GCI)-SM has been considered by combining the spatial modulation (SM) and code IM-spread spectrum for higher data rate, spectrum utilization, and EE transmission [29]. In a GCI-SM, the active antenna indices carry both information bits with spreading code in the spatial domain but increase the system complexity and hardware implementation cost. The trade-off between the SE and EE applications have developed a novel quadrature tri-mode-IM to avoid system energy loss [30]. The pulse code modulation (PCM) has been proposed for multi-user applications by exploiting spatial resources [31]. However, the main demerit is performance degradation with increasing channel numbers. Recently a novel frequency-domain filter shape index modulation (FSIM) has been proposed to map data bits for SE transmission [32]. The main drawback is using the ISI cancellation to avoid ISI that increases computational power and system complexity. The digital platform also involves with sophisticated DSP.

The design and development of a new wireless communication system will lead the innovative principles and solutions for effective and efficient transmissions without FFT and IFFT computation. Therefore, the analog HG pulse signal is widely used for wireless telemetry in NB and Ultra-wideband UWB systems. The narrow-width AOP signal is used to transmit data bits symbolically to increase the transmission rate [33-36]. The time-frequency lattice structure carries over one symbol per grid to improve the data rate by n-

times using the toroidal waveform-based OFDM technique [34]. Similarly, the HG system increases the data rate by  $(n+1)$  more using superimposing  $n^{\text{th}}$  order AOP signal [37].

The sub-nanosecond pulse signal is typically used in wireless telemetry to transmit data bits symbolically through a wideband RF antenna for low-power, short-range communications [38-39]. It has developed many pulse-shaping techniques to encode the data bits using a group of symbols for SE wireless communication. But it disperses the energy in pulse shaping techniques to other sub-carriers with the channel dispersion [40]. The prolate spheroidal wave functions are used to design a time frequency division multiplexing (TFDM) system and avoid the pulse energy dispersion for multiple user applications [33]. However, inter symbol interference (ISI) and inter carrier interference (ICI) are the main issues in TFDM system. The summation of BPSK-modulated multi-order HG pulses has been proposed for a SE data communication [34]. These pulses are orthogonal and coexist with other applications; therefore, in the pulse transmission either a single-order/linear combinations of pulses are used that carry the transmitted bits.

Several analog pulse-based data encoding schemes have been proposed in recent years for single-bit or multi-bit coding using either a single or composite Hermite pulse. The multi-order AOP set encodes multi-bit data for multi-user applications to intensify the data rate by taking advantage of the orthogonal properties [41]. It has highlighted two encoding schemes. The first method transmits a composite pulse through a narrow-width analog pulse signal. The second method uses a set of multi-order pulses instead of a single pulse signal. The orthogonal pulse signal exhibit mutual orthogonality between different order pulses and their composite signal. Simultaneous pulse transmission is achieved

without collision in the wireless system due to the signal orthogonality; however, it limits by the channel numbers using a single pulse-based wireless data transmission.

Recently, a novel pulse index modulation (PIM) has been proposed that activates specific pulse shapes according to the incoming transmission bits [42]. The authors have proposed the PI encoding using a set of AOP signals, like SM, for SE multi-bit transmission. It generates the transmitted pulse signal like the OFDM-IM but doesn't require complex operations like *FFT* and *IFFT*. The pulse index (PI) bits are used as an extra dimension to convey the conventional constellation mapping information. The linear combinations of over one analog pulse signal are required to create the signal orthogonality for multi-bit encoding. In addition, the receiver model comprises matched filtering and a maximum likelihood detector to decode the transmitted bits information. Therefore, the existing HG pulse-based PIM using M-ary increases the system complexity for encoding and decoding architecture.

### **1.7 Problems Identification**

The radio-frequency spectrum is a finite resource. It is becoming saturated with the demand for new applications. Generally, telecommunications companies minimize the existing resource limitations to support the rapid growing IoT market. Therefore, high-volume data acquisition and transmission technique are applied to the research field in wireless communication. The new scheme advances the technological impact on human lives. Integrating many wireless sensor devices increase the demand for high-speed data transmission. However, the allocated spectrum does not meet the drastically growing demand of customers for commercial applications. The availability of frequency spectrum

for commercial and military applications are decreasing with the number of users, and their bandwidth requirements are increasing drastically. The existing spectrum aims to accommodate 1,000-fold more wireless devices under the same network and operate by sharing bandwidth for simultaneous connectivity with increasing network capacity.

The proliferation of wireless sensor devices for communication technology has also generated a large volume of data on the limited bandwidth and brought new challenges, including transmission bottlenecks, data latency, and network congestion. The resource-constrained IoT devices can't support high-volume data transmission due to the limitation of speed, power, and memory, which creates a network burden on the limited bandwidth. The computational complexity, such as *FFT* and *IFFT*, spread-spectrum modulation, and higher bandwidth requirements of the digital pulse signal, also pose significant challenges for limited resources of IoT devices. Therefore, most of the existing technology can't support the current demands of high-density data telemetry for IoT node-level implementation. The advanced technology also requires higher bandwidth, improved data rate, simultaneous connectivity, lower latency, and data security to meet the demands of the 5G network.

To remove the computational burden in digital communication, the researchers have investigated analog pulse-based communication for its variety of benefits, including coexistence properties and larger bandwidth. However, the proper orthogonal pulse generation and their higher-order derivatives are the main drawbacks in analog pulse-based data communications. In addition, selecting an appropriate encoding and decoding scheme is a significant challenge when designing pulse-based systems. Most recently, a novel PIM technique has been proposed that activates a specific pulse according to incoming data bits

[42]. The PIM technique generates the transmitted pulse signal like the OFDM-IM and doesn't require the *FFT* and *IFFT* computations, but it requires over one pulse signal to transmit multi-bit data. The receiver model is also a little complex to detect the receiving data bits for SE short-range wireless telemetry. In addition, the number of data channels also limits the single AOP-based system for high-density IoT applications. An innovative approach enables effective spectrum utilization and meets the demand for advanced IoT technology. Therefore, the wireless industry is always looking for novel data encoding techniques to address the upcoming challenges for SE high-density data transmission in IoT applications. The orthogonal pulse-based telemetry provides an excellent alternative to overcome the above limitations with reduced complexity and data compression.

### **1.8 Proposed Solutions**

This dissertation proposes AOP-based several innovative data encoding and decoding schemes for SE short-range wireless telemetry to support high-density IoT networks. The AOP set is generated using a simple architecture-based modified Hermite pulse generator to encode the data bits symbolically [14]. The AOP generator comprises two first-order differential equations and requires less computational complexity than standard HG pulse generation techniques. In this dissertation, two innovative data encoding and decoding schemes are proposed for AOP-based high-volume data compression to meet the requirements of next-generation IoT networks. The first method uses the distinct order AOP set where a single order pulse carries multi-bit data instead of a single bit. The multi-order AOPs encode different binary combinations of  $k$ -bit with a low-level physical layer security, where  $k$  is a non-zero integer number. The second method encodes the individual

data channel by sharing the frequency spectrum by distinct PS instead of the single-order pulse signal for wireless telemetry. Distinct PSs encode the multi-user data and transmits the compressed volume as a composite signal using single carrier frequency.

The correlator architecture-based pulse decoding scheme is also implemented at the receiver end to detect and recover the transmitted data bits. The cyclic pulse elimination (CPE) algorithm is developed and implemented to decode individual pulses cyclically from the composite pulse signal using the correlation peak analysis. Unlike standard digital pulse communication, the proposed time-domain orthogonal analog pulse-based data encoding technique doesn't require complex operations, including *FFT* and *IFFT* computation. Therefore, the main contributions of this dissertation are AOP-based data encoding and decoding algorithm development, implementation, and validation for multi-user data compression by utilizing the same frequency spectrum. The communication channel effects on AOP signal and object sensing are investigated extensively using the network parameter measurement to check the feasibility of the proposed analog pulse technology. It also configured a prototype test platform using the commercially available customized RF modules to validate the performance and compatibility of the proposed AOP-based data telemetry with standard communication architecture and network protocol. The proposed schemes' research outcomes significantly improve the transmission rate and high-volume data compression by supporting many IoT connections sharing the same spectrum.

### **1.9 Research Impact on Society and Economic**

The electromagnetic spectrum is an essential resource for many societal and economic sectors. Commercial applications such as wireless data communications,

navigation, and data telemetry compete for spectrum access to scientific activities, including radio astronomy, earth observation, polar research, and other vital spectrum-dependent services. The ongoing technological progress has created a situation where each application, action, and service seeks additional spectrum access. Therefore, the research outcome of SE high-density wireless telemetry will directly impact ubiquitous high-resolution monitoring, secure transmission, and support future IoT networks. It also germinates new and innovative ideas and applications, including but not limited to continuous tracking, faster data transmission, large-volume data compression, scientific discoveries, object sensing, detecting, assessment, autonomous controlling, etc. The SE wireless telemetry will also impact intelligent agriculture, autonomous vehicles to increase highway capacity and safety, more efficient cities, smart industry, biometrics screening, smart home automation, large-area observation, and medical applications.

The research on high-density wireless telemetry also has substantial merits in the benefits of the interest and economy of the U.S. The U.S. government tries to manage the spectrum with continuous growth in the commercial wireless services, including mobile phones, IoT devices, video streaming, Wi-Fi, etc. According to Accenture's economic analysis, the impact of 5G on the U.S. economy will drive up to \$2.7 trillion in total sales across all major industries and add up to \$1.5 trillion to the GDP. In addition, the 5G technology has the potential to create up to 16.0 million jobs across all sectors of the U.S. economy. The DoD also uses the existing frequency spectrum to enable modern military communications, navigations, radar, a non-intrusive inspection of aircraft, and other equipment. The DoD spectrum sharing strategy shows that emerging technologies also offer that the DoD and commercial systems share the same frequencies.



## 1.10 Dissertation Outlines

This dissertation covers several aspects of SE wireless telemetry for short-range IoT applications, including analog pulse generation, algorithm design and development for high-volume data compression and decompression, channel effect analysis on AOPs, and test platform development to validate the analog pulse transmission. The broad theme of this dissertation is to explore tradeoffs between the narrow-width pulse generation and the hardware limitations to support NB systems. The entire dissertation has been divided into **seven** chapters. The contributions of each chapter are as follows:

**Chapter 1. Introduction:** Introduction, the IoT market, IoT system, wireless data telemetry, standard communication technology, literature survey on modulation techniques, problems identifications, proposed solutions to support high-density IoT networks, research impacts on society and economy, and the dissertation outlines.

**Chapter 2. Analog Orthogonal Pulse Generation and Telemetry:** Introduction, architecture of analog pulse-based data telemetry, standard pulse generation schemes, AOP set generation and signal property analysis, and brief explanation of analog pulse-based proposed data encoding schemes.

**Chapter 3. Single Pulse-Based Multi-bit Encoding:** Introduction, transceiver architecture for single pulse-based multi-bit encoding, architecture of proposed PI encoding, pulse randomization scheme, security analysis, and significant improvement of proposed encoding, and simulation results.

**Chapter 4. Pulse-Sequence Based Encoding and Data Compression:** Introduction, PS-based data telemetry, PS generation and channel coding, Gold sequence generation, high-

volume data compression and decompression, missing data finding, significant improvement of PS scheme, simplify the receiver algorithm, and simulation results.

**Chapter 5. Channel Effects on Analog Pulses and Object Sensing:** Introduction, channel characterization,  $S_{21}$  parameter measurement setup and configuration, signal processing in time-frequency analysis, measurement results and channel effects analysis, investigate different case study, modification of the receiver architecture, and summary.

**Chapter 6. Prototype Development and Test Results:** Introduction, Arduino implementation, configuring communication architecture, design and implementation mixer driver circuit and LPF circuits, prototype test platform, experimental results and discussions, BER and PER investigation for k-bit, test results for PS measurements, summary and discussion.

**Chapter 7. Conclusion and Further work:** Conclusion and future extension of the AOP-based short-range wireless data telemetry for high-density IoT applications.

**Appendix A. List of Publications**

**Appendix B. Correlation Peak Table**

**Appendix C. Pseudo Code for Algorithms**

## CHAPTER 2

### ANALOG ORTHOGONAL PULSE GENERATION AND TELEMETRY

#### **2.1 Introduction**

Orthogonal pulse-based wireless data telemetry is a new technology to support large-volume wireless sensor devices by sharing the same frequency spectrum with other applications. It improves data transmission rate by high-volume compression without standard algorithms or sophisticated signal processing for short-range IoT applications. It also shows several advantages, including relatively large bandwidth, robustness to multipath interference, less implementation complexity, low power requirements, and coexistence with other applications. This chapter highlighted the architecture of analog pulse-based wireless telemetry, AOP generation, time-frequency domain representation, analyzes the signal property, and provided the brief of different AOP-based data encoding schemes for high-volume data compression.

#### **2.2 Analog Pulse-Based Data Telemetry**

The AOP-based communication paradigm is a new technology to support high-volume data for SE wireless telemetry. The orthogonal pulse transmission reduces the system complexity, computational power, and integrates easily with the conventional communication architecture and network protocol. The signal orthogonality of analog pulse transmission scheme also compresses the high-volume sensor data without any

standard compression algorithm. Fig. 2.1 shows the generic system model of analog pulse-based transmitter and receiver architecture for SE wireless telemetry. It comprises of two sub-blocks leveling as pulse-based RF (a) transmitter and (b) receiver.

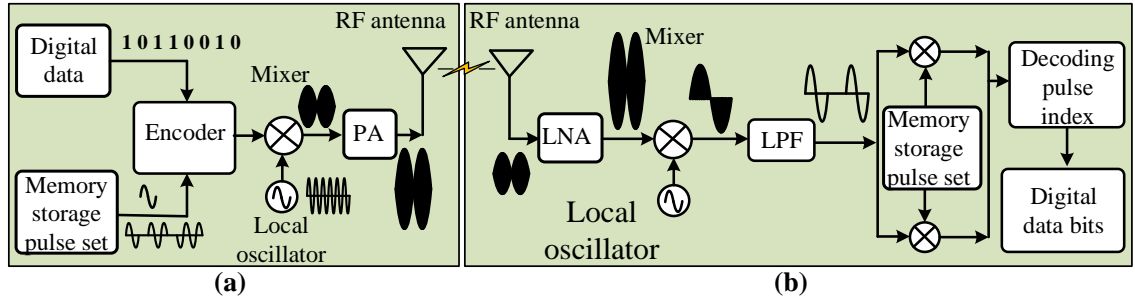


**Figure 2.1:** The AOP-based transceiver architecture (a) transmitter and (b) receiver.

### 2.2.1 Analog Pulse-Based RF Transmitter

Fig. 2.1(a) shows the block diagram of an AOP-based RF transmitter. It comprises memory storage multi-order analog pulses, data encoding, and an RF chain block. A power-efficient pulse generator generates the AOP set explained in **section 2.4** and stores it in the microcontroller flash memory for further signal processing. The sensor data encodes by a single pulse or a sequence of pulses using OOK technique. Then the data-encoded low-frequency baseband signal is translated to high-frequency at 500 MHz using carrier multiplication. Finally, the transmitted signal strength is increased by a PA before transmitting RF antenna for propagation through the channel.

### 2.2.2 Correlator Based Pulse Decoding Receiver

Fig. 2.1(b) shows the architecture of the correlator-based pulse decoding receiver model. The Rx antenna collects the transmitted composite pulse signal, reconstructs them, and maps the symbols into a binary bit using a prior known encoding template to decode the information bits of the individual data channels. First, the received composite pulse

signal passes through the RF chain to amplify the signal strength by a low-noise amplifier (LNA), down-converts the carrier frequency by the same carrier signal multiplication, and recovers the baseband frequency after passing through a low-pass filter (LPF). Then, the pulse-decoding algorithm is applied to decode the individual pulse signal from the received composite signal using correlation peak analysis. The memory storage AOPs are used as template to check autocorrelation sequentially with the received composite signal. The decoding algorithm checks the correlation peak sequentially and stores the PI corresponding to highest peak. Finally, the eliminated PI is mapped and compared with the prior known encoding template.

### ***2.2.3 Communication Channel***

The RF signal has the capabilities of multi-path propagation, penetrating through dielectric media, and experiencing reflection from surrounding objects for short-range wireless communications. The communication channel represents the effects of signal distortions, attenuations, and time delay when traveling through it. The most critical issue in analog pulse telemetry is the pulse shape distortion, spreading, and time delay in the transmitted signals propagating through indoor environments. The indoor communication channel involves different dielectric materials, including wooden doors, bricks wall, foam layers, metal furniture, concrete construction, electronic devices, etc. Typical indoor scenarios are considered, including the line-of-sight (LoS), room-to-room, within-the-room, and hallways to investigate the channel effects when propagating through a communication medium. Interference on the system with other applications is multiple access that also impacts the communication channel.

### 2.3 Conventional Pulse Generation Scheme

The UWB requires generating sub-nanosecond analog pulses to implement wireless data communication technology. The proper pulse generation and their higher-order derivatives are the main drawbacks in analog pulse transmission. In previous, the pulse was generated by spark gap techniques, but the pulse generation technique has changed with time. Literature review shows, a lot of works have done towards developing different innovative analog pulse generation techniques [43-58]. The Gaussian function, Haar function, Hermite polynomial, and modified Hermite polynomial are primarily used to generate pulses for UWB applications [43]. Gaussian, monocyclic and poly-cycle pulses with sub-nanosecond time windows are considered as UWB pulses. A pulse width of 100 ps is required for using the entire allowable frequency band in the UWB system [44]. A monocycle and doublet pulse signal is generated using a photonic microwave delay line [45]. It also shows Gaussian monocycle and different order pulses with their frequency spectrum. A new UWB pulse generator scheme has been proposed for different pulse widths that satisfy the FCC specifications on UWB communication [47].

Unfortunately, the widely adopted Gaussian monocycle exhibits a low-power efficiency and poor fit to the FCC power spectral mask that prevents practical usage. A new pulse generator is designed corresponding to the dominant eigenvector of a channel matrix constructed by sampling the power spectral mask [48]. The generated pulse meets the power spectrum and spectral emission constraint; however, it doesn't achieve the most efficient spectral utilization [49]. The prolate spheroidal wave function-based pulse meets the spectral power constraint but complicates implementation [50]. A digital filter based on the semidefinite programming algorithm has exploited to optimize the transmission

power by generating analog pulses [51]. It also proposed the linear variety of Hermite functions to eliminate the requirement of accurate time delay and increase the power efficiency for analog pulse generation [52-54]. The super-orthogonal convolutional code and orthogonal waveforms can affect higher data rates with better error performance [52]. However, a precise delay of 40 ps is required to generate the pulse set using the procedure of linear combinations, and it can't implement accurately by modern hardware technology.

Recently, the UWB pulse with a center frequency of 110.25 MHz and a bandwidth of 41.5 MHz (fractional bandwidth of 0.376) has been generated using a FPGA. Still, it is unsuitable for through-wall detection [55]. The proposed FPGA-based pulse generation could achieve a bandwidth of 1.6 GHz (fractional bandwidth of 1.033) and improve the transmitting frequency bandwidth for radar applications [56]. Later, the FPGA scheme is developed by arm swing motion to detect live human subjects behind the wall [57]. The multi-order analog pulse set was also recently generated using the FPGA to detect human subjects' respiration underneath the rubble and locate them based on the range estimation [58]. However, the FPGA scheme comprises three parts: digital clock manager, four-delay-paths stratagem, and edge combiner. Therefore, the power-efficient analog pulse generation scheme is also required for resource-constraints IoT node-level implementation for short-range wireless data telemetry. Most recently, the Hermite polynomial function has been simplified to generate multi-order analog pulses in a power-efficient way [41].

## **2.4 Analog Orthogonal Pulse Set Generation**

The power-efficient AOP set generator is crucial for high-density data telemetry in WSNs. The orthogonal Hermite function has signal orthogonality, but proper AOP

generation using Hermite polynomial raises the computational complexity with hardware implementation cost. However, the MHP-based pulse generator has less computational complexity than Gaussian pulse or other orthogonal pulse generations. This section describes the MHP-based orthogonal pulse set generation for analog communication.

#### **2.4.1 Mathematical Model**

A power-efficient multi-order analog pulse generator based on a neurotrophic circuit architecture has described as reducing the computational complexity and power dissipation for sub-GHz UWB communication [59]. The MHP-based orthogonal pulse set generator is a simplified method. Unlike the existing pulse generation methods, the developed mathematical model offered less computational power and reduced system complexity. In this work, the simplified MHP-based pulse generator is adopted from the previous works. It comprises two first-order differential equations (1) and (2), where ‘ $\tau$ ’ is the time scale factor,  $h_n$  is the  $n^{\text{th}}$  order Hermite variable, and  $h_{n-1}$  shows the previous state of pulse order. The higher-order MHPs can be generated by changing the value of ‘ $n$ ’, where ‘ $n$ ’ is non-negative integer and varies from 0 to  $n$  for various order pulse generation.

$$\tau * h'_n(t) = -\frac{1}{2}h_n(t) + nh_{n-1}(t) \quad (1)$$

$$\tau * h'_{n-1}(t) = +\frac{1}{2\tau}h_{n-1}(t) - h_n(t) \quad (2)$$

#### **2.4.2 MATLAB Simulink Model**

Fig. 2.2 shows the MATLAB<sup>®</sup> Simulink model of pulse set generator. This power-efficient simplified model consists of 2-integrators, 5-multipliers, 3-adders, and a Sawtooth wave generator. The constant value ‘ $n$ ’ defines the pulse order and the factor ‘ $\tau$ ’ decides the pulse duration. So, the different order pulse signal can be obtained through changing the value of ‘ $\tau$ ’ when  $n$  is given for both NB and UWB system. The simplified model is designed



for sub-GHz UWB communications to produce the AOP set with a pulse width of  $20\text{ ns}$ , but in this work, the  $2.0\ \mu\text{s}$  pulse width signal is generated for considering the trade-off between hardware implementation and test facilities. The NB pulse signal is generated using  $\tau = 1.0 \times 10^{-6}$  and setting the Sawtooth wave function at  $-5.0\ \mu\text{V}$  to  $5.0\ \mu\text{V}$ , and time period  $-1.0\ \mu\text{s}$  to  $1.0\ \mu\text{s}$ . By varying ' $n$ ' to different integers the pulse responses of two dynamic system  $n^{\text{th}}$  and  $(n-1)^{\text{th}}$  order derivatives are obtained which represents the AOPs. This pulse generation scheme is significantly less complex and power-efficient than others Hermite pulse generation technique.

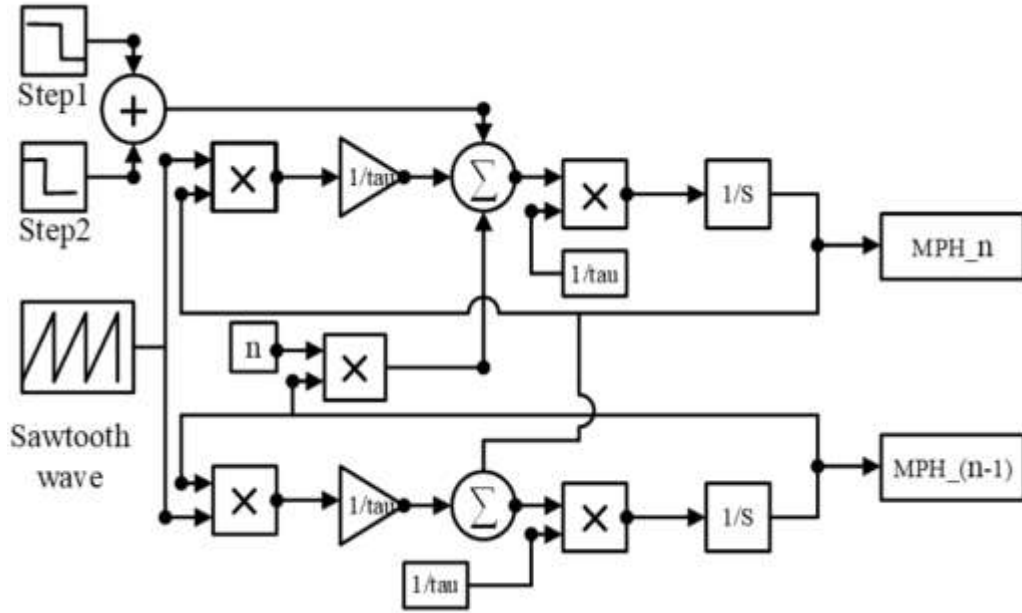
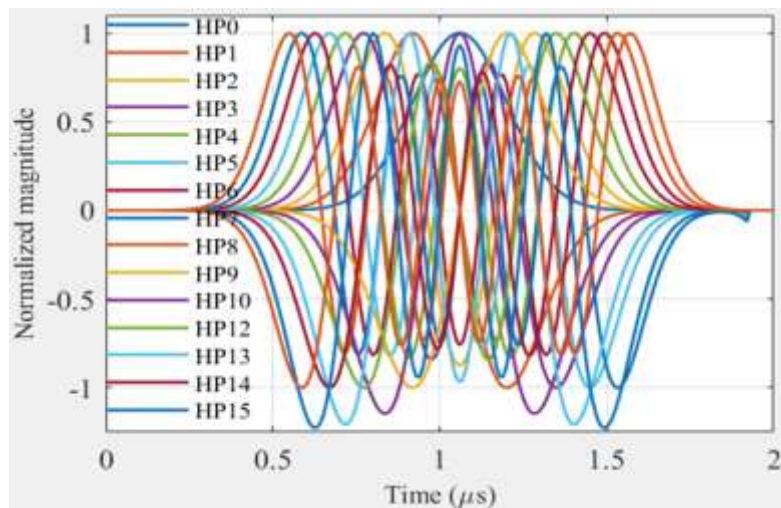


**Figure 2.2:** Simulink model of MHP-based multi-order analog pulse generator.

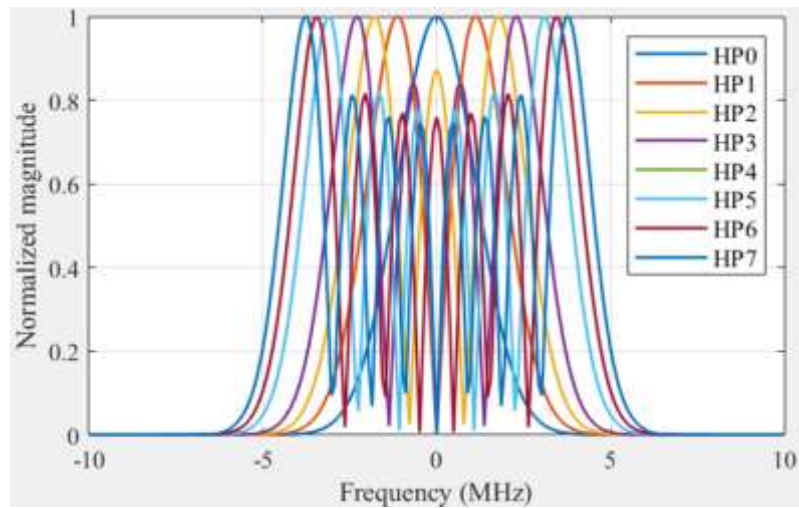
### 2.4.3 Signal Orthogonality

In this dissertation work, the multi-order AOPs are generated from 0 to  $7^{\text{th}}$  to implement the innovative SE data telemetry. Fig. 2.3(a) represents the multi-order AOPs generated by the MHP-based pulse generator described in the previous sub-section. As seen in Fig. 2.3(a), the pulse oscillation cycle increases with the Hermite pulse order. This

work generates distinct order of original and their  $180^\circ$  phase-shifted pulses. The pulse symbol from HP<sub>0</sub> to HP<sub>7</sub> represents the original, and HP<sub>8</sub> to HP<sub>15</sub> shows their shifted pulses of order zero to seven, respectively. Fig. 2.3(b) shows the frequency-domain representation of different Hermite pulses. The signal bandwidth describes the network throughput and refers to how much data information can transmit or receive across a connection in a certain period. In this dissertation, a  $2.0 \mu\text{s}$  width AOP signal is generated for short-range wireless data telemetry applications.



(a) Multi-order AOPs in time domain



(b) Multi-order AOPs in frequency domain

**Figure 2.3:** Different order AOP signal in (a) time-domain and (b) frequency-domain.

**Table 2.1:** Correlation coefficient peak table for individual AOPs.

	HP <sub>0</sub>	HP <sub>1</sub>	HP <sub>2</sub>	HP <sub>3</sub>	HP <sub>4</sub>	HP <sub>5</sub>	HP <sub>6</sub>	HP <sub>7</sub>
HP <sub>0</sub>	1.000	0.000	-0.218	0.0001	-0.186	0.0002	-0.168	0.0004
HP <sub>1</sub>	0.000	1.000	0.000	0.000	0.000	0.000	0.000	0.000
HP <sub>2</sub>	-0.218	0.000	1.000	0.000	-0.218	0.0001	-0.110	0.0003
HP <sub>3</sub>	0.0001	0.000	0.000	1.000	0.000	0.000	0.000	0.000
HP <sub>4</sub>	-0.186	0.000	-0.218	0.000	1.000	0.0001	-0.093	0.0002
HP <sub>5</sub>	0.0002	0.000	0.0001	0.000	0.0001	1.000	0.0001	0.000
HP <sub>6</sub>	-0.168	0.000	-0.110	0.000	-0.093	0.0001	1.000	0.0002
HP <sub>7</sub>	0.0004	0.000	0.0003	0.000	0.0002	0.000	0.0002	1.000

Table 2.1 shows the correlation coefficient peak tables of individual pulses. The correlation peak between the two signals shows how close they are to each other. The auto-correlation peak shows how the pulse signals are identical. The cross-correlation shows the mutual orthogonality among two different pulses. The cross-correlation coefficient '0' typically means two signals are at right angles. The auto-correlation peak '1' shows no orthogonality among them. The negative peak shows the correlation of the original pulses with their time-shifted pulses.

#### ***2.4.4 Pulse Signal Strength***

The signal strength of AOPs measured the consistent and stable wireless data transmission. In 2002 the Federal Communication Commission (FCC) defined the equivalent isotropically radiated power (EIRP) for indoor wireless communications. The power spectral density (PSD) is a good indicator of the minimum power requirements of a pulse signal for indoor communications. The PSD of the signal describes the power present in the signal as a function of frequency. It is commonly expressed in watts per Hertz. As per FCC guidelines, the normalization factor of PSD is the peak value -41 dBm/MHz for indoor communication allowed by the FCC. Usually, the PSD tells us at which frequency range variations are substantial. This information is helpful for further signal analysis.

Table 2.2 shows the spectrum bandwidth of the different order AOPs. All the pulses contain almost fixed 3-dB bandwidth around  $1 \pm 0.15$  MHz in frequency domain representation. Let us assume, the data transmission rate is 1.50 Mbps for 3-bit encoding using a 2.0  $\mu$ s AOP signal. The channel BW is around  $1 \pm 0.15$  MHz. The spectral efficiency,  $S_{eff}$  is,  $\frac{1.5 \times 10^6}{1 \times 10^6} = 1.5 \frac{bits}{Sec} / Hz$ . It shows that the 50% spectral efficiency obtained using a 2.0  $\mu$ s pulse signal for 3-bit encoding. If we use ns pulse signal and higher level of bit encoding then the spectral efficiency also improved. Fig. 2.4 shows the PSD plot of individual AOPs. MATLAB<sup>®</sup> simulation is performed to check the PSD of individual pulses after frequency shifting at 500 MHz. The PSD plot depicts that all the individual pulses meet the minimum EIRP requirements for AOP-based wireless data telemetry at 500 MHz.

**Table 2.2:** The half-power (3-dB) bandwidth for multi-order analog pulses.

Pulse signal	HP <sub>0</sub>	HP <sub>1</sub>	HP <sub>2</sub>	HP <sub>3</sub>	HP <sub>4</sub>	HP <sub>5</sub>	HP <sub>6</sub>	HP <sub>7</sub>	HP <sub>8</sub>
BW (MHz)	1.873	1.229	1.165	1.089	1.036	1.001	0.970	0.947	0.922
$S_{eff}$ (bps/Hz)	0.802	1.220	1.287	1.377	1.447	1.500	1.546	1.583	1.626

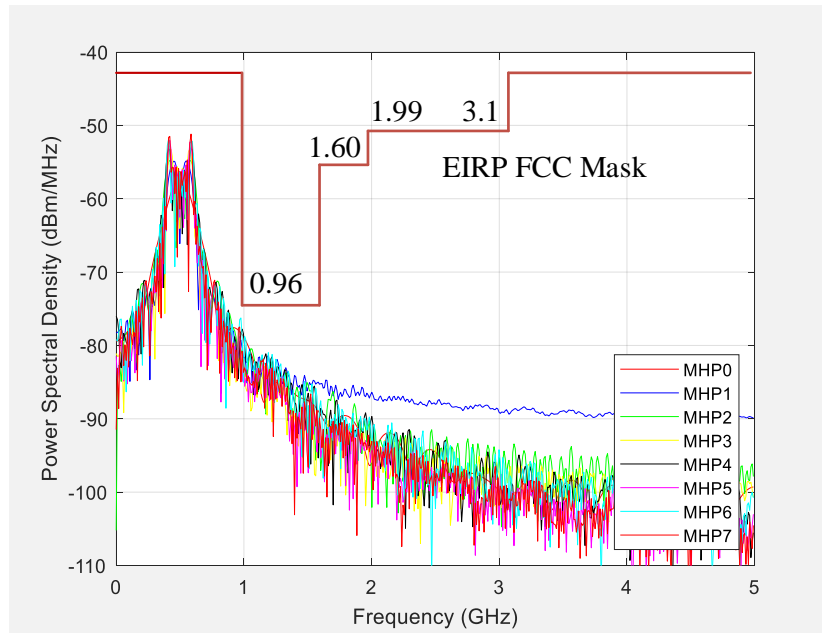


**Figure 2.4:** Power spectral density of different order pulses at 500 MHz frequency.

### 2.4.5 Orthogonal Shifted Pulse generation

The time-shifted analog pulses are also orthogonal with their original pulses. I also investigated the pulse generation scheme considering different time shift factor ranges from 20% to 70%. The lowest time shift factor is 20% with original pulses to maintain the signal orthogonality. In pulse communication, the main problem is proper orthogonal pulse generation with their higher-order pulses. The higher-order pulses contain many pulse cycles within a fixed time window, which is noise prone for wireless data telemetry. The time shift factor increases the number of pulses of the distinct order AOP set to remove the complexity of higher order pulse generation. Fig. 2.5 shows the orthogonal pulse generation results for different order AOPs and their various time shift factor. The red, blue, and green traces show the first, second, and third-order pulses. The pulse width of the original multi-order AOPs is  $20.0 \mu\text{s}$ . The pulse width of the new pulse set becomes  $34.0 \mu\text{s}$  considering a maximum 70% time shift factor.

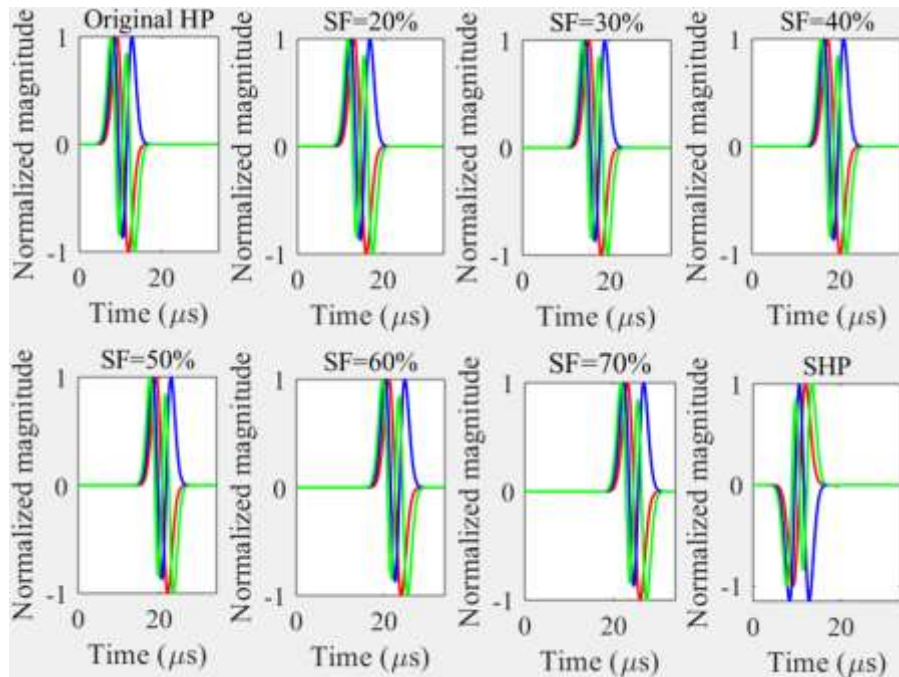


**Figure 2.5:** Multi-order analog pulses and their time shifted pulse signals.

## 2.5 Proposed Data Encoding Schemes

Integrating a large volume of recording channels is a big challenge in the wireless system, which causes a substantial growth in data volume into WSNs. Analog pulse-based multi-bit data encoding for the multichannel system has been discussed to achieve high data speed in WSNs. It developed various novel data encoding schemes based on the orthogonality and properties of Hermite pulses. In this Ph.D. dissertation, two innovative analog pulse-based data encoding schemes are proposed for SE short-range wireless telemetry to support the demands of next-generation IoT networks. The first scheme offers a single AOP signal to encode multi-bit data instead of single bit. Multi-order AOPs show different  $k$ -bit data binary combinations, where  $k$  is a non-zero integer number. In the second approach, a sequence of the pulse signal is used to encode the distinct data channels. The individual PS carries information bits corresponding to the data channel instead of a single-order orthogonal pulse. The serial-parallel data transmission technique is used in the PS scheme to represent the data bit. This section introduced different data encoding schemes with their architecture. On the other hand, the multi-bit encoding and PS-based channel coding are described broadly with high-volume data compression and decompression, transceiver architecture, algorithm development, and preliminary simulation results in **chapter 3** and **chapter 4** in detail.

### 2.5.1 Single Pulse Based Multi-bit Encoding

The single-order pulse-based multi-bit data encoding is a new scheme for high-density sensor applications. A set of AOP set is used to encode data bits and transmits as symbolically. In multi-bit encoding, a single-order analog pulse carries multi-bit data where the digital bits stream modulates by a set of AOPs. Fig. 2.7 shows the AOP set-based

multi-bit encoding. In this example, the  $k$ -bit encoding is explained for multi-user applications, and each single-order pulse signal carries 3-bit data instead of a single bit. The distinct pulse order of AOPs represents the specific data channels, and the time-shifted pulses create the number of pulse requirements to carry different combinations of 3-bit binary data. Fig. 2.7(a) shows the data encoding templates for sensor 1, where the SMHP<sub>1</sub> indicates the  $180^\circ$  phase shifted pulse and represents the '000' bits data. The symbol  $t_1, t_2, t_3, t_4, t_5,$  and  $t_6$  represents the time shift factors of 20%, 30%, 40%, 50%, 60%, and 70%, respectively, of the original pulses to encode data bits as per the encoding template. Similarly, MHP<sub>2</sub>, MHP<sub>3</sub>, and MHP<sub>4</sub> pulses and their time-shifted pulses will be used to modulate the data bits for sensor 2, 3, and 4, respectively. Fig. 2.7(b) shows the encoding scheme of multi-user data using AOP<sub>s</sub> at the sensor hub. Since all the distinct order analog pulses are orthogonal; therefore, all the pulses are superimposed to create a composite signal showing the compressed data volume for multi-user applications. **Chapter 3 describes** the multi-bit encoding using distinct AOPs with MATLAB<sup>®</sup> simulation results.

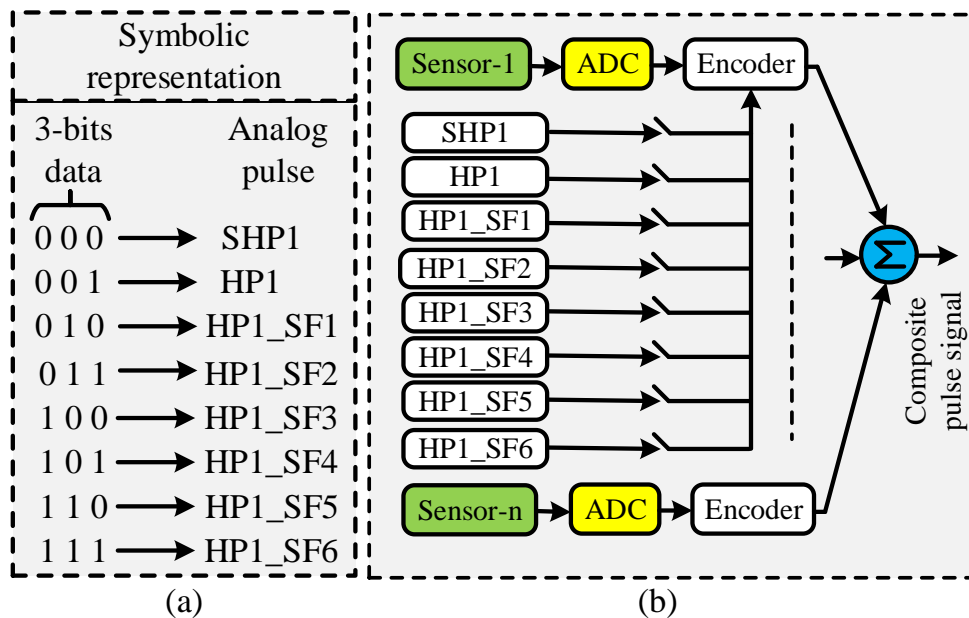


**Figure 2.6:** Analog pulse-based encoding using multi-order and their shifted pulses.

### 2.5.2 Pulse Sequence Based Data Channel Encoding

The novel PS-based data channel encoding uses a set of AOPs, where each PS represents a single data bit. The multi-order AOPs and their time-shifted pulses are used to generate the distinct PSs. PS-based encoding is another important contribution of this dissertation work for high-volume data compression. The PS-based data compression technique offers high-volume data monitoring and assessment to expand high-speed wireless telemetry. A PS encodes the digital data bits in time domain analogy with considering time shifting property of the orthogonal pulses. The distinct PSs are generated by considering the permutation-combination of the pulse positions in a sequence. The permutation of four different order pulses creates 24 distinct PSs. Table 2.3 shows the distinct PSs where individual PS offers the respected data channel.

**Table 2.3:** PS generation and channel encoding template for 4-pulse systems.

Seq. #	TS1	TS2	TS3	TS4	Cha. #
1	MHP <sub>0</sub>	MHP <sub>1</sub>	MHP <sub>2</sub>	MHP <sub>3</sub>	1
2	MHP <sub>0</sub>	MHP <sub>1</sub>	MHP <sub>3</sub>	MHP <sub>2</sub>	2
3	MHP <sub>0</sub>	MHP <sub>2</sub>	MHP <sub>1</sub>	MHP <sub>3</sub>	3
4	MHP <sub>0</sub>	MHP <sub>2</sub>	MHP <sub>3</sub>	MHP <sub>1</sub>	4
5	MHP <sub>0</sub>	MHP <sub>3</sub>	MHP <sub>1</sub>	MHP <sub>2</sub>	5
6	MHP <sub>0</sub>	MHP <sub>3</sub>	MHP <sub>2</sub>	MHP <sub>1</sub>	6
7	MHP <sub>1</sub>	MHP <sub>0</sub>	MHP <sub>2</sub>	MHP <sub>3</sub>	7
8	MHP <sub>1</sub>	MHP <sub>0</sub>	MHP <sub>3</sub>	MHP <sub>2</sub>	8
9	MHP <sub>1</sub>	MHP <sub>2</sub>	MHP <sub>0</sub>	MHP <sub>3</sub>	9
10	MHP <sub>1</sub>	MHP <sub>2</sub>	MHP <sub>3</sub>	MHP <sub>0</sub>	10
11	MHP <sub>1</sub>	MHP <sub>3</sub>	MHP <sub>0</sub>	MHP <sub>2</sub>	11
12	MHP <sub>1</sub>	MHP <sub>3</sub>	MHP <sub>2</sub>	MHP <sub>0</sub>	12
13	MHP <sub>2</sub>	MHP <sub>0</sub>	MHP <sub>1</sub>	MHP <sub>3</sub>	13
14	MHP <sub>2</sub>	MHP <sub>0</sub>	MHP <sub>3</sub>	MHP <sub>1</sub>	14
15	MHP <sub>2</sub>	MHP <sub>1</sub>	MHP <sub>0</sub>	MHP <sub>3</sub>	15
16	MHP <sub>2</sub>	MHP <sub>1</sub>	MHP <sub>3</sub>	MHP <sub>0</sub>	16
17	MHP <sub>2</sub>	MHP <sub>3</sub>	MHP <sub>1</sub>	MHP <sub>0</sub>	17
18	MHP <sub>2</sub>	MHP <sub>3</sub>	MHP <sub>0</sub>	MHP <sub>1</sub>	18
19	MHP <sub>3</sub>	MHP <sub>0</sub>	MHP <sub>1</sub>	MHP <sub>2</sub>	19
20	MHP <sub>3</sub>	MHP <sub>0</sub>	MHP <sub>2</sub>	MHP <sub>1</sub>	20
21	MHP <sub>3</sub>	MHP <sub>1</sub>	MHP <sub>0</sub>	MHP <sub>2</sub>	21



22	MHP <sub>3</sub>	MHP <sub>1</sub>	MHP <sub>2</sub>	MHP <sub>0</sub>	22
23	MHP <sub>3</sub>	MHP <sub>2</sub>	MHP <sub>0</sub>	MHP <sub>1</sub>	23
24	MHP <sub>3</sub>	MHP <sub>2</sub>	MHP <sub>1</sub>	MHP <sub>0</sub>	24

The permutation of  $n$ -distinct order AOPs and their shifted pulses are applied to generate the  $n!$  PSs. The time-shifted pulses also create another 24 PSs for 4-distinct orthogonal pulses. In this proposed scheme, each PS indicates a particular data channel to represent the digital bit stream. The analog pulse has the orthogonality property that coexists in a specific time slot, sharing the same bandwidth of each data channel. If superimposed all 24 PSs with their corresponding time slots to compress the data volume to create a unified composite pulse (UCP) before transmitting through the transmitting antenna. The UCP occupies a 4-time slot (TS) compared to a single TS in a conventional system. This data compression takes place without any sophisticated signal processing.

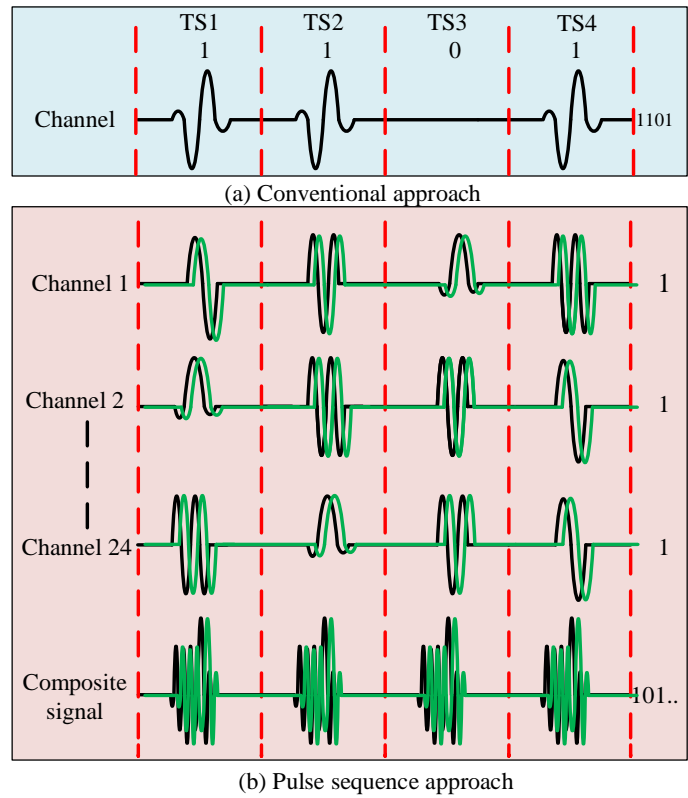


**Figure 2.7:** Data compression in PS-based encoding using original and shifted AOPs.

Fig. 2.7 shows the concept of the PS-based data encoding template using distinct PSs, where the presence of a PS indicates data bits and vice versa. Fig. 2.8(a) represents the conventional single pulse-based encoding, and (b) shows the PS-based scheme where the black and green trace depicts the PSs for original and shifted AOPs, respectively. Their corresponding UCP signal presents the compressed data volume. The PS encoding directly increases the data transmission rate by supporting a large volume of data. The proposed PS scheme improves  $(n-1)!$  times more data by supporting  $n!$  number of distinct channels for the  $n$ -Hermite pulse system. Similarly, the 25% time-shifted pulses of multi-order AOP signal also create another  $n!$  of PSs. Therefore, the  $n$ -distinct pulses and their time-shifted pulses create  $2n!$  PSs to support  $2n!$ -numbers of channels with  $2n!/(n+1)$  times data rate improvement. **Chapter 4 describes** the PS-based data encoding and decoding architecture, data compression and decompression algorithm, simply the missing channel finding by generating OPS, and preliminary simulation results to validate the theoretical concept.

## 2.6 Conclusion

This chapter presents a compact summary of AOP-based short-range wireless telemetry. A simplified and power-efficient AOP set generation model is described in detail by analyzing the signal properties. The modified Hermite polynomial comprises two partial differential equations compared to other Hermite polynomials and is implemented easily by MATLAB® Simulink to generate AOPs. The multi-order AOPs transmits high-volume data, either a single pulse or a sequence of pulses by utilizing the signal orthogonality. The various time shift factors are also considered and analyzed to remove the difficulties and complexities of higher-order pulse generation.

## CHAPTER 3

### ANALOG PULSE BASED MULTI-BIT DATA TELEMETRY

#### 3.1 Introduction

Indoor wireless data telemetry has become popular with the increasing of IoT devices deployment and communication technology. The analog pulse-based telemetry improves the transmission rate with high-volume data compression. It uses the pulse symbol, position, amplitude, time interval, etc., to carry the information bits. This chapter presents a novel analog pulse-based telemetry to transmit multi-bit data by PI encoding for wireless transmission. The proposed PI based data encoding supports the SE wireless telemetry, where a single order AOP signal represents  $k$ -bit data. The different PI represents the binary combinations of  $k$ -bit data. The PI encoding scheme encodes data-bit and transmits symbolically through channel media. It also randomized the template of PIs after a specific time interval,  $T_h$ , to add the security level. Therefore, the PI randomization technique increases data volume with an extra low-level physical layer security. The rest of this chapter describes the pulse index randomization (PIR), transceiver architecture, security analysis, improvements, and preliminary simulation results for multi-bit encoding.

#### 3.2 Pulse Index Encoding for Multi-Bit Data Telemetry

Fig. 3.1 shows the schematic diagram of the pulse-based wireless transceiver. It has two main components, the RF transmitter and the RF receiver. The transmitter encodes the

digital bitstream symbolically using a set of pulses and transmits via an RF antenna. The matching receiver receives the transmitted pulse pattern and decodes the transmitted data bits. The multi-order AOP set is generated using the pulse generator described in previous chapter and stored in flash memory for further signal processing.

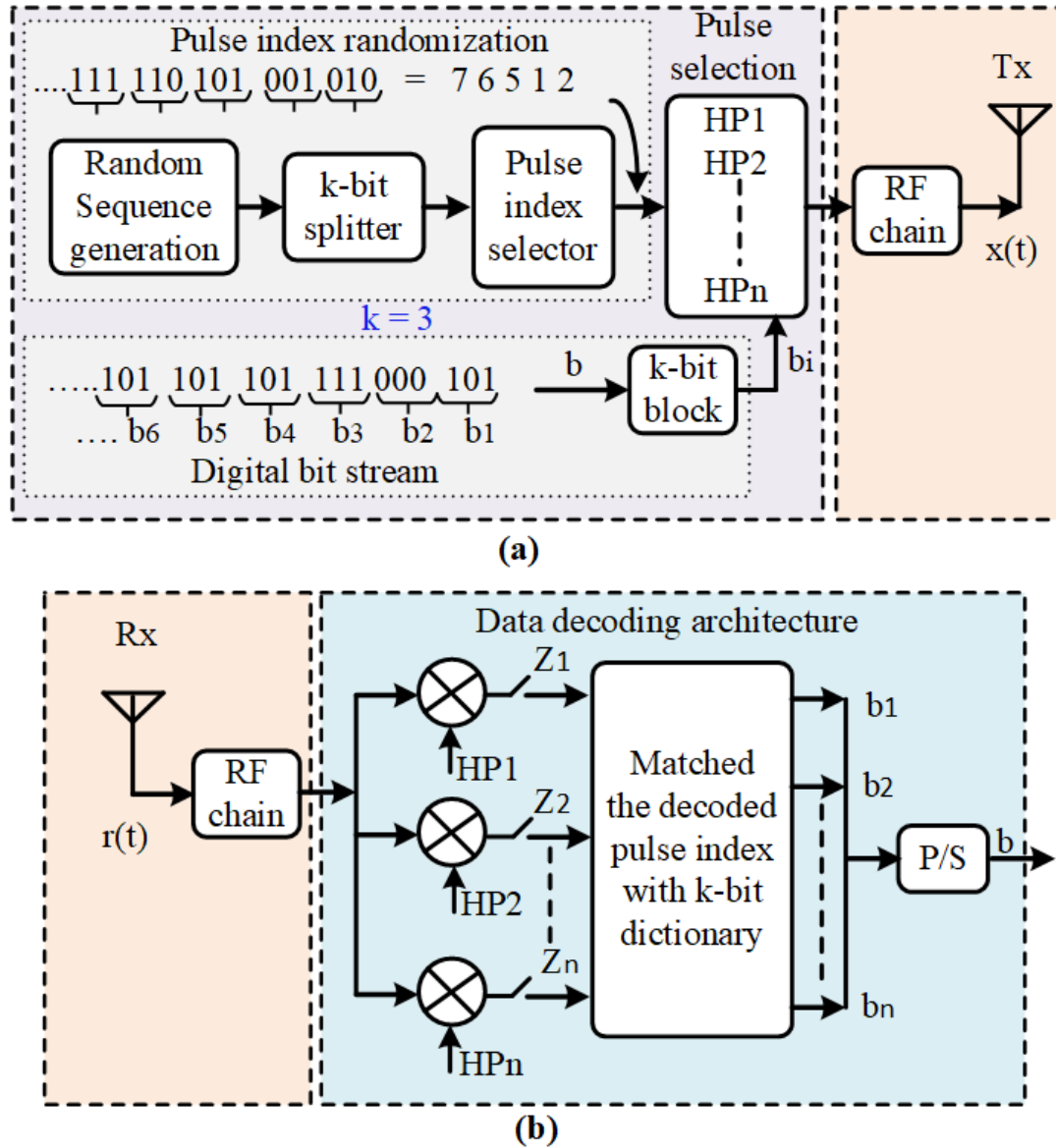


**Figure 3.1:** Transceiver block diagram of PI encoding (a) Transmitter (b) Receiver.

The generated multi-order analog pulse information is stored in the transmitter memory chip to implement the data encoding algorithm. A  $2^k * k$  bits random number is also

generated by the memory-based random number generator and divided by a  $k$ -bit splitter, where each  $k$ -bit random number represents the PI of the distinct AOP signal. The incoming data bits are divided into small  $k$ -bit sub-blocks and encoded by a single-order AOP signal among  $2^k$  pulses according to the template, where  $k$  is a non-zero integer number. The pulse selector determines the memory storage pulse indices representing the  $k$ -bit data symbolically. The data-encoded pulse train is then passed through the RF chain for carrier multiplication and amplification before transmitting via an RF transmitter. The Rx antenna sequentially collects the transmitted pulse pattern and passes through the RF chain again to increase the signal strength and frequency down-conversion. Then, it sends to the  $n$ -branch-matched filtering blocks to correlate with the memory storage template signal. If the received pulse signal matches the template pulse, it prints the index number. Finally, the pulse-decoded index is converted to the binary data bits using the prior known template.

### 3.3 Architecture of Proposed Pulse Index Encoding

The main goal of this section is to design and implement  $k$ -bit encoding with data security using the AOP-based packet-less communication paradigm. The proposed method also leverages the data density by supporting multi-bit data using distinct order AOP signals. A data unit protocol is constructed using different analog pulses whose index number is modulated based on the randomization template. This type of data encoding removes the pulse signal's periodicity by changing the PI randomly after,  $T_h$  sec interval to prevent the data-coded pulse positions from the hackers. The combination of  $k$ -bit encoding and the randomization technique has the potential to provide SE architecture for resource-constraint IoT devices. Fig. 3.2(a) shows the architecture of the proposed PI encoding using

the serial-serial data transmission by AOP signal of width,  $T_s \mu s$ . The baseline of the PI encoding contains a start pulse, i.e., sync pulse with a time window,  $T_p$ , at the beginning of the transmitted pulse train to identify the starting point of  $k$ -bit data. The time gap between two identical sync pulses represents the transmitted data bits. Figs. 3.2(b) and (c) illustrate the conventional single-pulse system where each pulse carries single-bit data and the proposed PI encoding. The OOK techniques are used to encode a single bit by a single-order pulse in the conventional system. On the other hand, the proposed scheme encodes  $k$ -bit data by single order pulse and requires  $2^k$  different numbers of orthogonal pulses.

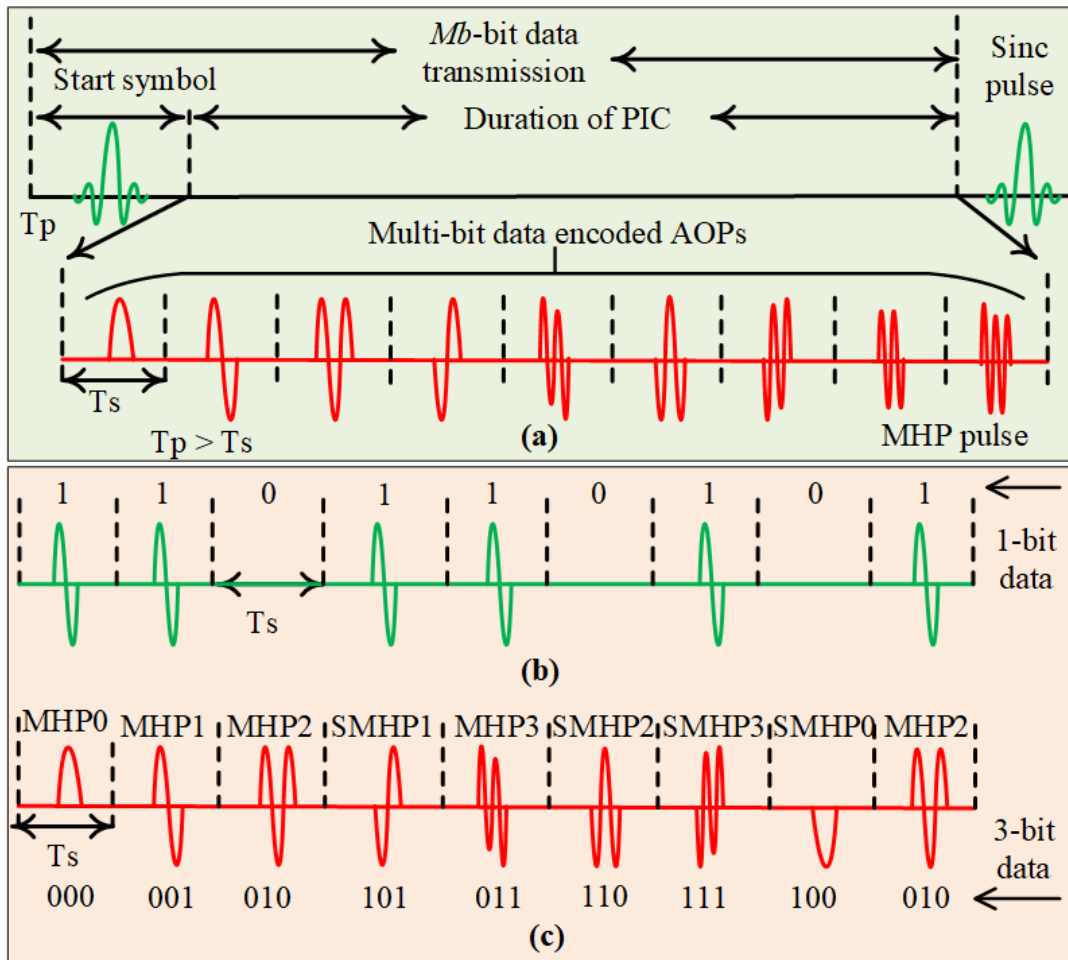


**Figure 3.2:** Data modulation (a) PI encoding architecture, (b) conventional single pulse system, and (c)  $k$ -bit encoding (here,  $k = 3$ ).

The pulse symbol  $MHP_0$  to  $MHP_3$  depicts the zero to third-order pulse signal with a constant time window of  $\delta = T_s$ . Typically,  $\delta$  is in nano/pico sec for high-speed data transmission. In resource-constraint wireless telemetry, power saving is another crucial factors for transmitting a large amount of time-series data. The compression technique reduces the transmission energy by compressing a large volume of data bits. The proposed scheme is a direct method to compress high-volume data symbolically. It is also an efficient approach for saving the computing power and time by AOP-based data compression. In addition, it reduces the data size by  $k$ -bit using a single pulse. It allows the transmission of data with a very low-energy budget in terms of few pulses compared to the conventional compression technique. The total number of pulses,  $N_P = 2^k$ , depends on the value of  $k$ -bit encoding. The data encoding algorithm is given in Appendix C, **algorithm C1**. It involves several steps. These steps are described in chronological order as below-

**Step 1:** Divide the information bitstream into a small groups with an equal size based on the length of the transmitted data frame. The data length is ‘n’ times of  $M_b$ -bit, where ‘n’ is an integer number and  $M_b = k\text{-bit} \times N_P$  bits.

**Step 2:** Perform the data encoding scheme according to the  $k$ -bit dictionary for each small series of binary data bits where the index number represents  $k$ -bit data.

**Step 3:** For each group of data bits, the pulse-encoded information is transmitted sequentially from the memory storage analog pulses according to the index number.

**Step 4:** Add an indicator pulse at the front of encoded pulses to identify a starting point.

**Step 5:** For multi-user applications, a single order pulse and their time-shifted (20% to 70%) pulses will encode each group of  $M_b$  bits data (Repeat steps 1 to 4).

### 3.4 Pulse Index Randomization Techniques

An attacker always tries to search the existing vulnerabilities at different layers of the communication networks. They attempt to access and manipulate the secret information transmitted through wireless media. Suppose the hacker gets access to the transmitting information. In that case, they can manipulate the bits by changing the intrinsic signal characteristics, i.e., the pulse shape, amplitude, or time interval of the arriving signal. The pulse randomization technique prevents physical attacks that require the attacker to know the shape of the pulses. The pulse randomization technique randomized the data-encoded PI using the customized Fisher-Yates shuffles algorithm with a random key  $K_i$ . To encode  $M_b$  bits of data, the required number of analog pulses is  $N_P$ , including the original and time-shifted pulses. The sequence of the randomized PI depends on the random key,  $K_i$ . The same algorithm is also required to retrieve the transmitted bitstream at the receiver end.

Initial pulse index			Index randomization at ' $T_h$ ' Sec.			Index randomization at ' $n*T_h$ ' Sec.					
Index	AOP set	3-bit data	Index	AOP set	3-bit data	Index	AOP set	3-bit data			
1	MHP0	0 0 0	1	SMHP0	0 0 0	1	MHP3	0 0 0			
2	MHP1	0 0 1	2	MHP2	0 0 1	2	SMHP1	0 0 1			
3	MHP2	0 1 0	3	SMHP3	0 1 0	3	MHP0	0 1 0			
4	MHP3	0 1 1	4	MHP1	0 1 1	4	SMHP0	0 1 1			
5	SMHP0	1 0 0	5	MHP3	1 0 0	5	MHP1	1 0 0			
6	SMHP1	1 0 1	6	SMHP2	1 0 1	6	SMHP2	1 0 1			
7	SMHP2	1 1 0	7	MHP0	1 1 0	7	MHP2	1 1 0			
8	SMHP3	1 1 1	8	SMHP1	1 1 1	8	SMHP3	1 1 1			
(i)			(ii)			.....			(n)		

**Figure 3.3:** Index randomization architecture (i) initial pulse dictionary, (ii) index randomization at  $T_h$  sec., and (n) randomization dictionary at  $n*T_h$  sec.

Fig. 3.3 shows the PI randomization based  $k$ -bit encoding architecture. In the proposed encoding the PI number changes randomly after time,  $T_h$  sec and encodes the information bits according to the  $k$ -bit dictionary. The same PI doesn't always indicate the



same  $k$ -bit data. Let us assume, the index number 3 for MHP<sub>2</sub> signal represents ‘010’ bits and transmits symbolically in the first  $T_h$  sec (Fig. 3.3 (i)). After  $T_h$  sec, the pulse randomization changed the index number randomly. Assume, the new index number is 9 for MHP<sub>2</sub> which represents now ‘100’ instead of ‘010’ bits (Fig. 3.3(ii)). Similarly, the PI of all the distinct  $N_P$  pulses change randomly and encodes the bitstream by a new template. Since the random key changes periodically and the index number of the distinct pulses also varies that creates a pulse blinding to third parties. Therefore, the proposed PIR technique maintains data privacy and keeps it hidden from an adversary for secure data transmission.

### **3.5 Security Analysis**

The proposed PI encoding scheme encodes the binary combination of  $k$ -bit data. The distinct order AOPs are used to distinguish the binary combinations of the  $k$ -bit data. The proposed method increased the security level by adding the randomness of the data-encoded PI. This section describes the data security enhancement by PI encoding based on the analysis of the threat model and index randomization technique.

#### ***3.5.1 Threat Model***

Let us assume a scenario where the sensor node transmits data bits to a local server. The sensor node and the local server have a shared secret and access to commonly used network standards and protocols. The hacker's primary aim is to hack the communication channel and breach data privacy. S/he has different intentions to perform security breaches, such as obtaining channel access, manipulating the source information, stealing data, and diverting the transmission channels. This work considers the man-in-the-middle attack threat model to explain secure data communication. It assumes that the attacker always

tries to intercept and read the transmitted message, not manipulate it. They also know the pulse set generation scheme,  $k$ -bit encoding using analog pulses, and random number generation techniques. The hacker is also familiar with decoding the message information from the symbolical representation of the transmitted pulses. They doesn't know the exact random pulse pattern, and will use a brute-force approach to decode the transmitted data.

**Table 3.1:** Average time required for exhaustive key searching.

Number of bits, $k$	Number of pulse, $N_p = 2^k$	Number of possible combinations, $N = N_p!$	Time required for 1.9 GHz processor, decode/sec	Time required for 2.9 GHz processor, decode/sec
2	4	24	$6.31 \times 10^{-9}$	$4.13 \times 10^{-9}$
3	8	$4.03 \times 10^4$	$10.60 \times 10^{-6}$	$6.91 \times 10^{-6}$
4	16	$2.09 \times 10^{13}$	3.81 hours	2.50 hours
5	32	$2.63 \times 10^{15}$	$2.19 \times 10^{18}$ years	$2.43 \times 10^{15}$ years

### 3.5.2 Exhaustive Key-searching

The pulse randomization technique can prevent physical attacks using narrow pulse signal. The cryptographic pulse blinding technique requires the attacker to know the physical characteristics of the pulses if the attacker gets access to the pulse-based transmitting information. However, by randomizing the PI, the attacker does not know which pulse belongs to which  $k$ -bit data. Table 3.1 represents the scenario of the proposed scheme based on the information about the average time required for an exhaustive key search. The total number of combinations of  $N_p$  pulse is  $N_p!$ . The more significant value of  $N_p$  shows better data security based on the average time required for an exhaustive key search. The expected number of trials is half the total number to get the correct combination. The time needed to crack the key also depends on the speed of the attacker's computer. It shows that eight or sixteen distinct pulses are required to encode 3-bit or 4-bit data. The 4-bit encoding has  $2.09 \times 10^{13}$  possible combinations of the pulses. The time of

re-randomizing should select the pulse encoding template considering the attacker's 1.9 GHz processor computer at  $T_h \geq 3.81$  ~hours and  $T_h \geq 2.50$  ~hours for the 2.9 GHz processor. If 32 pulses are used to map 5-bit data, then it would require about  $2.09 \times 10^{18}$  and  $1.43 \times 10^{15}$  years, respectively which are virtually impossible. The higher-bit encoding creates more randomness that requires a large amount of time to decode the information bits by brute-force methods. But, the onboard memory storage of IoT devices limits the number of higher bit encoding using the PI techniques. The threshold level of pulse randomization time,  $T_h$  sec should update according to Table 3.1 to ensure security. The new random number generates every  $T_h$  sec, which creates the randomness of the pulses and ambiguity for the hacker. Since the random key changes periodically and the index number of distinct pulses also varies that creates a pulse blinding to third parties.

### ***3.5.3 Time Interval and Amplitude***

The data security is also analyzed based on the pulse arrival time interval and amplitude variation. The attacker can also try to manipulate the pulse amplitude and the arrival time in the receiver to manipulate the transmitted bit information. Typically, time-of-flight (ToF)-based ranging systems rely on satisfactory time resolution to estimate distance correctly [70]. Typically, the Cicada attack exploits the search algorithm that uses ToF systems to detect the peak amplitude of the pulse and find the leading pulse edge [70]. The extended pulse systems are also inherently vulnerable to early detection and late commit (ED/LC) attacks [71]. The analog pulse-based data communication can be susceptible, like distance ranging by Cicada and ED/LC attack. In this attack, the attacker's primary goal is to inject extra pulses between the encoded pulse trains to manipulate the transmitted bit stream. When the receiver receives a misleading pulse, it generates wrong

information. This type of attack can minimize by generating a short symbol, usually a narrow-width pulse in *ns* or *ps*. It has developed a system to process short symbols by allocating energy within a time frame [72]. Therefore, a narrow-width pulse can be considered secure against such attacks because the next pulse will appear before calculating the time interval, and the attacker cannot mislead the pulses by adding an extra pulse.

In this chapter, a  $\mu\text{s}$  width analog pulse signal is used by considering the trade-off between the hardware limitations and facilities for demonstration by developing a prototype test platform in research lab environment; however, the pulse generator can also generate the *ns* pulse signal. The narrow width analog pulse reordering is a new technique that enhances the extended mode of IEEE 82.15.4f with cryptographic operations at the pulse level to prevent physical layer attacks, including the ED/LC [73]. Since a successful ED/LC attack is based on the attacker knowing the pulse shape, time interval, and the starts and ends point. Therefore, the PIR prevents these types of attack by blinding positions. It creates the ambiguity and they doesn't know which pulse belongs to which  $k$ -bits.

### 3.6 Simulation Results

In this section, the performance of the PI based  $k$ -bit encoding algorithm is verified using the MATLAB<sup>®</sup> simulation. The pulse error rate (PER) and the BER are evaluated using different set of digital bitstream and pulse numbers with varying the signal-to-noise (SNR) level from -5.0 dB to +15.0 dB to evaluate the performance of data encoding. MATLAB<sup>®</sup> built in additive white Gaussian noise (AWGN) model is used to represents the channel noise in computer simulation. In simulations, the SNR defines the ratio of energy per symbol to noise power. Fig. 3.4(a) shows the PER for 10  $k$ , 100  $k$ , and 1000  $k$

pulse transmission and reception with AWGN channel model. The simulation results show that, the PER increases by increasing the number of pulse transmission. It makes change because the error rate is related to the number of pulses.

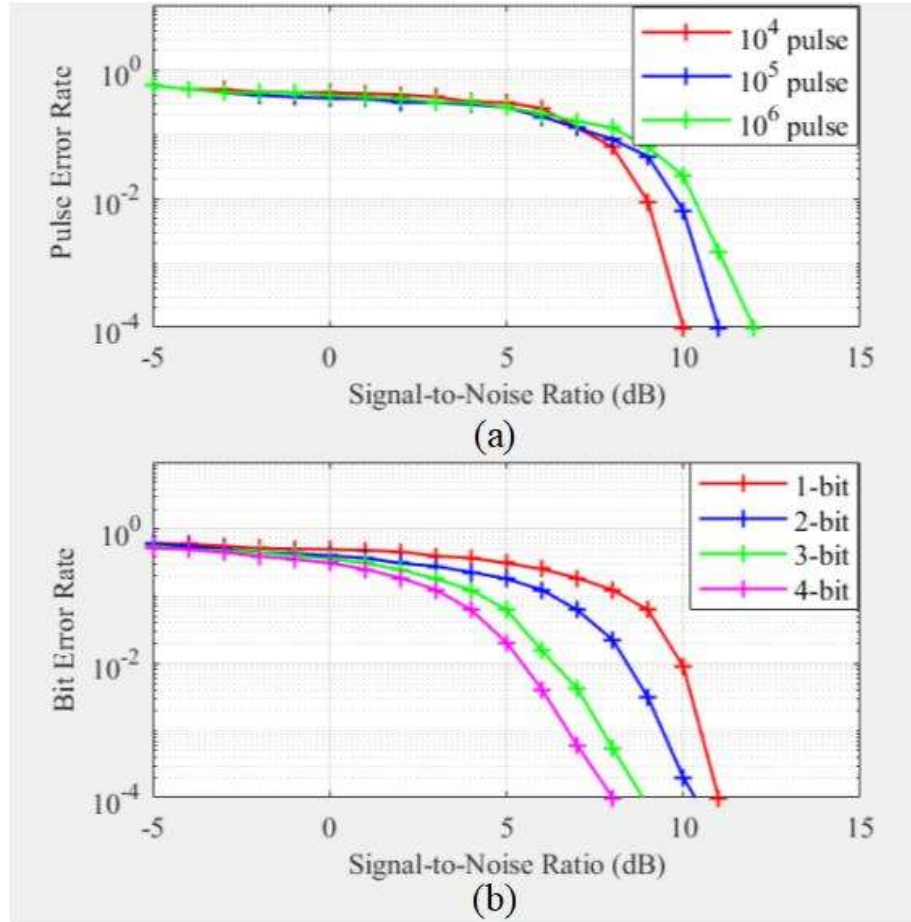


**Figure 3.4:** Simulation results of error vs. SNR at different (a) number of pulse transmission and (b) k-bit encoding for proposed PI encoding.

Similarly, the BER is also investigated to evaluate the performance of the proposed scheme. Fig. 3.4(b) shows the BER for different bit-level encoding by a single order AOP. This dissertation work has performed the computer simulation for 1-bit, 2-bit, 3-bit, and 4-bit encoding to investigate the effect of error rate with increasing the transmitted  $k$ -bits carried by a single pulse. The BER decreases with increasing the number of bits transmitted by single order analog pulse, like the M-ary PPM technique [60]. In M-ary PPM, the

theoretical relationship between the BER and the SNR is vice versa, and the BER is lower for higher numbers of M results [60]. In PI encoding, the BER also decreases by increasing the number of bits. It shows the BER is  $1 \times 10^{-4}$  around 11.0 dB SNR for 1-bit encoding and it reduces with increasing the bit/pulse.

### **3.7 Significant Improvements of the Pulse Index Encoding**

This section describes the meaningful improvement of the proposed PI encoding in terms of architectural simplicity, level of data compression and latency time improvement compared to the Huffman coding, and data rate improvement. The performance of the proposed encoding has also compared with the existing PI encoding using AOPs. The following subsections describe the performance improvements of PI encoding technique.

#### ***3.7.1 Architectural Simplicity***

The proposed PI encoding architecture differs from the existing scheme [42], where the multi-bit data is modulated by using two distinct order HG pulses along with the M-ary mapper to create the signal orthogonality. At first, the incoming information bits have divided into two sub-blocks. The HG pulses have encoded the first two bits by selecting the indices based on the look-up table [42], and BPSK methods modulated the last two bits. Finally, the data encoded pulse has multiplied by the output of the M-ary mapper and superimposed by time-domain summation. The composite HG pulse shows the multi-bit data within a single time window. It requires two different receiver models, i.e., Matched filter and maximum likelihood detection that increases the computational time and memory to recover the transmitted bits. On the other hand, this chapter presents a less complex and straightforward way to encode the same number of data bits using a single-order analog pulse. The proposed encoding also simplifies the transmitter architecture by carrying  $k$ -bit

data using a set of memory-based AOPs. It also minimizes the computational power by correlator-based decoding at the receiver end to recover the transmitted bit information.

### ***3.7.2 Level of Data Compression Improvement***

At the sensor node, the data transmission is the energy-saving source for high-volume wireless telemetry. Several research efforts have already done to reduce the data transmission energy using different compression techniques. The lossless data compression can reproduce precisely the original transmitted data information by the decompression process. On the other hand, the lossy data compression can't produce the exact transmitted information. Most works focus on lossless data compression with higher precision for high-accuracy applications. The PI randomization scheme encodes the binary bitstream, where each pulse represents  $k$ -bit data. Therefore, the PI encoding directly compresses the data volume by supporting  $2^{k*k}$  bits using  $2^k$  pulses. Table 3.2 represents the data compression and time latency improvement compared to the conventional Huffman scheme.

Table 3.2 shows that, the Huffman coding compressed the  $3 \times 10^6$  bits binary data to 26,11,529 bits in 0.5537 sec, while the  $k$ -bit ( $k=3$ ) encoding reduces the data volume by 2.61 times and needs a less amount of time 5.56 times lower than Huffman coding. The compression ratio has improved by 3.90, and 2.85 times for  $k = 4$  bits encoding, respectively. At  $k = 4$ , the ratio of time elapsed to compress the 4-bit data is lower than the 3-bit but higher than the Huffman coding. It is understandable that with increasing  $k$ , the requirements of total number of pulses increase as  $2^k$  and needs a higher processing time than lower bit encoding. However, the proposed scheme increased the data compression ratio and latency compared to the Huffman coding. The trade-off between compression and the number of pulse requirements may consider by selecting the value of  $k$ .

**Table 3.2:** Data compression and latency improvement compared to Huffman coding.

k-bit	Data volume (bits)	Compressed data Huffman	Compressed data k-bit	Ratio	Elapsed time (s) Huffman	Elapsed time (s) k-bit	Ratio
3-bit	3000000	2611529	1000000	2.61	0.553793	0.099545	5.56
4-bit	4000000	3906403	1000000	3.90	0.582006	0.204550	2.85

### 3.7.3 Data Transmission Rate Improvement

Throughput is one of the most critical requirements to estimate the quality of service in IoT networks. Typically, the communication capacity is limited by the low hardware specifications of the sensor nodes. The IoT devices are incompatible with the 5G technology for high-speed and large-volume, secure data transmission. Literature review shows it has published most of the research articles on EE scheme only and a few papers focused on data rate improvement by adopting compression techniques wireless communications [61-62]. The proposed PI encoding improves the transmission speed directly by compressing data volume without creating computational complexity. It encodes multiple data by a distinct pulse symbol and increases the transmission rate by  $k$ -times compared to the conventional single-bit system.

### 3.7.4 Data Accuracy Comparison

The proposed PI scheme's data accuracy also has compared with the Huffman coding in terms of BER investigation. Fig. 3.5 shows the data accuracy comparison between the proposed  $k$ -bit encoding and Huffman coding in terms of BER. In this experiment, the PI encoding compressed  $3 \times 10^6$  bits of binary data to  $1 \times 10^6$  bits using  $k = 3$ -bit encoding. Then the compressed bitstream is encoded by multi-order AOPs according to the pulse encoding template. The AWGN signal is added with the data encoded pulse train to represents the channel noise. Finally, the correlator-based receiver algorithm



decodes the transmitted pulses and converts them to binary bitstream using a prior known encoding template to find the missing bits. The BER is checked by comparing the transmitting and receiving bitstream with varying the SNR.

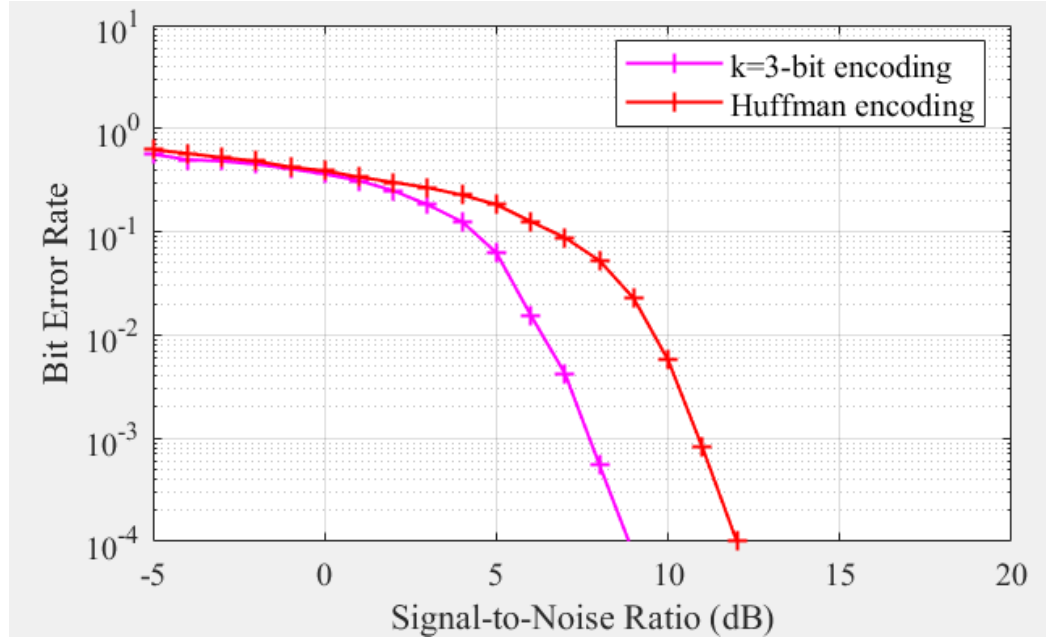


**Figure 3.5:** Comparison between the k-bit encoding and Huffman coding in terms of BER investigation.

On the other hand, the Huffman coding compressed the  $3 \times 10^6$  bits binary data corresponding to  $1 \times 10^6$  symbols (0 to 7) to 26,11,529 bits binary data. Then a single order analog pulse is used to encode the binary bitstream using the BPSK method. Similarly, the AWGN signal is added with the data encoded pulse train and applied the correlator-based decoding to decode the transmitting pulse train. Finally, convert the analog pulses to bitstream and find the missing data bits by checking the BER. The BER plot shows that the PI encoding has better data accuracy than the Huffman coding because of transmitting less number of pulses. Understandably, Huffman coding requires more pulse transmissions to transmit the same amount of data volume compared to the proposed scheme. The higher number of pulse transmissions increases BER than the lower pulse transmissions.

### 3.8 Conclusion

This chapter explores an innovative PI encoding architecture in the time domain for high-volume sensor data transmission in IoT networks. The multi-bit encoding is presented with the pulse randomization technique to add extra physical layer security at the transmitter. The correlation peak-based pulse detector is also used to simplify the decoding scheme in the receiver. Simulation results show that the proposed encoding improved the data compression ratio and time latency by 2.61-times and 5.56-times, respectively, compared to the standard Huffman coding. The AOP-based PI encoding supports  $2^k * k$  bits data by  $2^k$  different pulses and ensures low-level physical layer security, where  $k$  is a non-negative integer number. The proposed scheme provides low-power, cost-effective, and scalable data telemetry by changing the  $k$  value. Pulse randomization technique adds low-level security for reliable transmission in resource constraint IoT applications.

## CHAPTER 4

### PULSE SEQUENCE BASED ENCODING AND DATA COMPRESSION

#### 4.1 Introduction

The connected devices are increasing exponentially with the inception of IoT devices in WSNs. The high-speed, reliable data transmission supports numerous devices and it is crucial for the rapid growth of IoT networks. High-volume data compression is one of the keys to support more data within the existing capacity in high-density WSNs. The narrow-width orthogonal pulse signal can transmit data information symbolically for short-range SE IoT applications. It also has the data compression capability by carrying multiple bits using single-order AOP. However, the number of data channels limit the single pulse-based technology to support high-density IoT networks. This chapter presents an innovative encoding using a sequence of pulses to support high-volume data by sharing the same frequency spectrum. The PS encoding also compressed the data volume without compression algorithm and supported many channels without overburdening the communication network. The objectives of this chapter are to develop data encoding and decoding, compression and decompression, PS regeneration, and performance evaluation.

#### 4.2 Pulse Sequence Based Data Encoding and Compression

Spectrum sharing telemetry is a demanding issue for high-density IoT networks. The multi-order AOP signal contains the same bandwidth around a  $1 \pm 0.15$  MHz for pulses

of  $2.0 \mu\text{s}$  and coexists in the time domain. Therefore, the orthogonal AOP set can be used for multi-user applications with high-volume data compression. In the PS-based channel encoding, the multi-order AOP signal and its time-shifted pulses are used to create distinct PSs. The distinct PSs indicate individual data channels, and their composite signal represents the compressed data volume of the encoded channels. The PS-based encoding supports SE wireless telemetry. The constant bandwidth and signal orthogonality makes the AOPs suitable for high-density IoT devices sharing the same spectrum with other applications. The following subsections describe the architecture of PS generation, PS-based data encoding, and data volume compression algorithms.

#### ***4.2.1 Pulse-Sequence Generation***

This section describes the architecture of distinct PS generation with algorithm design and development. The PS generation is the central part of the proposed data channel encoding. It is based on the permutation and combination of pulse positions. It is developed by a simple switch matrix algorithm using the memory storage multi-order AOPs. The multi-order AOP set creates distinct PSs for transmitting the sensor data symbolically instead of a single pulse. Fig. 4.1 shows the architecture of different PS generations. The permutation matrix rearranges a number set,  $N$ , by reordering the position in a series. Therefore, the permutation concept is used to create a distinct PS. The total combinations of the number series are  $N!$ , where each permutation number series differs from another and represents an individual data channel.

The proposed PS generation technique creates a particular number of PSs by switching the pulse position in a sequence of pulses without repetition of the pulse order. It generates  $N_p!$ , numbers of distinct PSs for  $N_p$  number of multi-order AOPs. In Fig.4.1,

the first three order AOPs such as  $MHP_0$ ,  $MHP_1$ , and  $MHP_2$ , are used to generate the PSs, where the subscript shows the pulse order. The numerical numbers 1, 2, and 3 represent the PI of the AOPs. In three pulse systems, the permutation series for the PI set are 123, 132, 213, 231, 312, and 321. Therefore, the PS generation algorithm creates  $3!$  or 6-distinct PSs using the switch matrix technique by switching the positions of the PI. Similarly, the four-pulse system creates  $4! = 24$  distinct PSs by permutation of the PI. The proposed PS generation algorithm is given in Appendix C, **algorithm C2**. The generated PSs differ from each other and occupy an equal number of time slots. The unique sensor node is known as a channel and is represented by a dedicated PS.

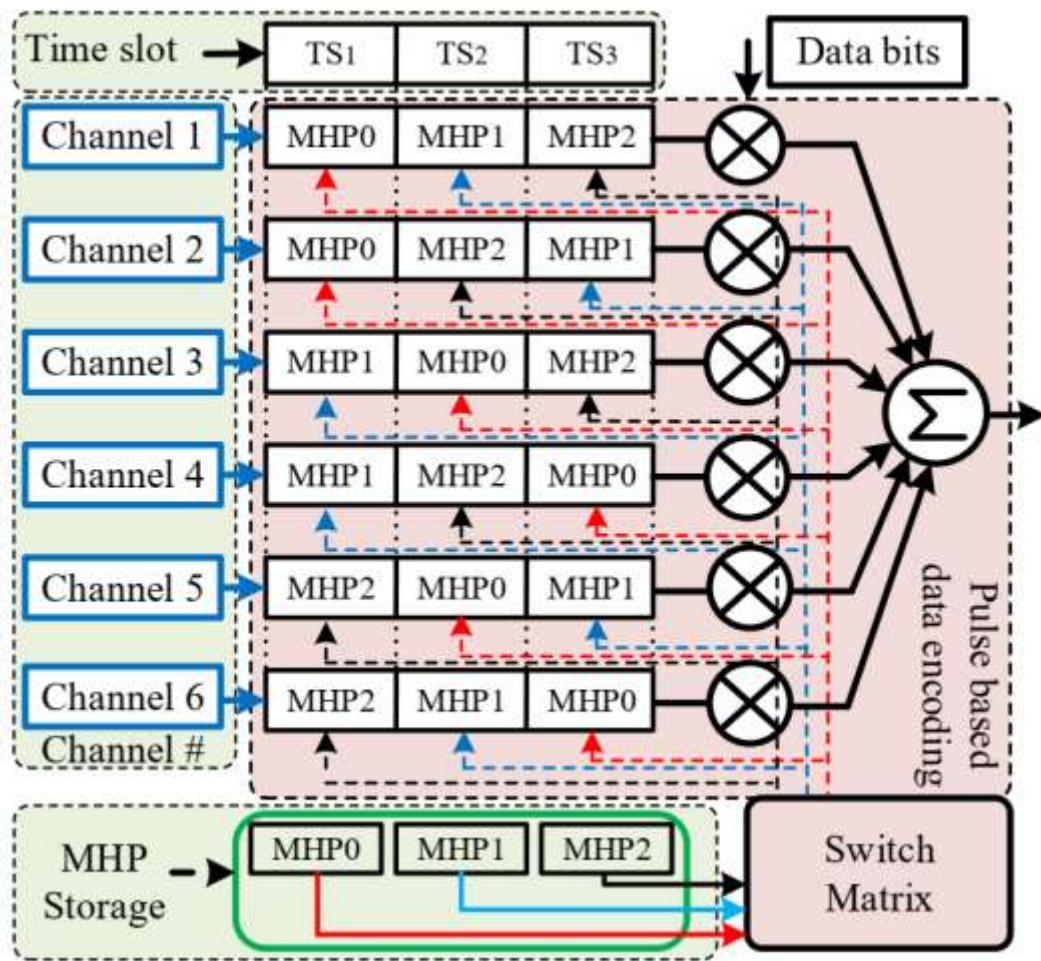


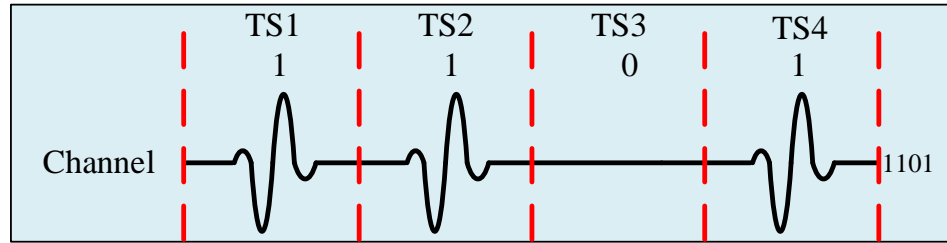
**Figure 4.1:** Distinct PS generation using switch matrix algorithm using AOP set.

#### ***4.2.2 Pulse Sequence Based Channel Encoding***

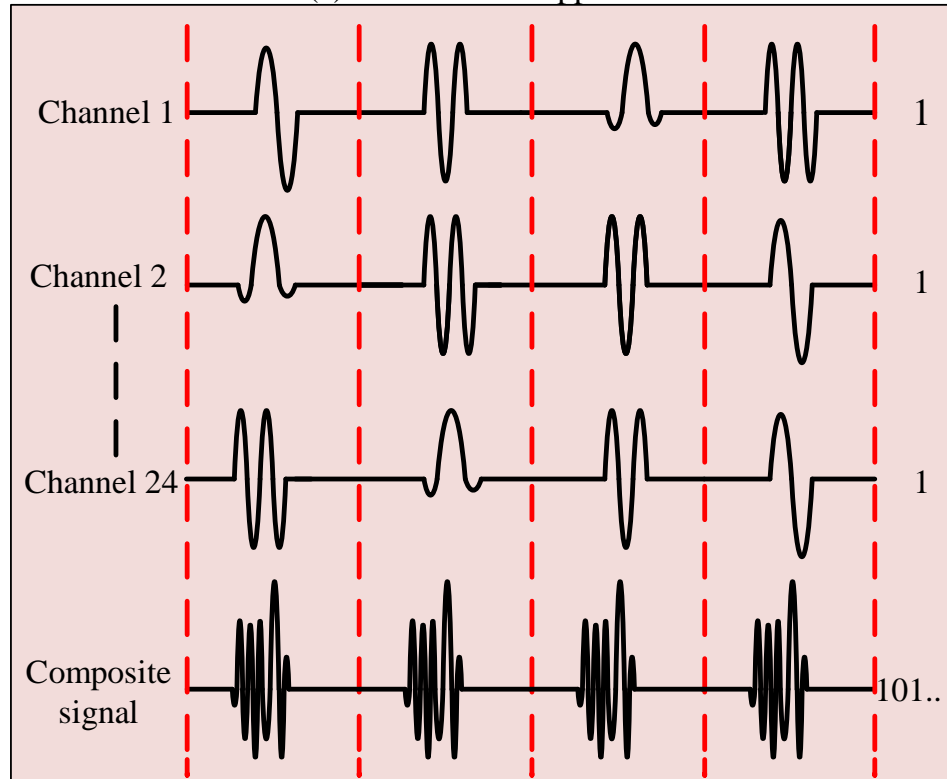
The PS-based channel encoding is an innovative AOP communication idea to support high-density wireless sensor devices. At the sensor hub, the multiple input single output (MISO) transmission technique enables multiple channels represented by distinct PSs as input. It transmits as compressed data volume by a UCP signal. This subsection presents the PS-based encoding for multi-user applications. According to the channel encoding template, a dedicated PS carries the information bit of a specific data channel. Fig. 4.2(a) represents the channel encoding using the standard OOK technique for a single pulse system. The presence of a pulse shows data bit '1' and vice versa. In the single-pulse system, multi-order pulse is used to differentiate the data channels, respectively. On the other hand, the PS scheme encodes individual data channels by a distinct PSs compared to the standard single pulse encoding. The unique PS is assigned to a particular sensor node to encode and transmit the data bits. The PS-based encoding also supports the conventional OOK techniques to share multi-channel data. Fig. 4.2(b) shows the multi-channel encoding using distinct PSs, where the presence of either original or shifted PSs offer bit '1' or '0'.

#### ***4.2.3 Pulse Sequence Based High-Volume Data Compression***

The main benefit of PS-based telemetry is the simultaneous spectrum sharing and supporting high-density data compression within the limited bandwidth. The pulse-based compression technique compressed the sensor data volume without creating computational complexity, sophisticated digital signal processing, or a standard data compression algorithm. Since all the distinct order pulses are orthogonal and coexist in the same time window; therefore, all the data-encoded PSs are superimposed on top of another corresponding to each TS to create the UCP signal.



(a) Conventional approach



(b) Pulse sequence approach

**Figure 4.2:** Data encoding scheme (a) single pulse and (b) PS-based compression.

The UCP signal represents the compressed data volume of the encoded channels. Compared to the single pulse transmission, the PS scheme increases the data volume by supporting more data channels. The four (4) distinct orthogonal pulses can create a total of  $4!$  or 24 different PSs, and the corresponding UCP signal occupy four-TSs compared to a single TS in a conventional single pulse system. However, the UCP signal depicts 24 bits of data instead of 4-bits compared to the single pulse system, thanks to the initial time redundancy in the formation of analog PS for supporting many data bits. The net data rate

improvement with the proposed scheme becomes  $24/4 = 6$  times more than the conventional system. This data compression takes place without using any sophisticated computation. That's why it is also defined as on-the-fly data compression. The proposed scheme initially sacrifices time for getting the ultimate gain of supporting extensive volume data by sharing the same frequency spectrum. The overall data rate improvement is  $(n-1)!$ -times for the  $n$ -pulse system by supporting  $n!$ -numbers of data channels, where  $n$  is a non-negative integer number. Another important benefit is it has transferred the complexity of high-density data telemetry from the transmitter side to the receiver side, enabling easy implementation of wireless transmitters, especially for resource constraint IoT networks.

### **4.3 Cyclic Pulse Elimination Based Data Decompression**

A conventional correlator receiver correlates the receiving pulse signal by a reference to recover the message data. Firstly, the received signal is multiplied by a locally available template waveform with multiple-access code synchronization. The product's output is then passed through an integrator to decode the pulses and convert them to message information. Typically, a coherent RAKE receiver architecture can track the energy associated with multi-path replicas [74]; however, channel estimation is critical for the pulse-based receiver. A suitable channel estimation algorithm is also needed through heuristic approximation to reduce the optimal detection scheme. The reference receiver decreases the channel estimation steps compared to the coherent reception; however, it possesses an inherent architectural complexity for low-cost implementations. It also employed the template waveform in the pulse decoding process comprising delayed replica in a differential receiver that creates the system complexity too.



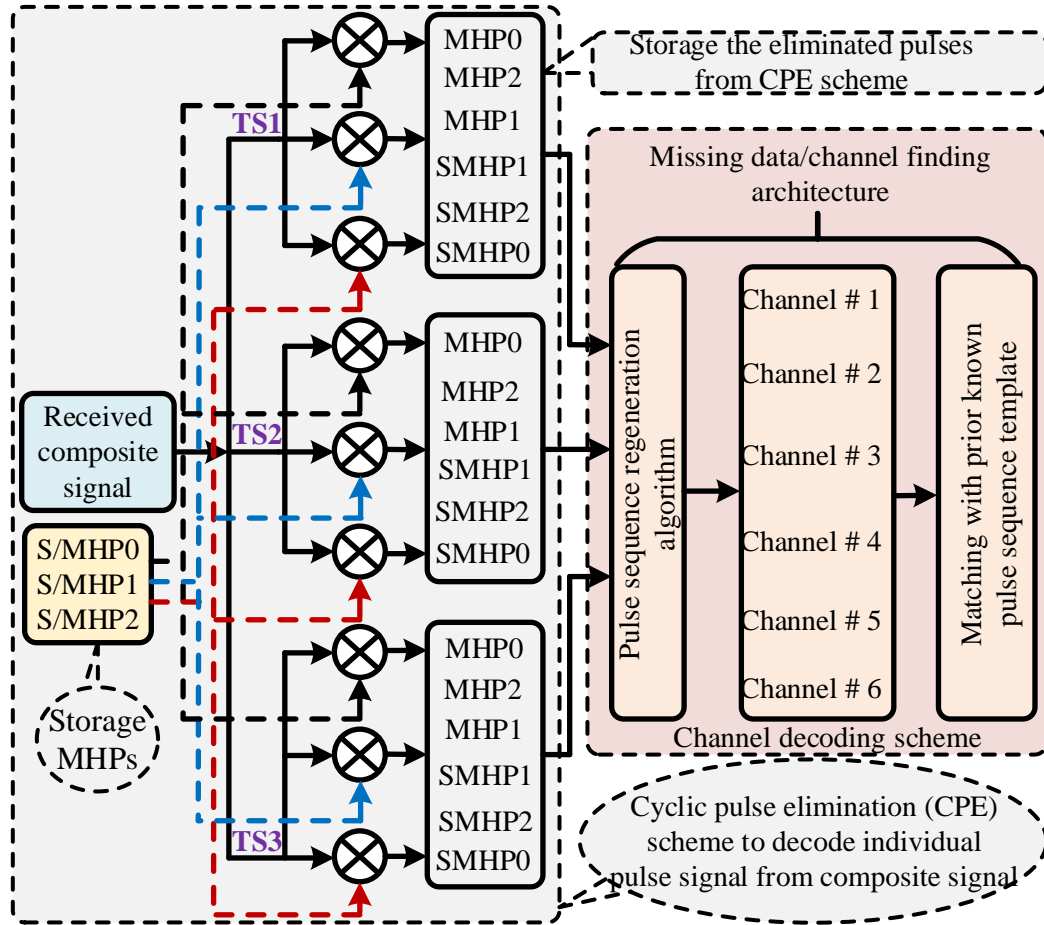


**Figure 4.3:** Data decoding architecture using cyclic pulse elimination algorithm.

This chapter also proposes a new channel decoding algorithm using correlation peak analysis to simplify the existing receiver architecture. Fig. 4.3 shows the correlator-based pulse elimination architecture to decode the transmitted data bits. First, the receiving RF antenna received the transmitted RF signal and passed through the RF chain to recover the baseband UCP signal. Then the pulse elimination algorithm is applied to the baseband signal to eliminate the individual pulses and store the index numbers. The PS regeneration algorithm is also developed after eliminating individual pulses from corresponding to each TS to find the missing data channel. In this dissertation work, the CPE algorithm is proposed and designed to eliminate individual pulses from the UCP signal cyclically

corresponding to each TS. A CPE-based channel decoding is the main contribution to correlator-based pulse elimination. The proposed CPE technique eliminated the pulses from the received composite signal by correlation peak analysis. Fig. 4.4 shows the flowchart of the CPE algorithm. First, in the CPE algorithm, the composite signal correlates sequentially with the individual pulses stored in the receiver memory. Then check the correlation peak of individual pulses with the composite signal and find the maximum peak. The pulse signal corresponding to the highest peak is subtracted from the combined signal and stored as the PI number. This pulse elimination process will continue until the correlation peak reaches below the threshold level, then exist the elimination loop.

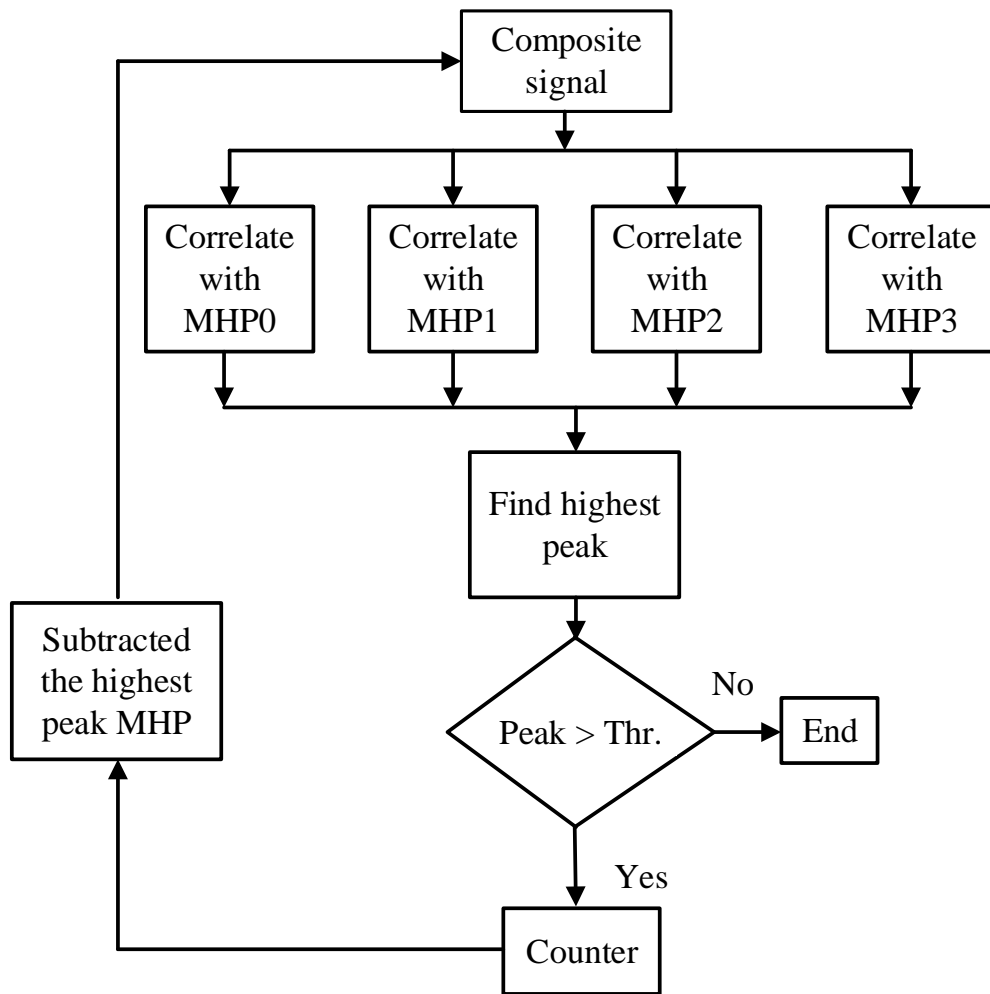


**Figure 4.4:** Flow chart of proposed CPE algorithm for single time slot.

In PS-based correlator receiver, the CPE algorithm is apply corresponding to each TS to decode individual pulses from the UCP signal. In appendix C, **Algorithm C3** shows the CPE-based decoding scheme. Time synchronization is a critical issue for correlation peak analysis with composite signal. Therefore, an extra pulse signal can be added in front of the UCP signal at sensor hubs for time-synchronization for correlation analysis. When, the receiver detect the time-synchronization pulse it starts to correlate the composite pulse with individual pulses corresponding to each TS. The second part of the channel decoding scheme is the index pattern regeneration using the eliminated PI. The eliminated individual PI is used to regenerate the PSs for finding the missing data channel by comparing with a prior known encoding template. Appendix C, **Algorithm C4** shows the PI pattern regeneration scheme from the stored index. The recreated index pattern correlates with the prior known channel encoding template to find the missing data channel. The decoded PS indicates the presence or absence of a data channel for high-density sensor networks. If the regenerated PS matched with the template PSs, then the corresponding data channel is present in the transmitted UCP signal. The presence of PS shows the corresponding channel transmits data bit. In OOK encoding, a threshold waiting time,  $T_w$  sec, offers either a specific channel is out of service or transmits a "0" bit. If a particular PS is continuously absent until  $T_w$  sec, then the corresponding data channel is out of service.

#### **4.4 Orthogonal Pulse Sequence Generation and Channel coding**

The orthogonal pulse sequence (OPS) generation and channel encoding is also presented in this dissertation work to simplify the decoding scheme for PS-based wireless telemetry. In previous section, the PS-based channel encoding and high-volume data

compression are described in details for short-range IoT applications. The analog pulses are orthogonal with other pulses and their composite signal, but the entire PSs are not orthogonal. The non-orthogonality of PSs arise the channel decoding complexity to find the missing data bits at the correlator based receiver. In this section, the gold code sequence generation introduces to create the OPSs for removing the decoding complexity at the receiver. Signal orthogonality of distinct PSs simplify CPE algorithm and eliminate entire PSs from the UCP signal by correlation peak analysis without sequence regeneration. Fig. 4.5 shows the OPS generation flowchart and correlation peak analysis shows in **Appendix B**. The correlation peak represents the correlation of individual OPSs with others and all the PSs have a positive peak that shows the orthogonality with others. Similarly, the OPS scheme also encodes data by distinct PSs and the UCP depicts the compressed data volume.

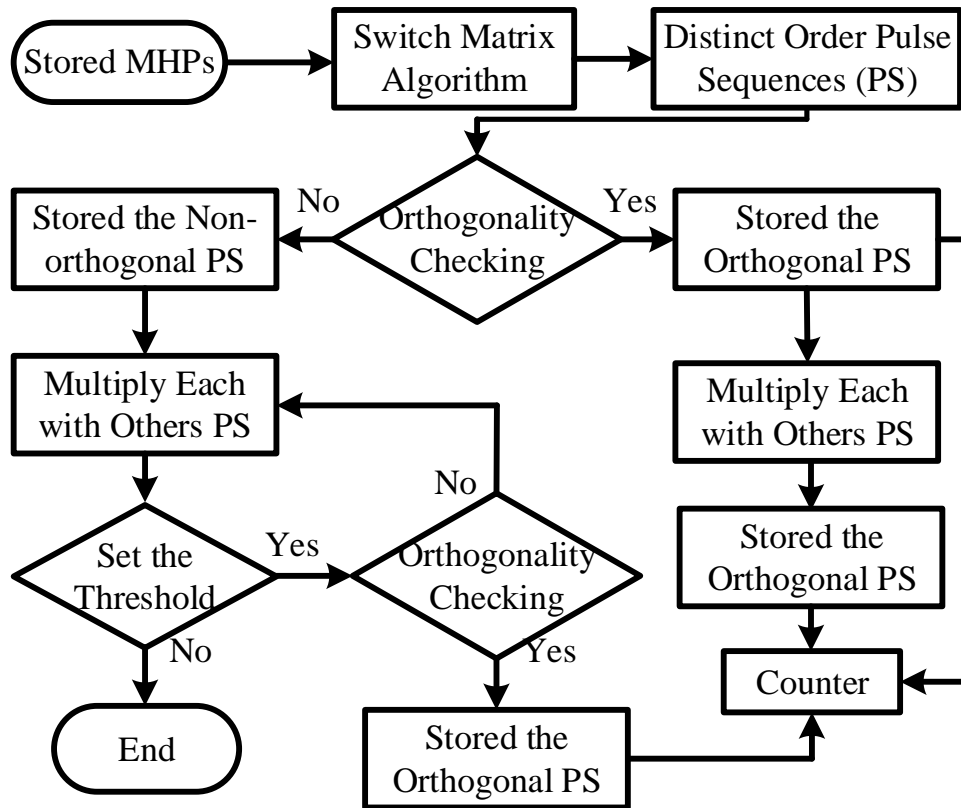


**Figure 4.5:** Flow chart of orthogonal pulse-sequence generation.

### 4.5 Orthogonal Pulse Sequence Decoding Scheme

The correlation peak analysis is used to decode the entire OPS from the UCP signal instead of using the CPE algorithm. Fig. 4.6 shows the channel decoding architecture. The received UCP signal is directly checked by the correlation peak with the individual PSs in parallel at the receiver. If any specific PS is present in the UCP signal then its correlation peak is higher than the pre-defined threshold and set the indicator flag '1' and vice versa. The indicator flag '1' and '0' represents the presence or absence of the corresponding PSs that depicts the status of data channels. The SPS and PS indicates the shifted and original OPSs, respectively. In BPSK data encoding, the PS indicates data bit '1' and the SPS represents bit '0' for any specific channels. The OPS-based channel decoding is much faster than the previously proposed CPE and simplify the missing data finding methods.

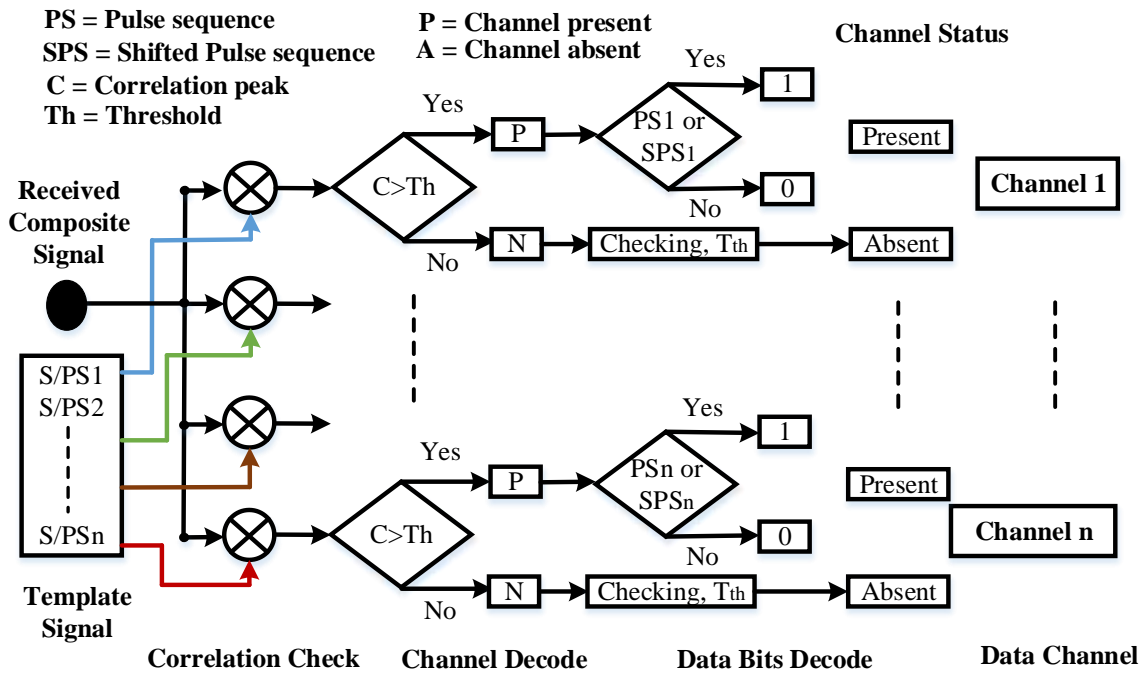


**Figure 4.6:** Correlation peak based OPS decoding for finding the missing data channels.

## 4.6 Simulation Results

The MATLAB<sup>®</sup> 2022 simulation tool is used to verify the performance of the proposed algorithm. The generated multi-order AOP signal is stored in MATLAB<sup>®</sup> work space for signal processing and algorithm development. At first, the AOPs are normalized within the amplitude +1 to -1. The signal orthogonality is also checked for considering different time shift factors using correlation peak analysis.

### 4.6.1 Permutation Technique

The PS generation algorithm creates a total of 24-distinct PSs, and each PS comprises 4-different order pulses in a sequence by changing the position without redundancy. Fig. 4.7 shows the simulation results of distinct PSs and Fig. 4.7(d) shows the UCP signal. In this dissertation work, the time shifted pulses are also used and verified by MATLAB<sup>®</sup> simulation. The 25% shift factor is used to create the shifted pulses and PSs to maintain the signal orthogonality. Fig. 4.8(a) shows the PS generation results, where the orange and blue traces indicate the original and shifted PSs. Fig. 4.8(b) shows the UCP signal for original and shifted PSs, respectively. The PS scheme is initially used an extra pulses to present a single data bit; but, the ultimate benefit is higher than the initial scarification of TS. Moreover, time-shifted AOPs also occupied an extra 25% TS of the original pulses; however, it also supports an extra data volume by increasing the number of channels. In conventional pulse system, only (4+4)-bit data is encoded by the four distinct AOPs and their shifted pulses, while the PS scheme transmits a total of 48-bit (24+24) data by 48-distinct analog PSs.

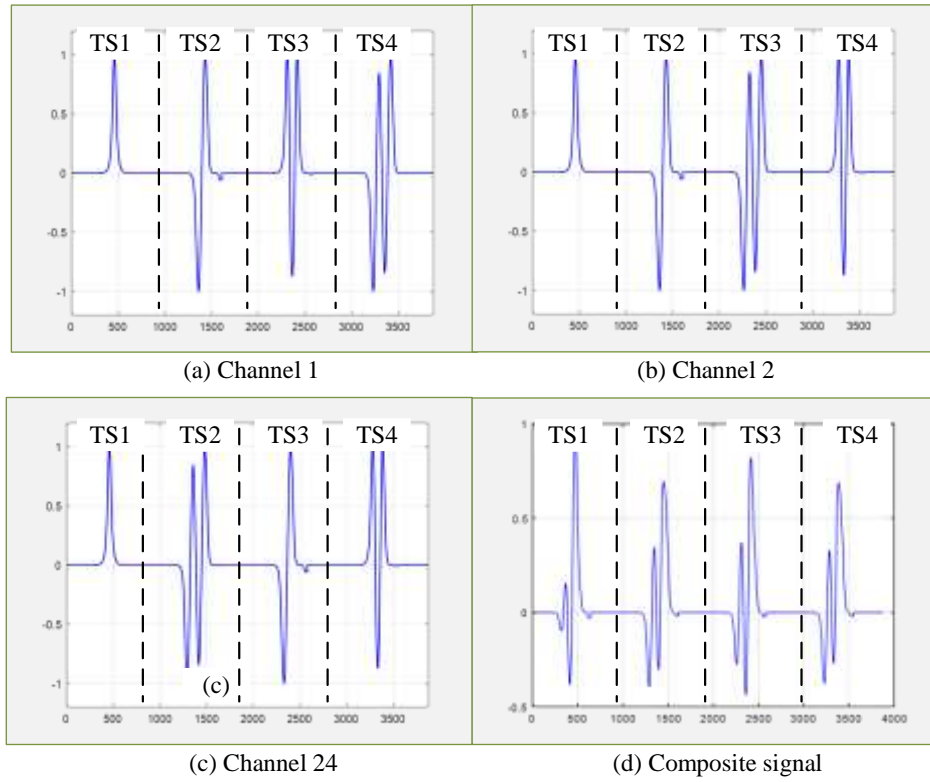


**Figure 4.7:** PS-based encoding channel (a) 1, (b) 2, (c) 24, and (d) UCP signal.

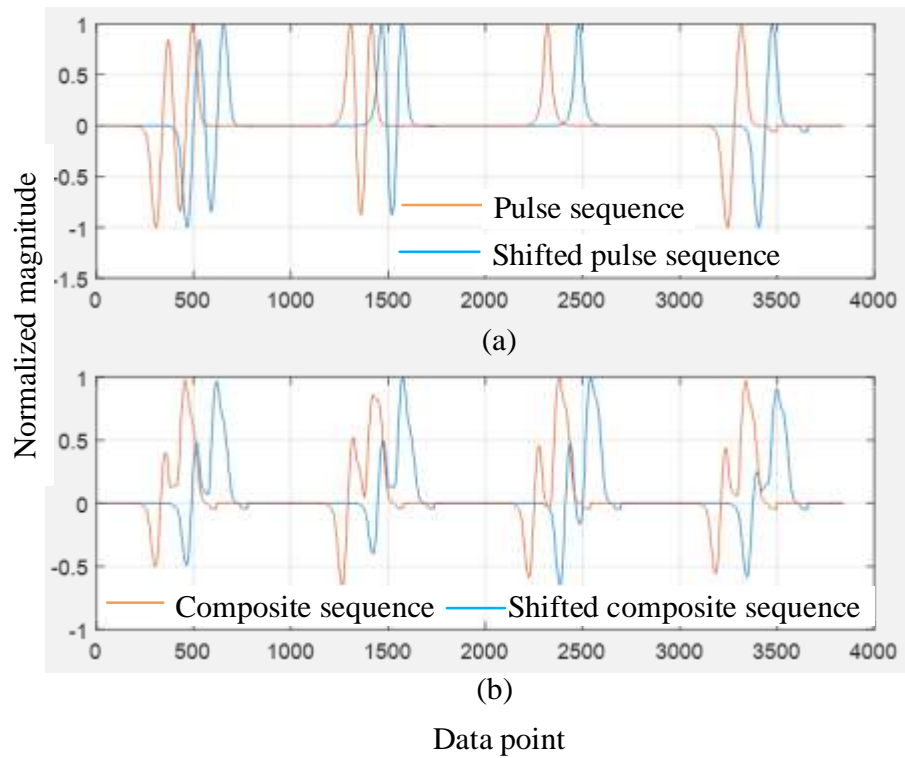


**Figure 4.8:** Simulation results for PS and UCP signals for original and shifted AOPs.

Fig. 4.9 shows the PSD plot of distinct AOPs and the corresponding UCP signals considering to the original and shifted pulses. Simulation results shows that all the individual pulses and the UCP signal are meet the power requirements defined by the FCC for indoor communications. The Comp.1 and Comp.2 represents the UCP signal corresponding the original and shifted PS based composite signal. The combined of Comp.1 and Comp. 2 is Comp.3 signal also meets the FCC requirements.

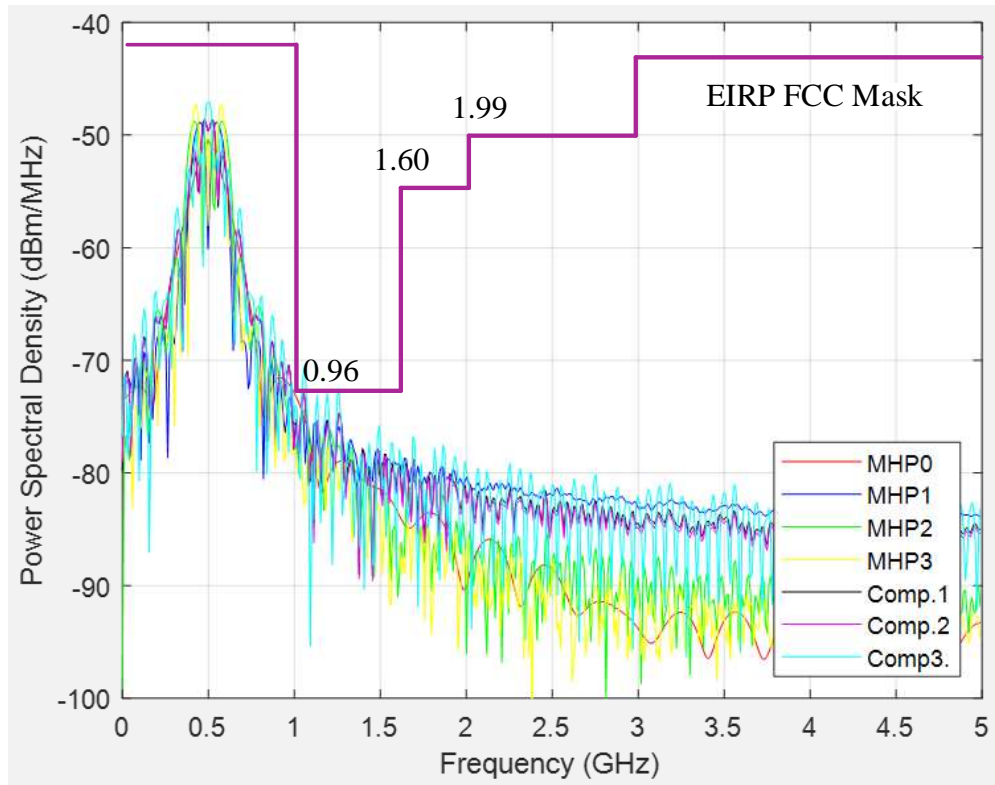
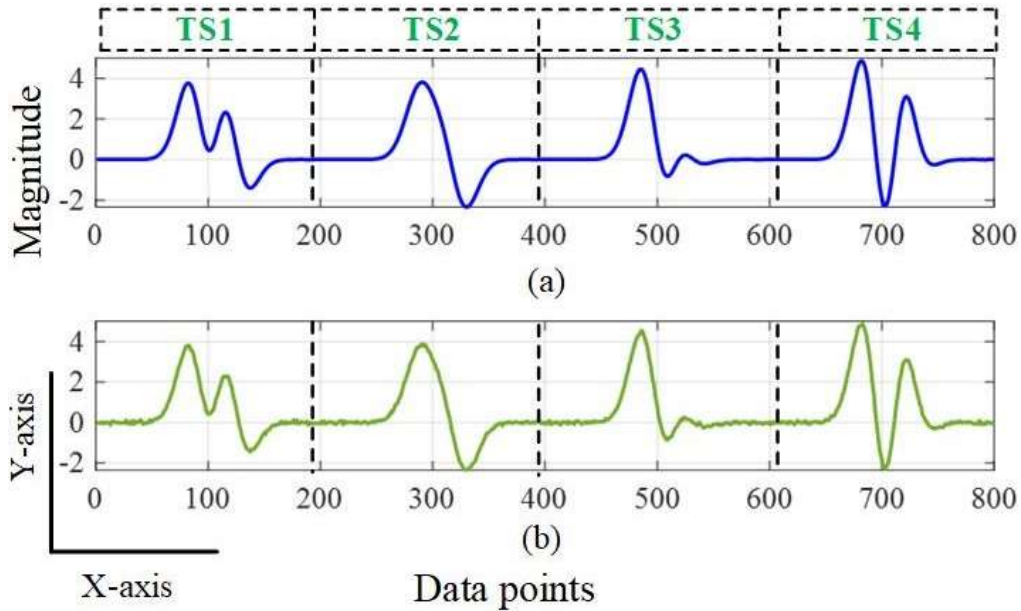


**Figure 4.9:** Power spectral density of individual pulses and their UCP signals.

The MATLAB<sup>®</sup> simulation tool is also used to verify the accuracy of the proposed CPE algorithm. Fig. 4.10 shows the composite signal with 20.0 dB AWGN channel model to represent the channel noise in computer simulation. The CPE algorithm divided the incoming UCP signal into  $n \times T_s$  sub-blocks, where  $n$  is the pulse number in a sequence. First, the CPE technique correlates the composite signal corresponding to a specific  $T_s$  with



the template pulse and checks the maximum correlation peak. If a specific pulse is present in the combined signal then its correlation peak is much higher than the pre-defined threshold,  $T_h$  and vice versa. Second, the pulse is subtracted from the received composite signal corresponding to the maximum peak value and stored the index number. The pulse elimination process will continue until the peak of individual pulses arrive below the  $T_h$ .



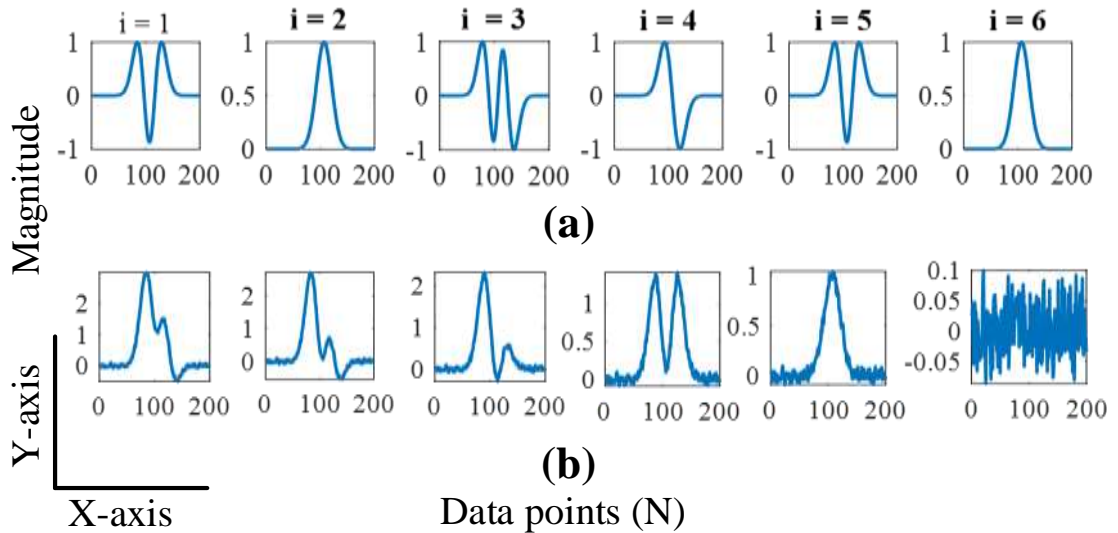
**Figure 4.10:** Simulation results of UCP (a) without and (b) with AWGN signal.

Fig. 4.11 shows the simulation results of CPE algorithm corresponding to the first, TS of the UCP signal. The UCP signal consisting of  $2MHP_0$ ,  $MHP_1$ ,  $2MHP_2$ , and  $MHP_3$  pulses. Fig. 4.11(a) shows the decoded pulses cyclically based on the highest correlation peak. Table 4.1 shows the correlation peak table corresponding to each iteration with the composite signal. Fig. 4.11(b) represents the remaining signal after eliminating all the pulses from the composite signal corresponding to the iteration. After decoding all the pulses from the composite signal, the residual signal contains only the AWGN, and the correlation peak of all the pulses reach below the threshold at 0.20. For the missing pulses

the corresponding correlation peak is lower than the threshold level. So, the correlation peak is also an indicator to find the missing pulse in the composite signal and it is also help finding the missing data channels.

**Table 4.1:** Correlation between composite pulses with distinct AOPs.

Ite. #	Composite signal						Residual signal
	1 <sup>st</sup>	2 <sup>nd</sup>	3 <sup>rd</sup>	4 <sup>th</sup>	5 <sup>th</sup>	6 <sup>th</sup>	
MHP <sub>0</sub>	0.3958	<b>0.5789</b>	0.2846	0.3546	0.4785	<b>0.9911</b>	<b>0.0561</b>
MHP <sub>1</sub>	0.3768	0.4579	0.5388	<b>0.6714</b>	0.0056	0.1008	<b>0.0596</b>
MHP <sub>2</sub>	<b>0.6210</b>	0.3039	0.4446	0.5540	<b>0.7476</b>	-0.2128	<b>0.0187</b>
MHP <sub>3</sub>	0.4173	0.5072	<b>0.5968</b>	0.0120	0.0162	0.0238	<b>0.0782</b>



**Figure 4.11:** Simulation results (a) decoded pulses and (b) residual signal.

In this dissertation work, four different experiments has performed to validate the CPE and PI regeneration algorithms. Fig. 4.12 shows the corresponding UCP signal in different test conditions and Table 4.2 represents the performance of the channel decoding scheme. In experiment-1, the CPE algorithm decoded all the individual pulses from the composite signal corresponding to each TS and regenerated the PI pattern successfully. The PI pattern regeneration scheme also finds the missing channels by comparing them with the prior known channel encoding template. The results show that the decoding

scheme decoded all the transmitted channels from the UCP signal. Similarly, the transmitted and missing channels are also decoded successfully from the UCP signal in experiments 2, 3, and 4. Therefore, the proposed CPE algorithm with the PI regeneration can apply to decode the transmitted data channels for PS-based wireless data telemetry.

**Table 4.2:** Test validation for CPE based channel decoding.

Exp.	Channel encoding						Channel decoding					
	PS <sub>1</sub>	PS <sub>2</sub>	PS <sub>3</sub>	PS <sub>4</sub>	PS <sub>5</sub>	PS <sub>6</sub>	PS <sub>1</sub>	PS <sub>2</sub>	PS <sub>3</sub>	PS <sub>4</sub>	PS <sub>5</sub>	PS <sub>6</sub>
E <sub>1</sub>	P	P	P	P	P	P	P	P	P	P	P	P
E <sub>2</sub>	P	P	A	P	A	P	P	P	A	P	A	P
E <sub>3</sub>	A	P	P	A	P	P	A	P	P	A	P	P
E <sub>4</sub>	P	A	P	P	P	A	P	A	P	P	P	A

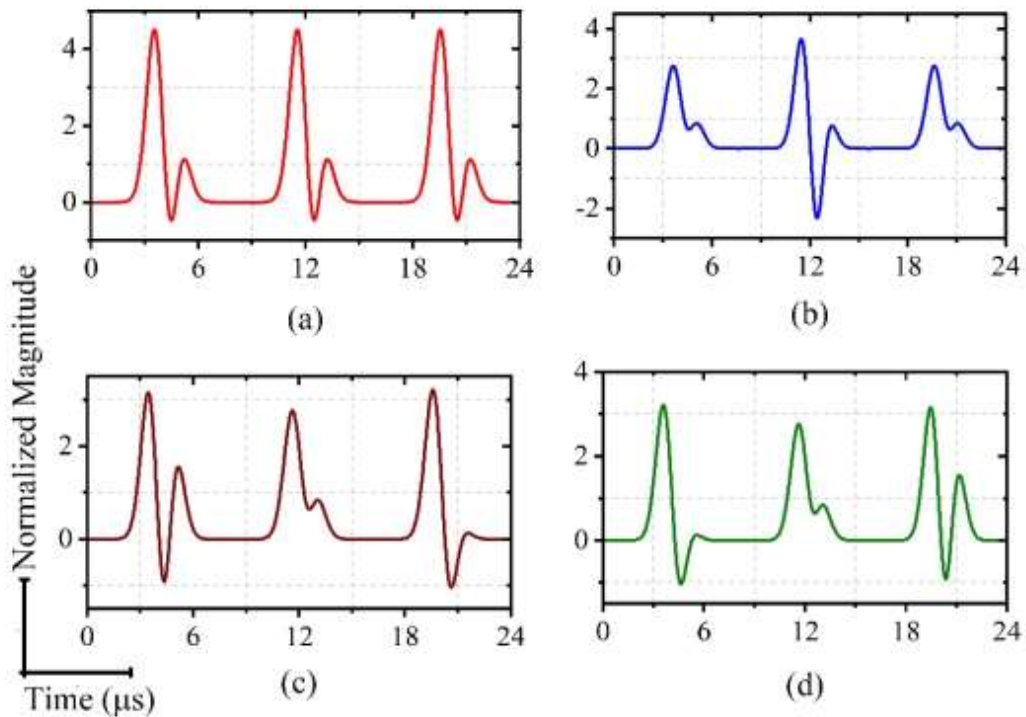


**Figure 4.12:** Composite UCP signal corresponding to each time slot.

#### 4.6.2 Gold sequence Results

The gold sequence-based OPS generation is the following approach of the permutation-based PS generation. The permutation technique generates  $n!$  distinct PSs by

changing their positions. The OPS generation creates PSs by multiplying two non-orthogonal PSs and finding the cross-correlation peak with others. The product of two non-orthogonal PSs make an orthogonal PS and co-exist in their composite signal. Fig. 4.13 shows the MATLAB® simulation results of OPSs generation.

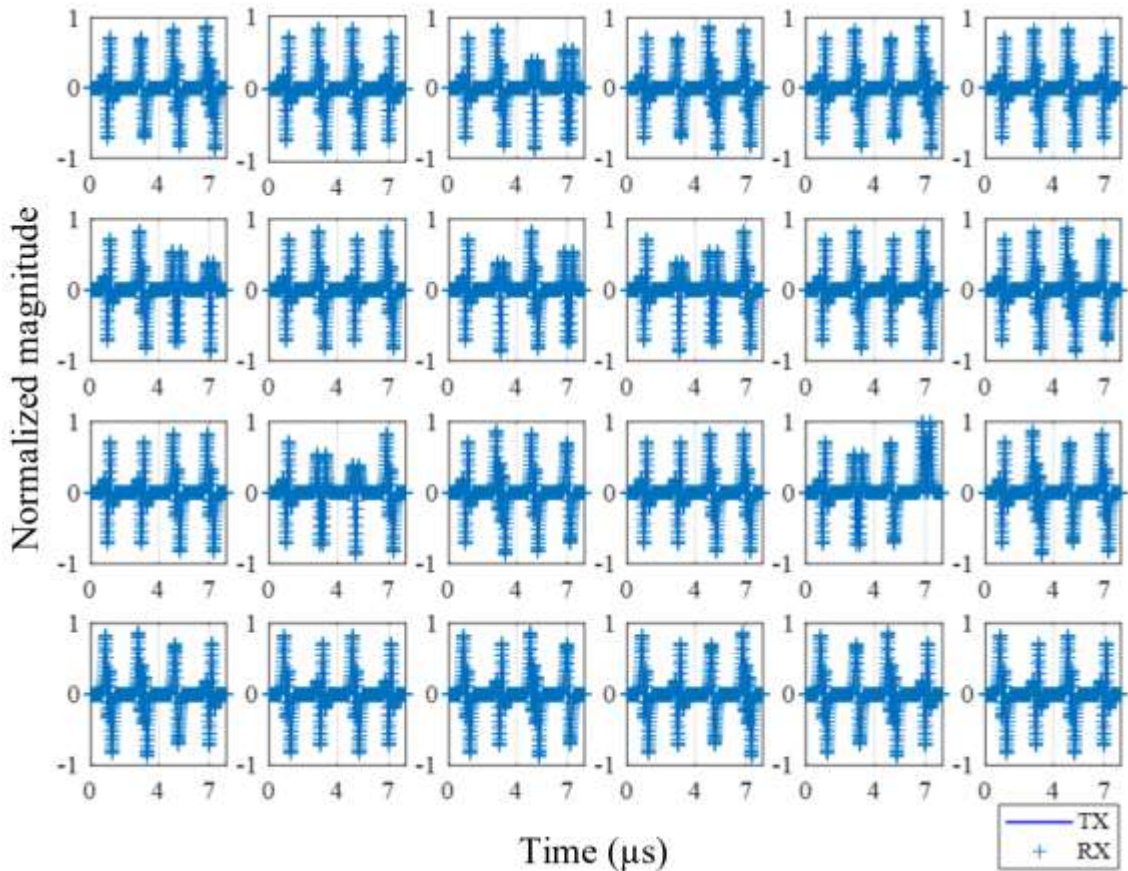


**Figure 4.13:** Simulation results of distinct OPS generation using Gold code method.

In Fig. 4.13 shows the channel encoding signal by distinct OPSs and decoding sequence from the corresponding UCP signal. All the individual PSs are orthogonal and coexists with their UCP signal. The composite signal represents the compressed data volume and supports multiple sensor data. The correlation peak analysis is the most thrifty and easiest way to decode the orthogonal signal from the composite signal. This experiment selects the threshold point at  $0.550$  to decode the individual OPSs from the combined signal

by correlation peak analysis. The OFDM based wireless communication reduces the BER over the multipath channels with system noise [75]. Simulation results show that, if any specific OPS is present in the composite signal then its peak is higher than the threshold level. If the correlation peak is higher than the threshold level, it prints the index number corresponding to that particular PS and decodes from their composite signal without the CPE algorithm. The missing data finding scheme also simplifies without PS regeneration and doesn't require rearranging the PI to reform the sequences. Fig. 4.14 shows the performance evaluation of PS-based data transmission. The BER is investigated by  $1 \times 10^6$  binary data bits. The OOK encoding technique encodes data bits using an OPS and decodes the missing bits using a correlator-based decoder. MATLAB® simulation results shows BER decreases with a higher SNR and it arrives at  $1 \times 10^{-4}$  around 13.0 dB SNR.

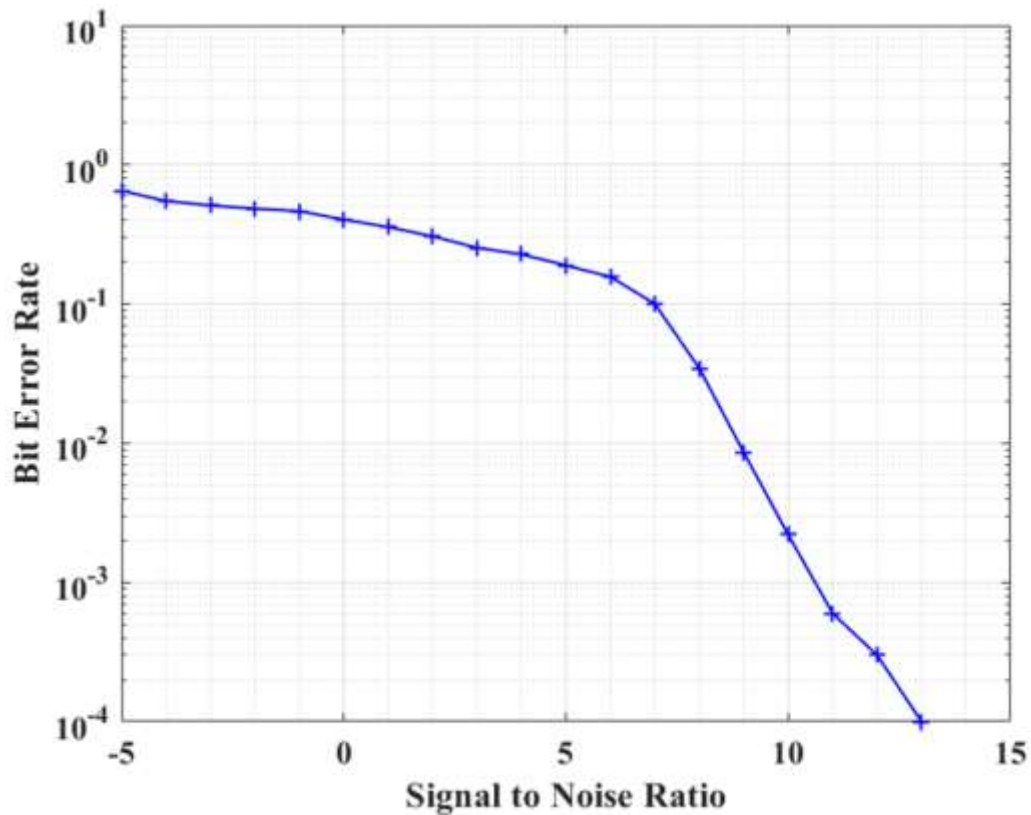


**Figure 4.14:** Simulation results for BER investigation for OPS-based encoding scheme.

## 4.7 Significant Improvement

The innovative PS-based encoding increases the significance of the data channel numbers, high-volume data compression, and SE communications. The benefit of narrow-width AOP-based combinatorial PS encoding is simultaneous spectrum sharing and recovering each PSs by applying a pulse decoding approach. The HG pulse system increases the data rate by  $(n+1)$  times using orthogonal polynomial waveform by superimposing  $n^{\text{th}}$  order orthogonal pulses applying the OFDM technique, where  $n$  is the order of the orthogonal polynomial [34]. On the other hand, the PS scheme improves the data volume by  $(n-1)!$ -times and data transmission speed by  $(n-1)!/TS$  Mbps. The proposed PS scheme uses an extra  $(n-1)$  redundant pulse signal to create each sequence but it supports numerous data channel  $n!$  for  $n$ -pulse systems. Table 4.3 shows the summary of significant improvements of the proposed PS scheme.

**Table 4.3:** Significant improvements of the proposed PS-based data channel encoding.

Number of pulse	Number of PSs	Data volume, bits	Data channel improvement	Data rate improvement
1	1	1	No	No
2	2	2	No	No
3	6	6	2 times	2 times
4	24	24	6 times	6 times
5	120	120	24 times	24 times
n	n!	n!	(n-1)! times	(n-1)! times

In a 3-pulse system, the proposed scheme supports a total of 6-channels instead of 3-channels by sharing the spectrum and improves the data transmission rate double compared to the conventional single-pulse system. A significant improvement will occur for the  $n \geq 4$  system. At the pulse width of  $1.0 \text{ ns}$ , the data transmission rate is  $400.0 \text{ Mbps}$  for a single pulse system, while in the PS scheme is  $2.4 \text{ Gbps}$  supporting 6-times more data channels by sharing the same frequency band for a 4-pulse system.



Similarly, if the pulse width is  $1.0 \text{ ps}$ , then the data rate will be  $2400.0 \text{ Gbps}$  for the 4-pulse system in the proposed scheme than  $400.0 \text{ Gbps}$ . Therefore, compared to the standard single pulse system, the proposed analog PS-based encoding scheme improved the data transmission rate  $(n-1)!$ -times more by compressing and supporting extensive volume data sharing the same frequency spectrum for SE telemetry.

#### 4.8 Conclusion

This chapter presents multi-channel encoding using an innovative PS scheme. The PS-based data compression and CPE based decompression algorithms are also developed and verified through MATLAB<sup>®</sup> Simulation. Test results shows that the proposed encoding increases the network capacity by supporting multiple channels using distinct number of PSs while sharing the same spectrum. The CPE algorithm also decoded all the channels successfully from the received UCP signal to find the missing data bits. The PS generation scheme created a total of  $n!$ -number of distinct PSs to support  $n!$ -data channels and increased data transmission rate by  $(n-1)!$  times more for the  $n$ -pulse system. The gold sequence scheme also simplifies the decoding algorithm compared to CPE algorithm to support high-density short-range IoT networks.

## CHAPTER 5

### CHANNEL EFFECT ON ANALOG PULSES AND OBJECT SENSING

#### 5.1 Introduction

A communication channel refers either to a physical transmission medium such as a wire or wireless connection over a radio telecommunications and networking. A channel is used for information transferring through a noisy environment. The message information is represented by an electromagnetic wave and sent it to a receiver, where the signal is contaminated by noise. Signal distortion, high noise prone, signal corruption, and time synchronization are the major issue in pulse communication. The channel effect investigation is critically needed for analog pulse communication. This chapter presents a simplified signal processing method to verify the feasibility and compatibility of AOP-based short-range wireless data telemetry. The channel effect on AOPs and object sensing is performed by measuring the network parameters at different case studies. The numerical simulation results show that the impact of channel noise on AOP signal. It also shows the actual scenario of communication channel effects due to the variation of dielectric media, reflection of object materials, and sensing capability of the AOPs in an indoor environment. The investigation also highlights some critical findings from the extensive analysis that help design the receiver architecture to decode the individual pulses from the received composite signal. The  $S_{21}$  measurements and numerical simulation results suggest that the AOP set can transmit compressed data volume for short-range wireless data telemetry.



## 5.2 Communication Channel Characterizations

Accurate channel characterization and modeling is the main prerequisite to design the wireless transceiver effectively and efficiently for indoor IoT networks. Many research works have been done to characterize the wireless channel in indoor communication, underground mining and underwater communications, BAN, etc. The physical layer is characterized at 2.45 GHz in terms of path loss, delay spread, etc., by investigating the wireless channel between the human body and the antennas at different locations in BAN [63]. The network parameters are measured using a vector network analyzer (VNA) and calculated the time-domain signal using *IFFT* [64]. Research efforts also have focused on the characterization of wireless channel for specific configurations of the transmitter and receiver antenna, different corridor obstruction angles, and indoor locations. The authors evaluated the path loss effect considering LOS and channel obstructions in an indoor environment, the room structure consists of gypsum board, plywood door, metallic cabinets, brick, foam layer, wooden structure, and dry concrete walls [64, 65].

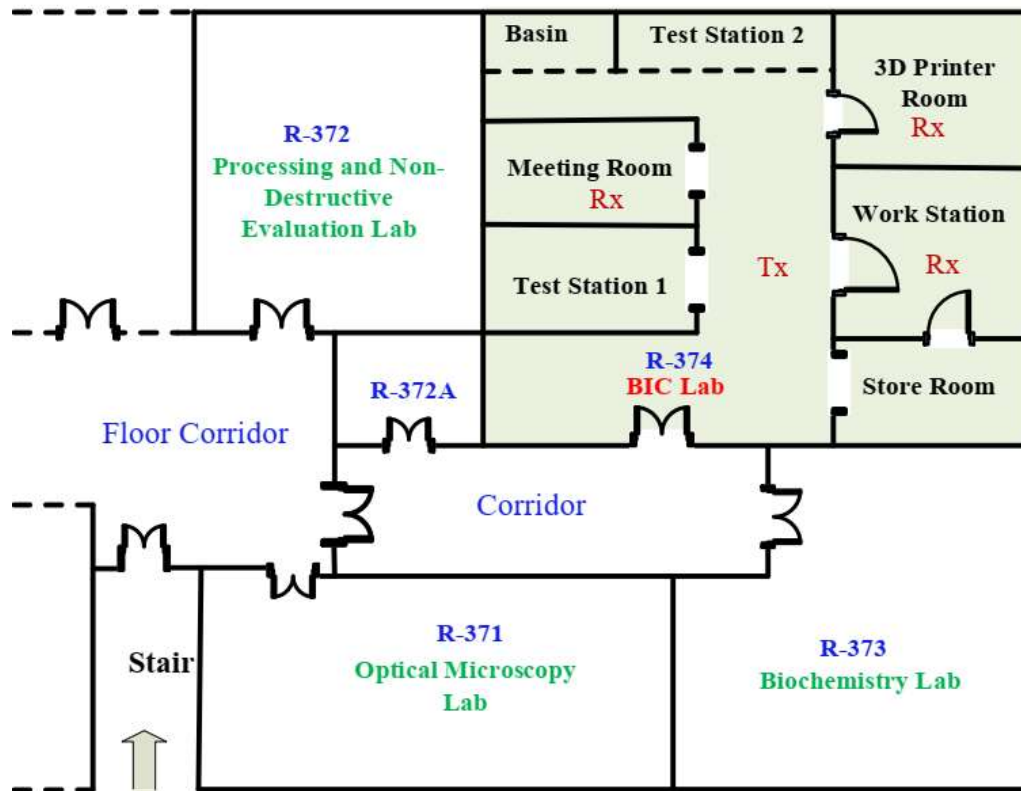
The channel measurements are performed in wideband frequency at the carrier of 433 MHz in a factory hall of a steel mill with large metal objects both in indoor and outdoor locations [65]. The automation floor dimension is  $29 \times 15 \times 7.3 \text{ m}^3$  with a metallic ceiling, a concrete floor, and some open metallic joists were performed channel measurements using a broadband channel at 5.85 GHz carrier frequency for industrial radio communication systems. The room size  $4.3 \times 7 \times 3 \text{ m}^3$  and  $6 \times 25.77 \times 3 \text{ m}^3$  were characterized by placing the antenna in the middle of the room and between the tables [66]. A long path THz wireless channel was also characterized by using on-chip generated pulses to evaluate the path loss, atmospheric absorption, and signal distortion [67]. The physical

channel effects on RF signal depends on the permittivity and permeability, when traveling via communication media. Thus, the impact of channel obstruction, characteristics of propagation media, and frequency-response of the time-varying RF signal is also crucially important designing the receiver for AOP-based indoor telemetry. This chapter investigated the channel effect by time-frequency domain computation using the measured S-parameters with a bench top VNA [68-69].

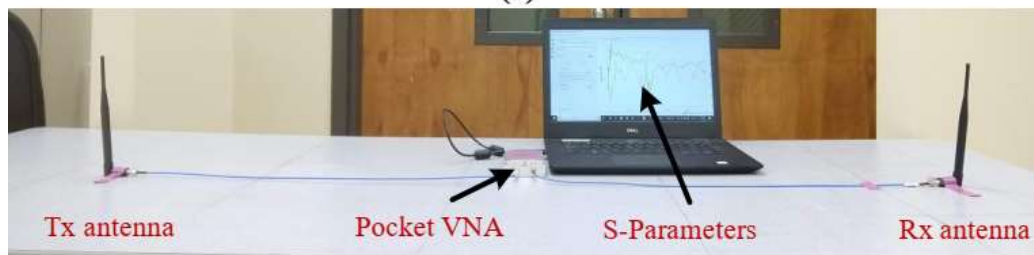
### **5.3 Measurement Setup and Configuration**

Two identical 1/4 wavelength Monopole 433 MHz antennas with a length of 20.7 cm, a diameter of 1.3 cm, and gain +3.0 dBi are placed at various positions on the table in different indoor locations. The antennas are placed in faced to each other with lined up for maximum power transfer in LOS communication to measure the network parameters. The characteristics of the propagation channel depends on the height of the antenna above the floor surface. Therefore, the antennas are placed on top of the table at 78.0 cm above of floor surface and measured the channel parameters in different obstacle. In this chapter, the channel properties are investigated at various locations of the room size of  $6 \times 4.5 \times 3 \text{ m}^3$ ,  $6 \times 3.5 \times 3 \text{ m}^3$ , and others locations of the BIC design lab Room # 374. Fig. 5.1(a) shows the floor map of the indoor test environment in BIC design lab, at UAB. The measurement points are selected by considering the reflection of the wall, ceiling, floor, electronics devices, furniture, and channel media on analog pulse signal for observing the real scenario in the indoor wireless environment. Fig. 5(b) shows the S-parameter measurements setup for different communication channel obstructions. The S-parameter is measured by a portable 2-port VNA known as Pocket VNA. This portable VNA can measure DUT's

frequency response up to 4.0 GHz. The VNA is calibrated before measuring the S-parameters using the standard calibration kits. The Tx and Rx antenna are connected with pocket VNA port 1 and port 2 via the calibrated co-axial cable in 2.0 ft, 4.0 ft, 6.0 ft, and 8.0 ft, respectively. The channel obstruction sample is also placed in between the Tx-Rx to characterize the channel. The VNA's built-in source provides a stimulus signal that is injected into DUT and measured the frequency response by changing from 100 kHz to 1.0 GHz in a total of 200 sample points in a linear scale.



(a)



(b)

**Figure 5.1:** Indoor S-parameter measurements (a) floor map and (b) test setup.

## 5.4 Signal Processing in Time-Frequency Analysis

The straightforward signal processing scheme is presented in frequency domain computation. The *FFT* and *IFFT* techniques are used to convert the time-varying signal from time-domain to frequency-domain and vice versa without losing any information. Fig. 5.2(d) shows the numerical simulated composite pulse signal comprising with MHP<sub>1</sub>, MHP<sub>2</sub>, and MHP<sub>3</sub>. First, the channel frequency response is obtained by measuring the  $S_{21}$  components (Fig. 5.2(e)). Then, MATLAB<sup>®</sup> Simulation is performed to transform the time-varying signal,  $X(t)$  to frequency-domain,  $X(\omega)$  using the *FFT*. Fig. 5.2(a) and (c) shows the modulated composite signal at 500 MHz before and after traveling through the channel media, respectively. The output signal,  $Y(\omega)$  is calculated by the frequency domain multiplication of  $X(\omega)$  and  $S_{21}(\omega)$ . Finally, the time-varying output signal (Fig. 5.2(d)) is obtained by taking the *IFFT* of the calculated signal,  $Y(\omega)$ .

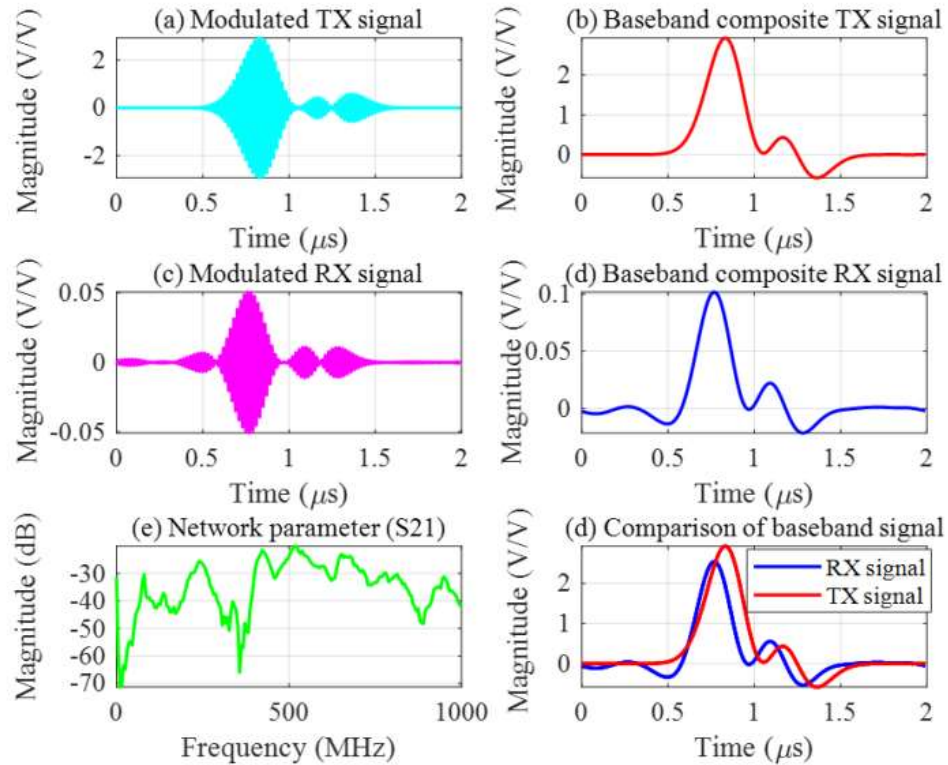


**Figure 5.2:** Signal processing steps for numerical simulation using S-parameter.

## 5.5 Measurement Results and Channel Effects

The analog pulse based data transmission reduced the transceiver complexity and bandwidth requirements with enhancing high volume data by compressing the digital bits into analog format. The network parameter is measured to investigate the pulse based telemetry feasibility considering different test conditions. Fig. 5.3(a) shows the measured transmission gain versus frequencies corresponding to the  $T_X$ - $R_X$  separation. The measured  $S_{21}(f)$  parameter indicates the power loss of a propagating signal through a communication channel. In this section, different case studies are considered to analyze the channel effects on time-varying analog pulses. The path loss is measured by measuring the  $S_{21}(f)$  components by VNA and calculated the corresponding numerical simulated output signal through simplified signal-processing scheme. Fig. 5.3(b) shows the numerical simulated response from 0 to 2.0  $\mu$ s for measured  $S_{21}$  parameters with the variations of distances.

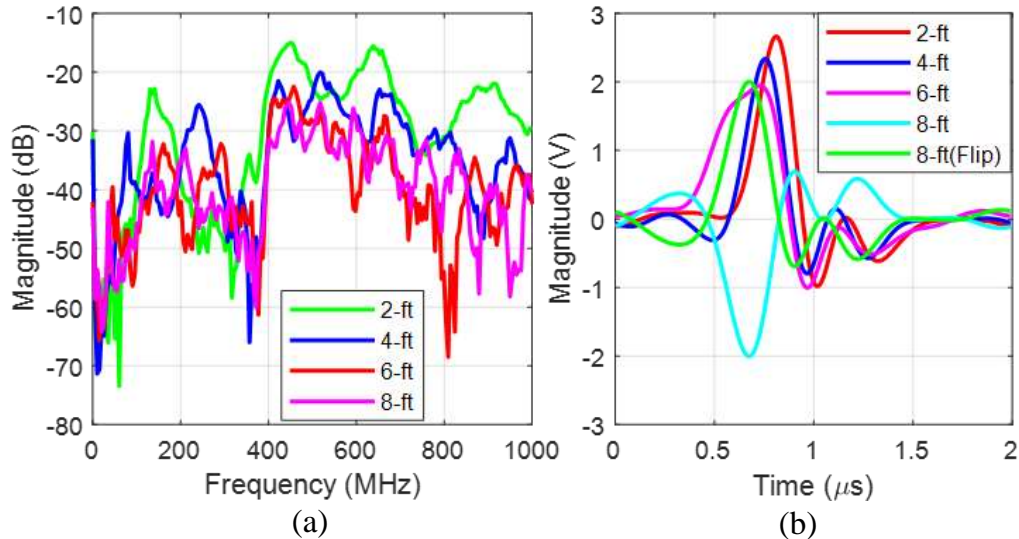


**Figure 5.3:** Measurement results (a) S-parameters and (b) numerical simulation.

The forward transmission loss and the distortion of an RF signal is also evaluated in the presence of channel obstacle materials, reflection, multi-path interference, fading propagation, etc. The green, blue, orange, and purple trace indicate the individual measured

S-parameters' corresponding to the antenna separation for 2.0 ft, 4.0 ft, 6.0 ft, and 8.0 ft, respectively (5.3(b)). The receiving antenna received both the direct signal and reflected signal from surrounding objects that create multi-path interference in the same or out of phase. The multi-color trace indicates the output signal obtained from the individual channel measurements data. Fig. 6.2(d) shows the measurement results where the normalized magnitude of the output signal is around 0.1 after propagating through a lossy media. The output signal is scaled up by a multiplying factor, 20 of each measurement. In Fig. 5.3(b), it is also noticeable that the path loss increases with increasing the distances.

### 5.5.1 Variation of Antenna Positions in Between $T_X$ - $R_X$ Separation

The energy loss and signal distortion also the function of dielectric constant of the propagation media. This chapter investigates the impacts of different dielectric materials on the AOPs for indoor wireless telemetry applications. The measurement on three different channel obstruction conditions are considered, such as middle in the  $T_X$ - $R_X$ , nearest to  $T_X$ , and  $R_X$  antenna conditions for an indoor environment.

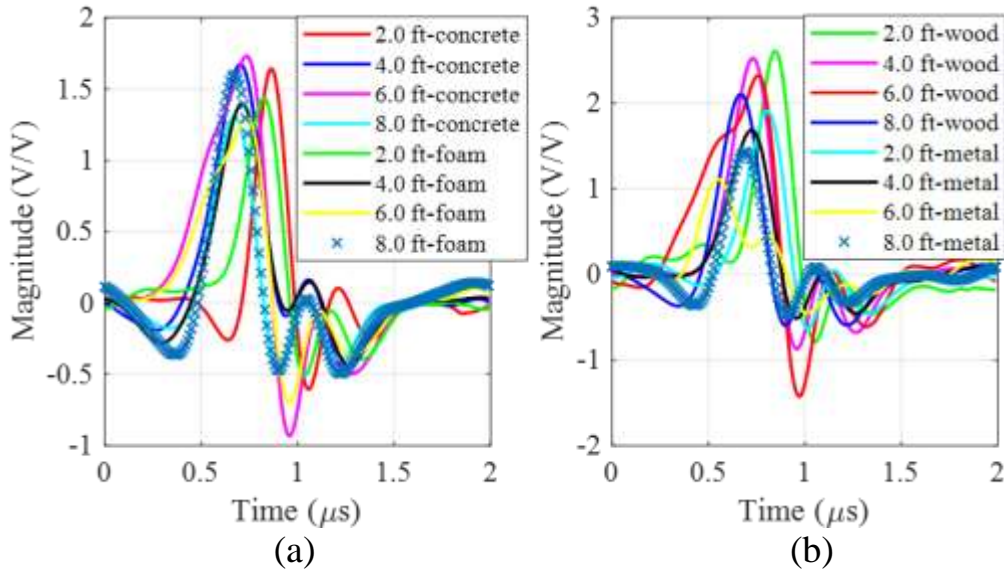


**Figure 5.4:** Numerical simulated results for channel obstructions (a) concrete and foam and (b) wood and metal in the middle of the  $T_X$ - $R_X$  position.

### 5.5.1(a) Middle in the $T_X$ - $R_X$ Separation

The path loss, signal distortion, and phase variation occurs from material to material of the channel obstacles. Fig. 5.4 shows the measured signal for concrete, foam, wood, and metal channel obstruction in the middle of the  $T_X$ - $R_X$  position. The signal penetration capability of AOPs are investigated for channel obstruction using different blockages. The external effect is significantly noticeable on AOP signal for wooden and metal blockages at the higher  $T_X$ - $R_X$  separation. To decode the individual pulses, the measured signal is boosted by a factor of 30 for concrete and foam and 50 for wood and metal block.

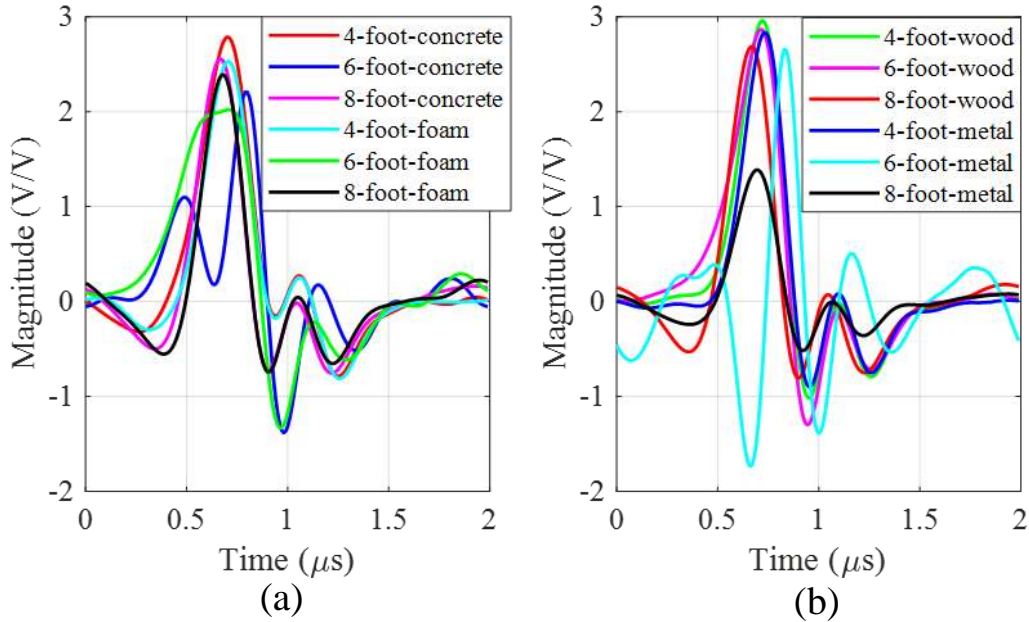


**Figure 5.5:** Numerical simulated results for channel obstructions (a) concrete and foam and (b) wood and metal in the nearest to the  $T_X$  antenna.

### 5.5.1(b) Nearest to the $T_X$ Antenna

This work also investigated the nearest and remote channel obstruction effect on AOPs by placing the channel obstacle material at 1.0 ft away from the antenna. Figs. 5.5(a) and (b) shows the numerical simulated output for channel blockages nearest to the  $T_X$  antenna for concrete, foam block, wood, and metal block in the variations of  $T_X$ - $R_X$



separations. Test results also indicate the strength of AOP signal after penetrating the obstacle materials. The numerical simulated output is multiplied by a factor 30 for concrete and foam and 50 for wood and metal blocks to increase the magnitude.

### 5.5.1(c) Nearest to the $R_X$ Antenna

Figs. 5.6(a) and (b) shows the signal penetration capability of AOPs after traveling the channel path for LOS communications. This chapter investigated the signal capability to penetrate the channel obstruction at different dielectric material blockages by placing the obstacle at 1.0 ft away from the  $R_X$  antenna. In Fig. 5.6(b) the output signal is spread more at 6.0 ft distance for metal blockages. However, the individual pulse is decoded from the composite signal by adjusting the magnitude.

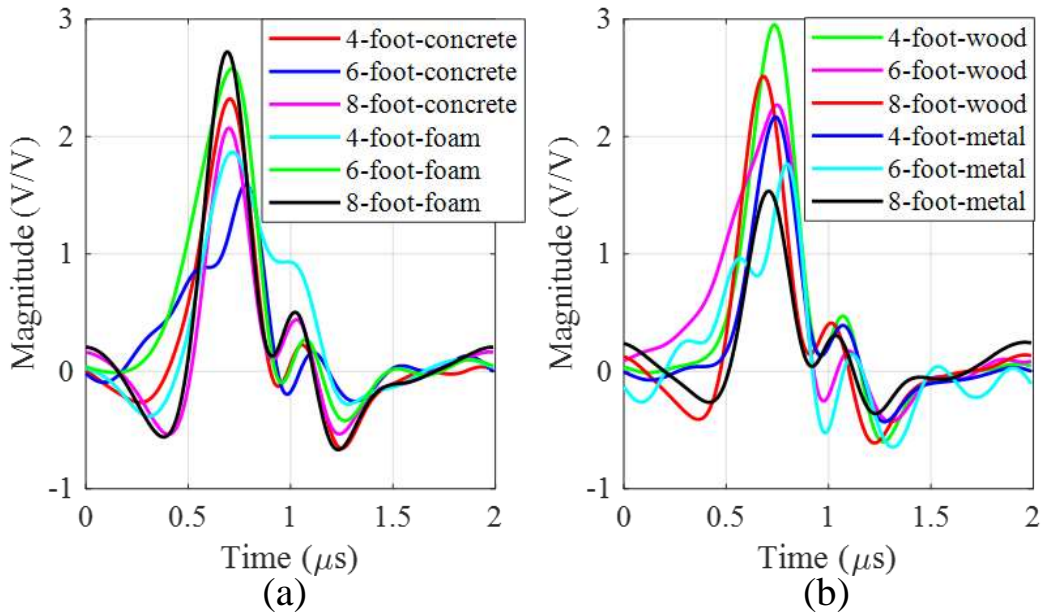


**Figure 5.6:** Numerical simulated results for channel obstructions (a) concrete & foam and (b) wood & metal in the nearest to the  $R_X$  antenna.

### 5.5.2 Variation of Channel Obstacle Combinations

This subsection presents the effect of channel media on proposed AOP signal at different combinations of the material blocks for LOS communication channel obstruction.



To investigate the channel effects and dielectric variations at different blockage materials such as concrete, metal, wooden sample block, etc., are used as the communication channel obstruction. Test results also indicate the real scenario of an indoor communication channel with varying the combinations of materials. This paper also investigates the effect of moisture content on the AOP signal using a thin water pipe attached with the channel blockage material. The water content absorbs the RF signal when propagating through any wet blockage materials. The numerical simulated signal is multiplied by a factor 50 to recover the individual pulse successfully.

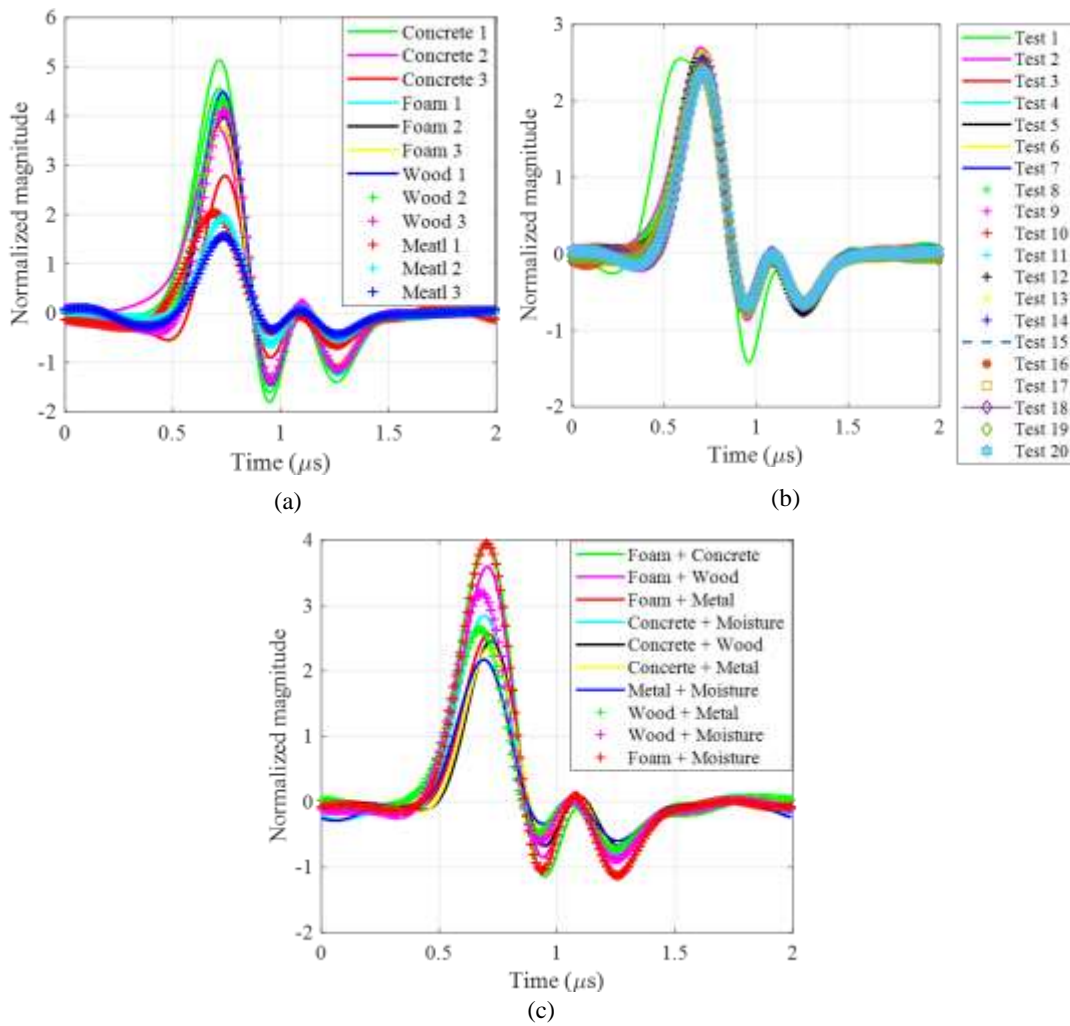


**Figure 5.7:** Numerical simulated results for different cases (a) object size, (b) different indoor locations, and (c) objects combinations.

### 5.5.3 Variation of Channel Obstacle Size

The energy loss and signal distortion are also investigated using variations of the channel blockage thickness. The material permittivity also varies with changing the cross-sectional area and the thickness of sample. Table 5.1 shows the sample thickness variations of different channel blockage materials. Fig. 5.7(c) depicts the signal attenuation from sample to sample in same types of blockage materials. The S-parameter measurements are performed at different cross sectional areas of samples to verify the AOPs compatibility. Test results also indicates the analog pulses can penetrate and propagate through different dielectric media with the variation of magnitude and phase from material thickness to thickness. However, the individual pulses are decoded from the numerical simulated output signals by scaling their normalized magnitude above 1.75 V/V.

**Table 5.1:** List of different size of communication channel blockages.

Size (inch <sup>3</sup> )	Concrete	Foam	Wood	Metal
Sample 1	6 × 4 × 2	13 × 12 × 1	16 × 16 × 0.7	12 × 12 × 0.08
Sample 2	6 × 6 × 3	18 × 12 × 1.5	16 × 16 × 1.0	12 × 12 × 0.1
Sample 3	6 × 6 × 6	18 × 12 × 4.5	16 × 16 × 1.5	12 × 0.8 × 0.125

### 5.5.4 Measurements at Different Location

In this study, the channel effect is also investigated in different locations by measuring 12 different measurements for the entire room instead of investigating the individual indoor environments separately. Fig. 5.7(b) shows the path loss for the investigated room size of 6 × 4.5 × 3 m<sup>3</sup> and 6 × 3.5 × 3 m<sup>3</sup> by placing the T<sub>X</sub> and R<sub>X</sub> antenna in different locations. The measurement results are valid for LOS communication in the specified 4.0 ft T<sub>X</sub>-R<sub>X</sub> separation; however, it works for further distances. The investigated channel effects also include the signal reflection, multi-path interference, fading propagation to the concrete wall, wooden door, furniture, electronics devices,

metallic almirah, etc. In all cases, the decoding scheme decodes the individual pulses from composite successfully. Test results also indicate the pulse-based data transmission is valid for a similar indoor environment.

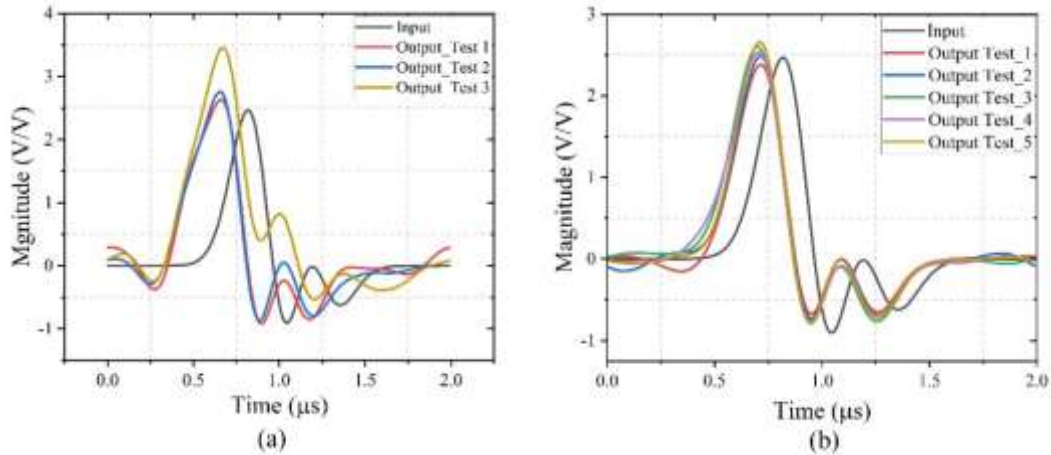


**Figure 5.8:** Simulated results for (a) room to room and (b) corridor communication.

### 5.5.5 Room to Room Measurements at Different Location

This chapter also investigates the room-to-room channel effects by placing the  $R_x$  antenna inside and the  $T_x$  antenna outside of the room. The room size is  $5.13 \times 2.43 \times 2.74 \text{ m}^3$ ,  $3.35 \times 2.74 \times 2.74 \text{ m}^3$ , and  $3.35 \times 3.35 \times 2.74 \text{ m}^3$  with consisting gypsum board, wooden door, computer desk, chair, and dry concrete walls. Fig. 5.8(a) shows the comparison results of the simulated numerical output at different indoor room sizes. The numerically simulated signal produced pulse spreading, time delay, and an initial negative dip after penetrating the walls. It makes sense the physical signatures occur for the presence of channel obstruction, reflection by furniture, etc. Test results also shows similar characteristics in different channel blockages with materials, sizes, and their combinations as shown in Fig. 5.7. However, the individual pulses are decoded from the composite signal by increasing the signal magnitude. Test results also represents the propagation capability of the composite pulse signal through penetrating the room walls. Fig. 5.8(b) shows the

test results at different positions, considering both narrow and wider spaces of the floor corridor. Test results validates the real scenario of indoor pulse transmission.

## **5.6 Modification of Receiver Architecture**

The extensive analysis using network parameter measurements helps design the pulse decoding receiver architecture. The numerically simulated output is obtained from the measured  $S_{21}$  component, considering different case studies for indoor environments to analyze the feasibility of the proposed measurement scheme. This section is divided into three subsections and discuss as follows with a brief description.

### ***5.6.1 Automatic Gain Control***

The AGC is implemented in a radio receiver to maintain a constant output signal due to the fading propagation. The amplitude of an incoming signal in the receiver varies over wide dynamic ranges depending on the channel characteristics. AGC provides a relatively constant amplitude by adjusting the gain parameters continuously. Test results show that the AOP signal distortion, spreading, and phase shifting occurs with variation of dielectric properties of obstacle materials, multi-path interference's, and indoor wave propagation. These external factors significantly affected the transmitted signal and attenuated randomly for the variation of channel properties. The previous section discussed the impact of signal magnitude variation in detail to decode individual pulses from the composite signal. The individual pulses are decoded using correlation peak analysis form the received composite after boosting the magnitude by different factors to maintain a fixed level. Though the LNA is amplified the signal level to a fixed stage of the received RF signal; however, further magnitude adjustment is required to obtain a certain level from

1.75 to 2.75 for multi-path reflections and fading propagation. Therefore, an AGC is critically needed to maintain a fixed magnitude around 2.50 by controlling the variable gain based on the variations of the incoming received signal at the receiver.

### ***5.6.2 Threshold Level Section for Pulse Elimination***

Recovering the transmitted pulse signal is essential in the promising AOP-based SE wireless data telemetry to support large volume sensor channels in high-density IoT networks. The correlator-based pulse decoding scheme is used to decode individual pulses from the composite signal by correlation peak analysis. The evaluation of the pulse decoding scheme shows the threshold level varies between  $\pm 0.45$  to  $\pm 0.60$  from case to case study for eliminating all the individual pulses sequentially. This chapter also verified the decoding scheme by creating a composite signal using different order AOPs. The critical finding through extensive measurements shows that the threshold selection significantly affected by presence or absence of  $MHP_0$  pulse in composite signal. However, all the distinct order pulses are successfully decoded from the combined signal by sliding the threshold level. The optimal threshold level is also selected at  $\pm 0.45$  through the investigation of channel effect analysis. The decoding scheme first checks the phase status of the received signal. If the combined signal is out of phase, then select the threshold level at -0.45; otherwise, it will 0.45 to decode the pulses from the composite signal successfully.

### ***5.6.3 Pulse Elimination Results***

Fig. 5.9 (a) shows the pulse decoding results in 8.0 ft antenna separation. The eliminated pulses ( $R_X$  pulse) are plotted in the same figure to compare with the transmitted pulses ( $T_X$  pulse). In the correlator receiver, the received composite signal is correlated with the individual template pulse signal sequentially and finds the correlation peak. If the

correlation peak is greater than the predefined threshold level, the corresponding analog pulse is eliminated from the composite signal, and the index is set equal to '1'. If the correlation peak is lower than the threshold value, the index is set to '0', which means the corresponding pulse is absent in the received signal. After eliminating all the distinct pulses, it compared with a prior known encoding template to find the missing data channel.

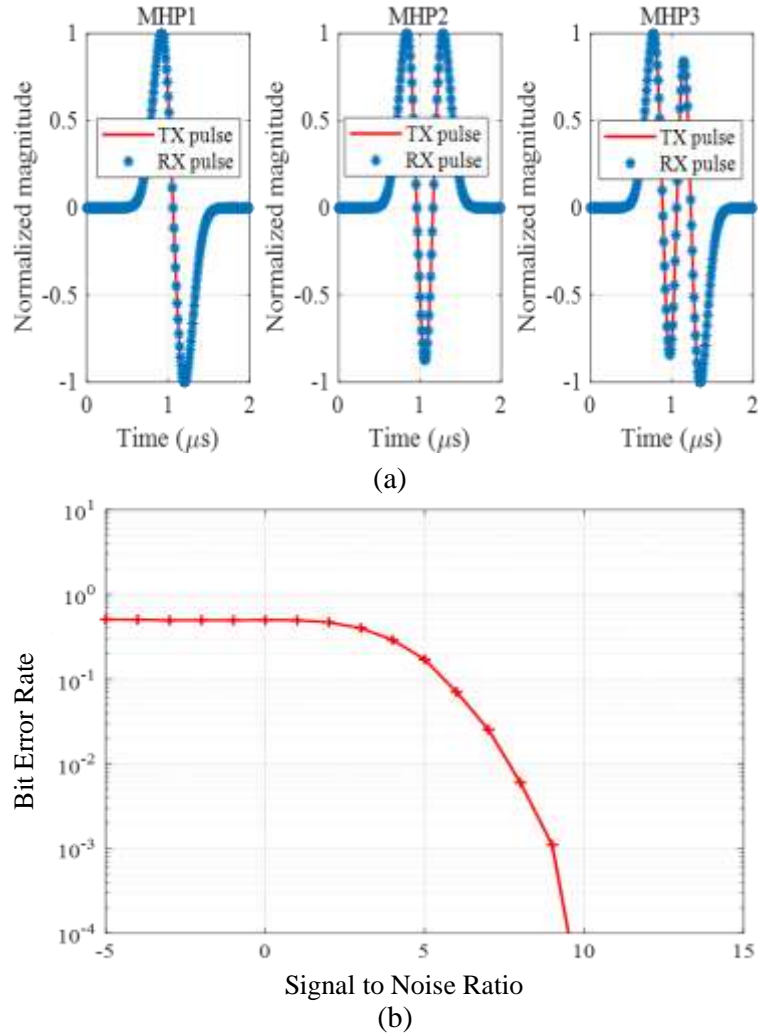


**Figure 5.9:** Simulation results (a) encoded and decoded pulses and (b) BER.

Fig. 5.9(b) shows the performance of an AOP-based data transmission scheme for single-user applications by analyzing the BER. In this experiment, the analog pulse is used to modulate  $1 \times 10^6$  bits by OOK modulation. The 500 MHz carrier is used for frequency

shifting the encoded pulse train. Then the signal processing is applied to get the simulated numerical output by the measured  $S_{21}$  component. The numerical simulated output is down-converted using the same carrier to get the baseband signal and checked the BER. In this dissertation work, the BER is checked by adding the AWGN channel model by varying the SNR from -5 dB to +15 dB. The investigation results also shows the critical finding for optimal threshold level at  $\pm 0.45$  and maintains the magnitude  $\sim 2.0$  to decode all the pulses from the composite signal successfully. Test results also suggest the pulse-based data telemetry is suitable and feasible with the existing communication architecture, network protocol, and spectrum sharing for supporting high-density IoT devices. The BER analysis also verifies the performance of analog pulse transmission for IoT data telemetry.

## 5.8 Conclusion

This chapter presents the channel effects on the AOPs for pulse-based data transmission that is critically needed for indoor wireless telemetry and object sensing applications. The extensive channel effects investigation verifies the feasibility of the AOP transmission technology for the next generation high-density IoT networks in indoor applications. The less complex signal processing for time-frequency analysis provides the real scenario of the communication channel impacts on AOPs for indoor environment. Measurements results shows that the physical signal distortion of analog pulses for the propagation through the wireless communication channel and finds critical improvement for optimal threshold selection to decode individual pulses from their composite signal. It also suggest the proposed pulse-based scheme is feasible with the existing communication channel and limited spectrum for sensor data transmission.

## CHAPTER 6

### PROTOTYPE DEVELOPMENT AND TEST RESULTS

#### **6.1 Introduction**

In this chapter a prototype test platform is developed and configured using the existing communication architecture and network protocol to validate the proposed AOP-based short-range wireless data telemetry. The prototype platform is built using the commercially available customize RF modules. Prototype development includes the Arduino programming, configuring the transceiver, design and development of RF mixer driver, and LPF circuit. Test results shows the evaluation of individual encoding and decoding schemes for analog pulse-based high-volume data compression and decompression. This chapter is divided into three (03) main sections to develop the prototype test platform and validate the proposed scheme for wireless data telemetry.


#### **6.2 Arduino Implementation**

Arduino MKR WiFi 1010 allows the building of an innovative project. It is easy to implement the Arduino platform and IoT cloud-compatible boards. It can connect devices, visualize the testing data, and control and share projects through the IoT cloud from anywhere in the world. The Arduino MKR1010 is the economical, simplest, and most accessible platform to develop WSNs for IoT connectivity. Table 6.1 presents the technical specifications of the MKR1010 microcontroller board. It has a 48.0 MHz clock speed and



256 kB flash memory storage. The MKR1010 board has one analog output,  $A_0$  pin and seven analog input,  $A_{in}$  pins. Also, it has the popular Arm® Cortex®-M0 32-bit SAMD21 processor with a large variety of shields to build projects. The MKR1010 board is selected in this work to demonstrate analog pulse-based telemetry for short-range IoT applications.

**Table 6.1:** Technical specifications of MKR1010 microcontroller board.

Image	Specification	Feature	Specification	Feature
	Name	MKR WiFi 1010	Clock speed	48 MHz
	Board	SAMD21 cortex	I/O voltage	3.3 Vdc
	LED pin	6	I/O current	7.0 mA
	Digital I/O	8	Memory	256 kB flash
	ADC pins	7 (8/10/12 bit)	UART	Yes
	DAC pin	1 (10 bit)	I2C	Yes
	PWM pins	13	SPI	Yes

The distinct PSs are created by utilizing the memory-storage analog pulses. The PS generation, data encoding, and compression algorithms are implemented into the MKR1010 board using the Arduino platform to verify the proposed data telemetry. The encoding schemes are verified by MATLAB® programming first, then developed by Arduino programming for experimental validation. In this dissertation, the NB communication is chosen with a constant pulse duration of  $T_S = 600 \mu s$  based on the trade-off between hardware limitations of the MKR1010 board, laboratory test facilities, and pulse transmission rate. The multi-order AOP information is stored in the SD card, where each analog pulse comprises 136 samples and the total memory occupied by ~4.0 kB for 4-distinct pulses. The pulse information is obtained from the SD card through serial communication and stored in a dummy variable in MKR1010 flash memory to develop the PS generation and data encoding for rapid prototyping. The data-encoded pulse train or UCP signal is directly taken from the  $A_0$  pin of the MKR1010 board. This dissertation work interface the analog output of the MKR1010 signal with the RF chain via a driver circuit

to drive the mixer module by the low-power microcontroller signal. The prototype Tx and Rx model is configured to validate the analog pulse-based high-density wireless telemetry.

### 6.3 Configuring Communication Architecture

A prototype test platform is configured by using the commercially available RF modules. The standard communication architecture, network protocol, transmitter and receiver model, and channel has been used to configure the test platform. Table 6.2 represents the list of customized RF modules. In this work, the individual RF modules are integrated into the Tx and Rx model to validate the system experimentally. All the RF modules, co-axial cables, and RF connectors are calibrated using the VNA before integrating into the communication system. The system configuration has checked using a sync pulse signal. The lab equipment's used for RF signal characterization including the frequency spectrum analyzer to observe the signal spectrum and measure the frequency spectrum and strength. After configuring the communication channel, the analog pulse-based encoding is developed into the MKR1010 board and integrated into the communication platform with the commercially available off-the-shelf RF modules.

**Table 6.2:** Selected customize mini-circuits RF modules for transceiver configuration.

RF modules	Frequency range	Model number	Source
Mixer-1	0 to 1.0 MHz	ZAD-8+	Mini circuits
Mixer-2	1 to 500 MHz	ZX05-1-S+	Mini circuits
Power amplifier	1 to 1000 MHz	ZFL-1000B+	Mini circuits
Low noise amplifier	1 to 1000 MHz	ZFL-1000 LN+	Mini circuits
Oscillator	300 to 525 MHz	ZOS-535+	Mini circuits
RF antenna	433 MHz	ANT-4WHIPH-SMA-ND	Digi-key

A prototype test platform is developed to validate the pulse-based telemetry considering a double-stage superheterodyne radio transmitter and receiver architecture.

First, the low-frequency test signal, Sync pulse is translated to 1.0 MHz by mixer-1, ZAD-8+ using a sinusoidal carrier signal generated by the function generator to meet the input requirements of mixer-2, ZX05-1-S+. The second stage frequency conversion is occurred by mixer-2 using a 500 MHz local oscillator, ZOS-535+ signal. Then the output of mixer-2 is amplified by a PA, ZFL-1000B+ before transmitting through the RF antenna, ANT-4WHIP3H-SMA of band frequency ranges 430 MHz to 470 MHz for wireless transmission. The local oscillator signal feeds to both mixers via RF-splitter, ZESC-2-11+ with an equal length of co-axial cable to modulate and demodulate the baseband signal using the same carrier multiplication.

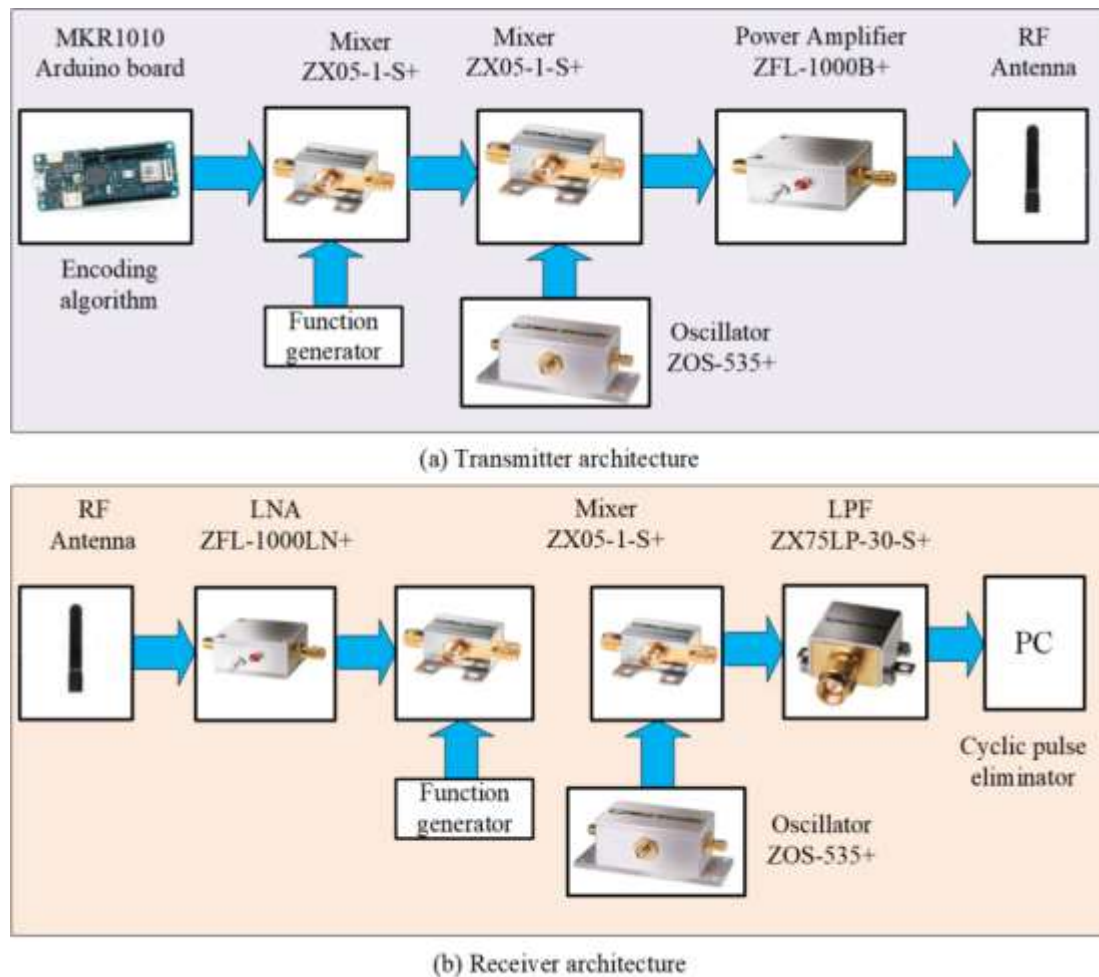


**Figure 6.1:** Configuring transceiver architecture using RF modules (a) Tx and (b) Rx.

At the receiver, the transmitted analog pulse train is received by the RF antenna and passed through the RF chain again for signal amplification by LNA, ZFL-1000LN+, frequency down conversion through step by step using 500 MHz carrier multiplication in Mixer-2, ZX05-1-S+ and 1.0 MHz carrier multiplication in Mixer-1, ZAD-8+. The frequency-demodulated signal is passed through a LPF circuit to recover the baseband signal frequency. The circuit design and implementation of the RF-module driver and the LPF are discussed in the next section.

#### **6.4 Design and Implementation of Driver and LPF circuit**

The serial transmission analog out of the microcontroller board represents the analog pulse signal, which contains  $0.75 V_{dc}$  offset and provides insufficient power to drive the RF mixer-1, ZX05-1-S+. Therefore, a low-power analog circuitry-based driver circuit has been designed and implemented to drive the RF mixer module using the low-power microcontroller signal. Similarly, the LPF has been designed and implemented to retrieve the baseband signal after removing the high-frequency noise. The circuit design and implementation are described in the following subsections.

##### ***6.4.1 Driver Circuit Design for RF Mixer Module***

Fig. 6.2(a) shows the configuration of the RF driver and RC filter circuit. It comprises the DC filter, buffer, level shifter, and current amplifier. The RC filter removes the dc offset from the analog pulse signal. The buffer is a unity gain amplifier whose primary function is to transform the impedance from one circuit to another and isolate the source. In this circuit, the buffer is used to match the impedance with the RF mixer and isolate the microcontroller board from the next stage current amplifier to avoid damage.

The second stage of the RF driver circuit is designed with the first-order Butterworth filter to pass a specific passband signal and avoid the anti-aliasing effect along with increasing the signal strength. In this application, the Butterworth low-pass filter is designed with a cut-off frequency of 1.5 kHz and with a passband gain of 0.5 to adjust the input power requirements of the RF module. The final stage of the driver circuit is the current amplifier or level shifter to increase the current level of the analog pulse signal without increasing the magnitude. The level shifter circuit is designed by using BJT. The input power requirement of the RF mixer module is  $50.0 \text{ mW}_{\text{rms}}$  with a  $50 \Omega$  input impedance. The current buffer is designed to increase the level and meet the input power at a fixed  $1.0 \text{ V}_{\text{pp}}$  low-frequency signal to drive a  $50 \Omega$  resistive load.

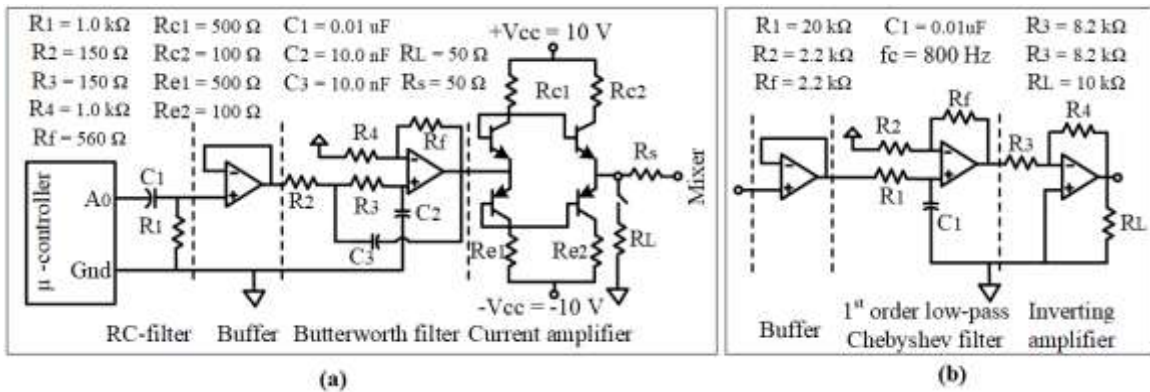


**Figure 6.2:** Design and implementation of (a) low-power driver circuit and (b) LPF.

#### 6.4.2 Low Pass Filter Design

Fig. 6.2(b) shows the LPF circuit to recover the base band signal. The LPF module consisting with buffer amplifier, first-order low pass filter, and non-/inverting amplifier. The buffer amplifier isolates the received signal from the RF-module. The received signal amplitude is few mV and remain under the noise signal. The first order LPF removed the unwanted noise signal and passed the desired frequencies 0 to 1.0 kHz without increasing the signal magnitude. The passband cut-off frequency is designed corresponding to the transmitted baseband signal frequency. The last

stage of a LPF module is the signal amplification to increase the strength for better visualization and adjust the magnitude for correlation with the template to decode the transmitted data bits.

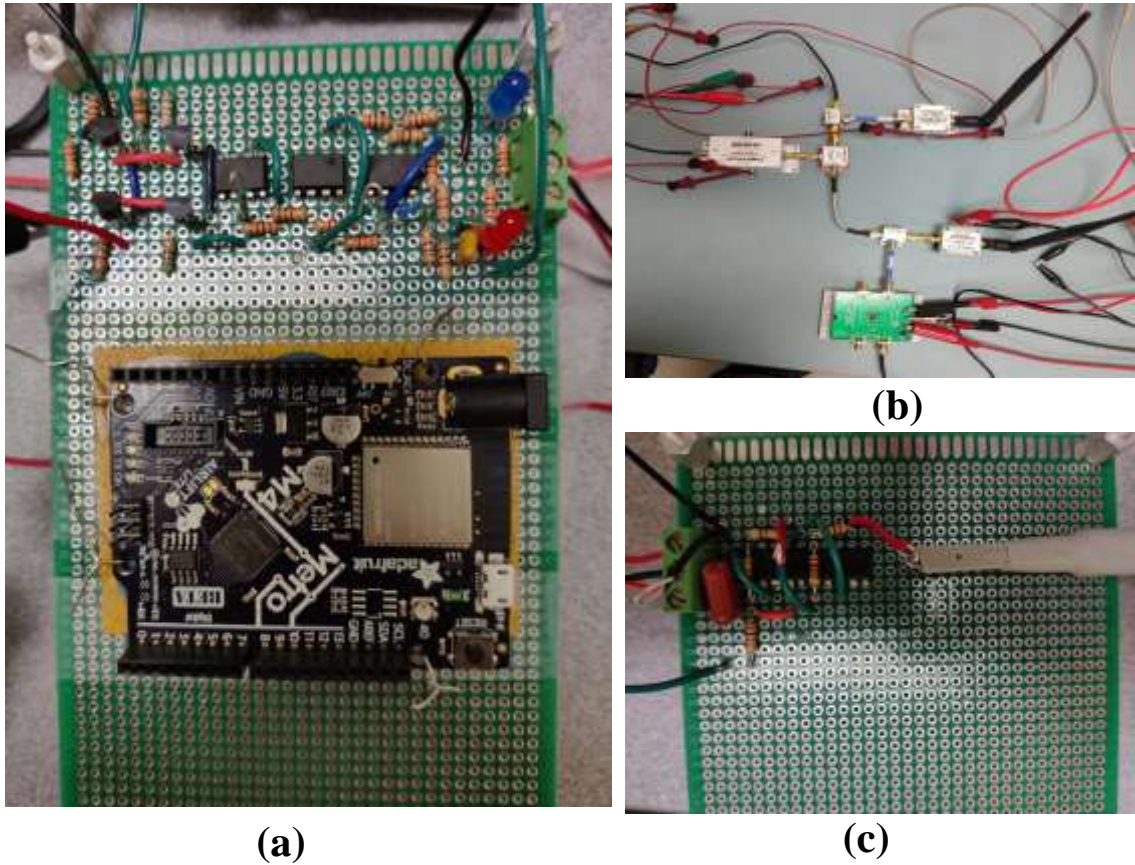


**Figure 6.3:** Prototype design (a) driver circuit, (b) evaluation board, and (c) LPF.

#### **6.4.3 Experiment Test Results for Driver and LPF Circuit**

Fig. 6.3(a) shows the hardware implementation of the RF mixer driver circuit. The driver circuit comprises dc filtering, level shifting, and a current buffering section to drive the mixer block. The driver circuit first designs and simulated by LTSpice simulation tools to select the component values and performance. Then it implements into a hardware circuit using a vector board for rapid prototyping. Fig. 6.3(b) shows the customized evaluation board of LPF to retrieve the baseband signal after frequency down-conversion using the same carrier multiplication. The commercially available LPF module can't

recover the baseband signal frequency in the proposed analog pulse communication. The baseband frequency of the pulse signal is in a few Hz levels, while the customize LPF module is available in a few kHz to MHz. In this dissertation work, an LPF circuit is also designed and implemented to recover the low-frequency signals. Fig. 6.3(c) represents the LPF circuit implemented into the vector board. The cutoff frequency is chosen based on the multi-order AOPs and their composite signal, then simulate the circuit in LTSpice simulation environment to select the component and circuit parameter's value. Finally, the filter circuit is implemented into the vector board.

Fig. 6.4 shows the hardware-implementation results of the RF mixer driver circuit. After design and hardware implementation, the circuit performance is evaluated using a known sync pulse signal. The yellow and green traces in Fig. 6.4(a) show the mixer input and output signal, respectively. A 1.0 kHz sync pulse is generated using the function generator and fed to the driver circuit input. The driver circuit's output is then fed to the RF mixer input terminal, and the mixer output signal is observed. Fig. 6.4(b) shows the analog pulse test results. The yellow and green trace shows the output and input of the driver circuit. In this test, the microcontroller analog signals feed to the driver input terminal and take the production after connecting the RF mixer block. The output signal of the driver circuits shows it can increase the power level without signal distortion and drive a resistive load. However, the signal level goes to zero at the driver output terminal after connecting the RF module. There were two reasons (i) impedance mismatching and (b) input frequency range of the RF mixer input terminal. First, the baseband analog pulse is multiplied by a 1.0 MHz sinusoidal carrier signal. Then it passes through the RF chain via the microcontroller and driver circuit to solve the mismatching issue.





**Figure 6.4:** Driver circuit test using (a) known sync and (b) proposed analog pulse signal.

Fig. 6.5 shows the carrier-modulated multi-order AOPs. Finally, the channel has been configured by the commercial RF modules for indoor environment testing and validating the AOP-based short-range wireless data telemetry.

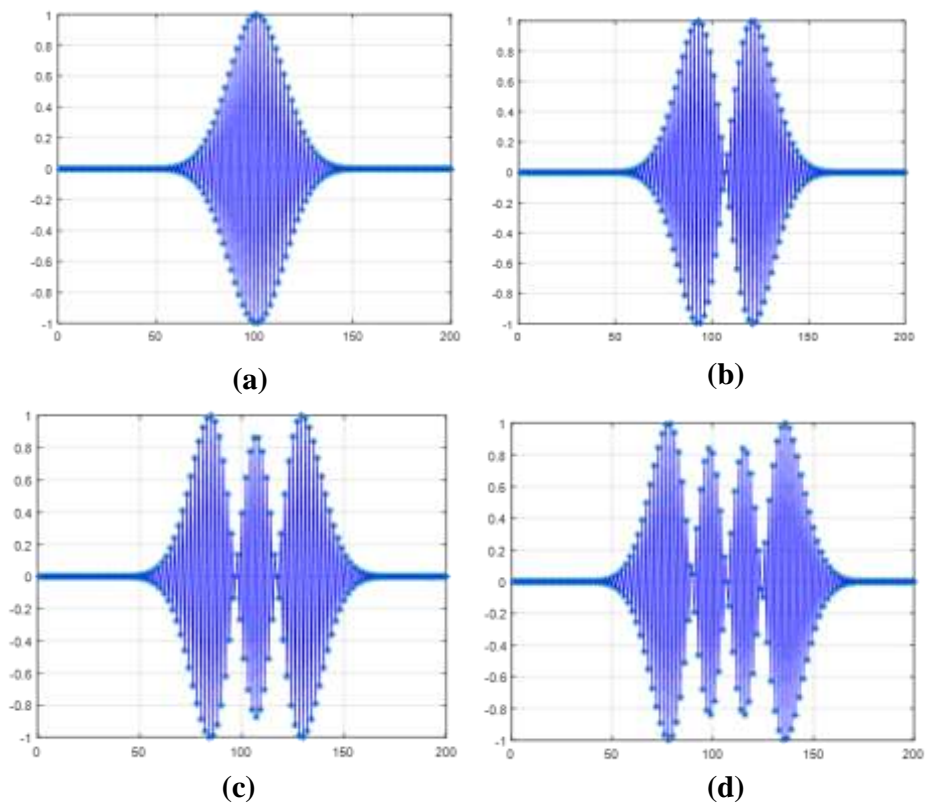


**Figure 6.5:** Amplitude modulated of multi-order AOPs by 1.0 MHz carrier frequency.



Fig. 6.6: shows the test results of RF transceiver configuring using the customize RF modules for analog pulse-based wireless data telemetry. In all the test, channels 1, 2, and 3 in Fig. 6.6 represents the received signal, RF mixer input/driver output signal after connecting the RF mixer, and transmitted signal at 500 MHz. This test fed the microcontroller signal to the RF mixer input terminal through the RF driver circuit. The driver circuit is designed and implemented to match the mixer module's input impedance and power requirements. Then, the mixer output signal is amplified by a PA before transmitting via an RF antenna. The RF antenna receives the transmitted signal in the receiver and passes through the RF chain to recover the baseband signals.

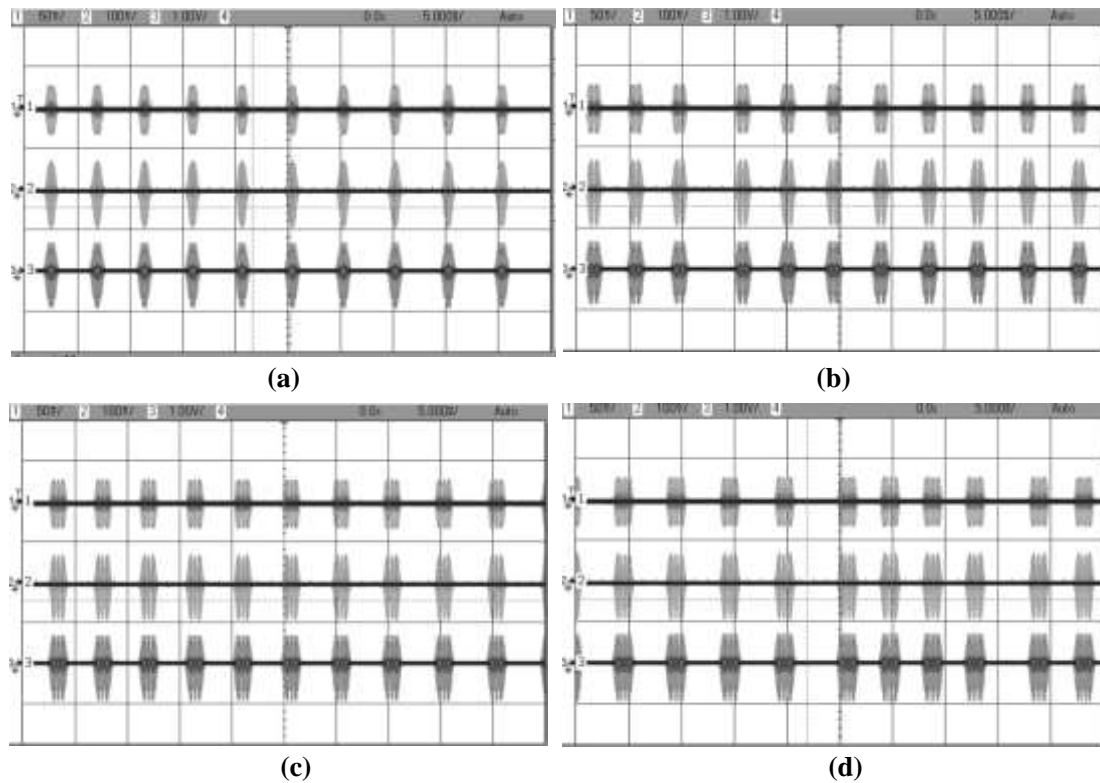


**Figure 6.6:** Test results for the (a) MHP<sub>0</sub>, (b) MHP<sub>1</sub>, (c) MHP<sub>2</sub>, and (d) MHP<sub>3</sub> signal.

Fig. 6.7 shows the frequency spectrum of the proposed analog pulse signal for indoor wireless data communication. The analog pulse signal is translated to higher

frequency by a 500 MHz carrier signal. Fig. 6.7(a) shows the frequency spectrum of a single order AOP signal at center frequency 490 MHz with a signal bandwidth 1.0 MHz. Fig. 6.7(b) shows the spectrogram of the multi-order analog pulse train. The frequency spectrum is observed in the full range of the spectrum analyzer from 0 Hz to 3.0 GHz. There are six spectrum corresponding each pulse signal at 490 MHz frequency band within the full frequency span. This results shows that the proposed AOP signal is capable and compatible for indoor short-range wireless data telemetry.

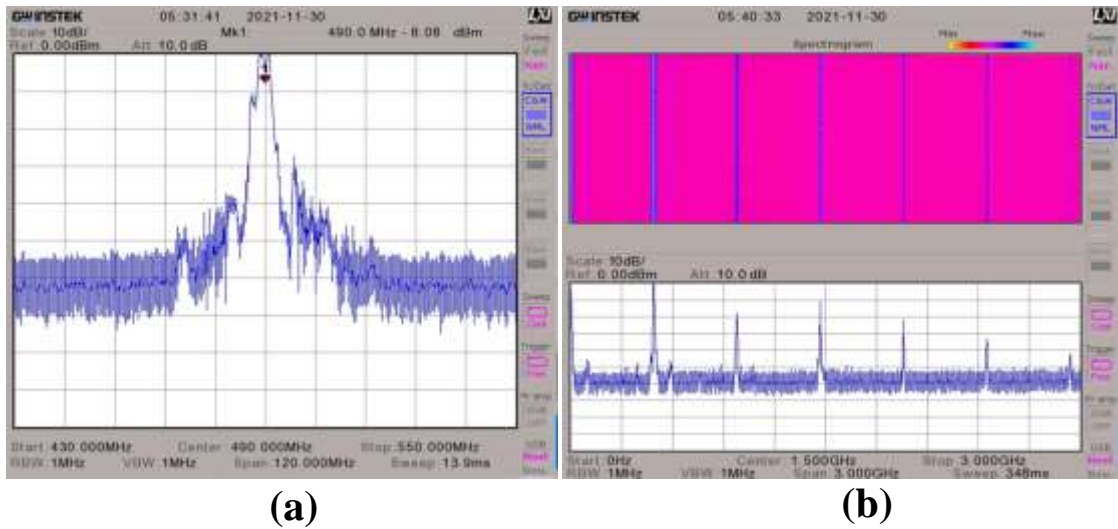


**Figure 6.7:** Test results (a) frequency spectrum and (b) spectrogram of AOP signal.

Fig. 6.8 shows the test results of transmitted RF and received RF signal via the RF transceiver for indoor wireless communication. The transceiver model has been revised and configured according to the superheterodyne architecture to solve the input frequency requirements of mixer ZX05-1-S+ module. The microcontroller signal is first translated into 1.0 MHz by mixer ZAD-8+ module. Then the output of first stage mixer is once again shifted to 500 MHz sinusoidal carrier signal by second stage frequency up-conversion. Similarly, the received signal is down-converted into two stage by the same carrier frequency, respectively. Fig. 6.8(a) the yellow and green trace shows the second stage

frequency down-converted of the received signal, the input of LPF circuit which contains high frequency noise signal. The LPF circuit is designed and implemented to remove the high frequency noise and retrieve the transmitted base band signal as shown in green trace. The RF mixer module inherently added noise with the base band signal by back propagation. Fig. 6.8(b) shows the transmitted and received pulse signal. The orange and green trace indicates the received signal at LPF and the driver circuit, respectively.

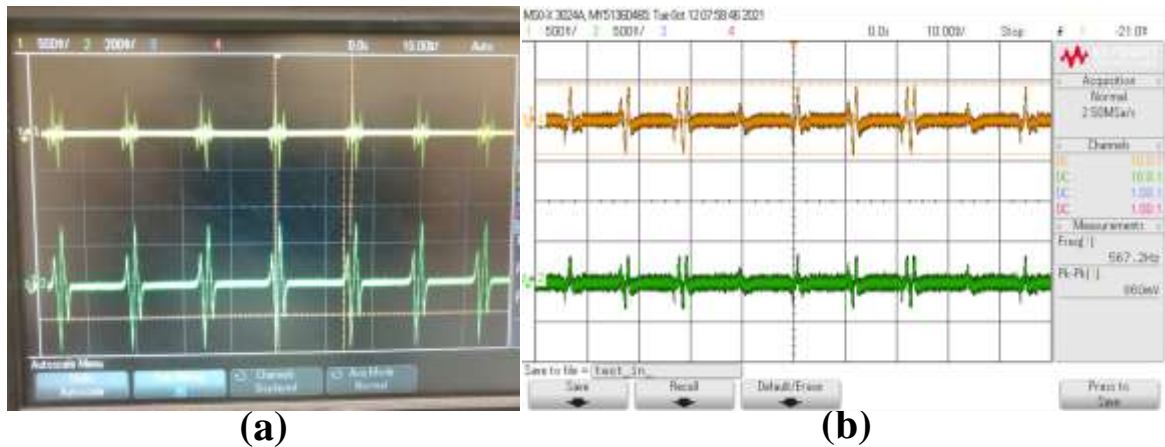


**Figure 6.8:** Test results (a) without LPF and (b) with LPF to remove noise signal.

Fig 6.9 shows the test results of analog pulse transmission using for short-range wireless telemetry in indoor environment using the conventional communication architecture and network protocol. The orange, green, and blue traces indicate the received and transmitted analog pulse train, and the carrier modulated signal at 500 MHz, respectively. In this demonstration, the different order analog pulse signal is stored in microcontroller flash memory and fed the analog out pin signal to RF mixer through driver circuit. The rest results shows that the multi-order analog pulse signal is capable and compatible with the existing communication architecture for short-range wireless data telemetry. The existing FPGA based transceiver architecture has been designed and implemented only for digital pulse communication which is incompatible for analog pulse

format. This prototype development also validated the hardware implementation of the transceiver for analog pulse transmission for wireless telemetry.

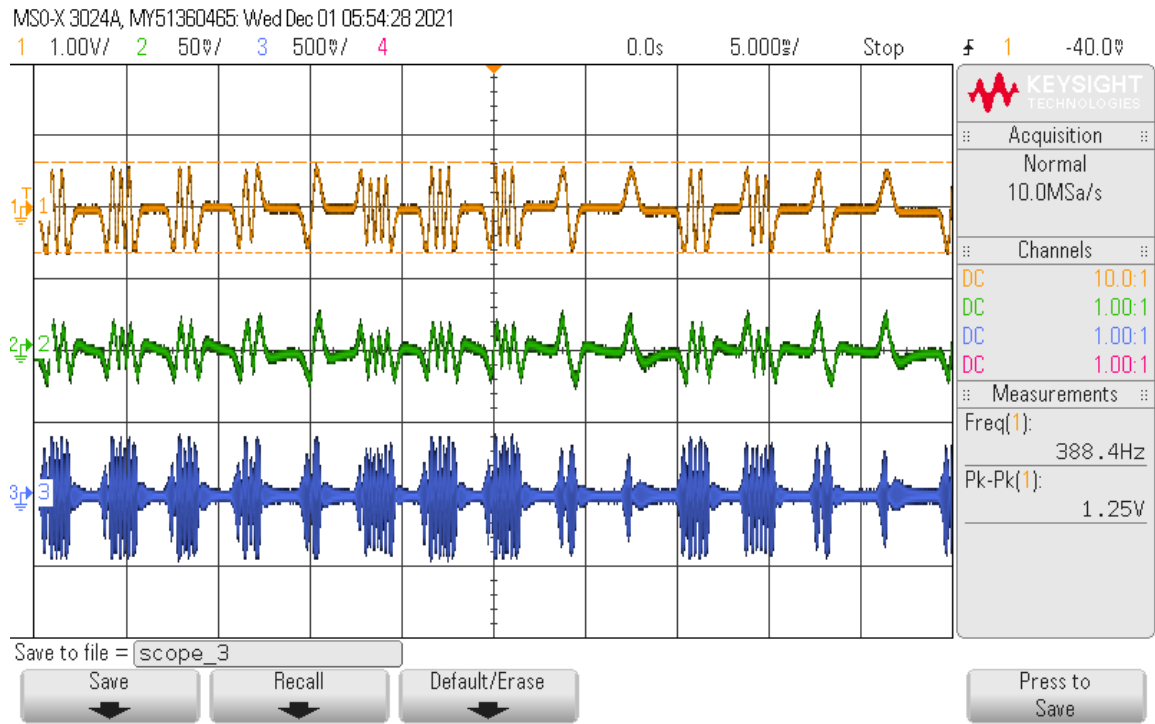
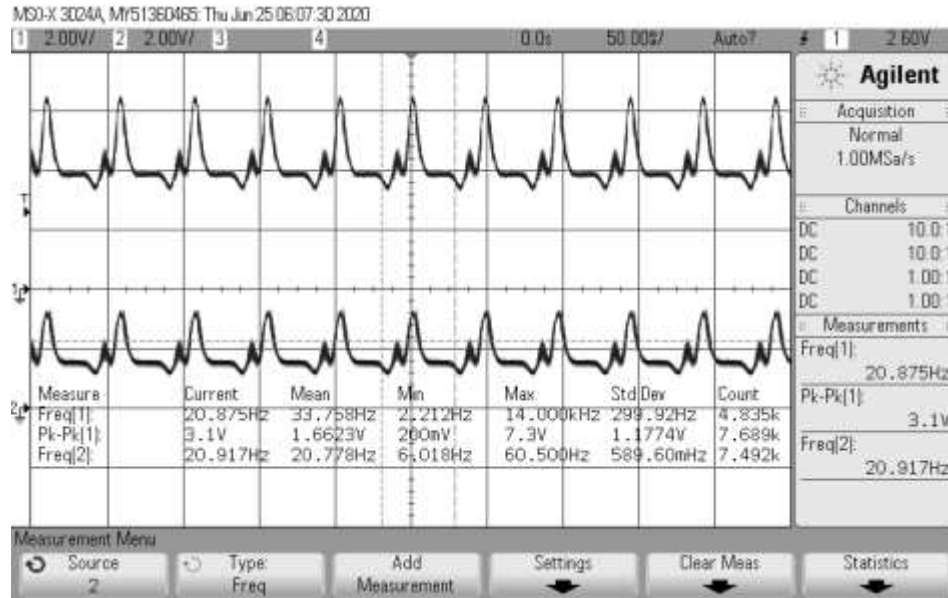


**Figure 6.9:** Test results for different order AOPs in short-range wireless telemetry.

Fig. 6.10 shows the test results for composite signal. The performance of the RF mixer driver circuit is tested using the composite pulse signal. In Fig. 6.10(a), channel 1 and 2 indicates the input and output composite signal of the driver circuit. Test results shows that the driver circuit successfully drive the RF mixer using composite pulse signal which comprises multiple peak value. The analog circuitry based level shifter and filter circuit is capable to recover the small dip without the signal distortion. Fig. 6.10(b) represents the frequency spectrum corresponding the composite signal. Test results shows the signal has the spectrum in the center frequency at 490.31 MHz.



(a)

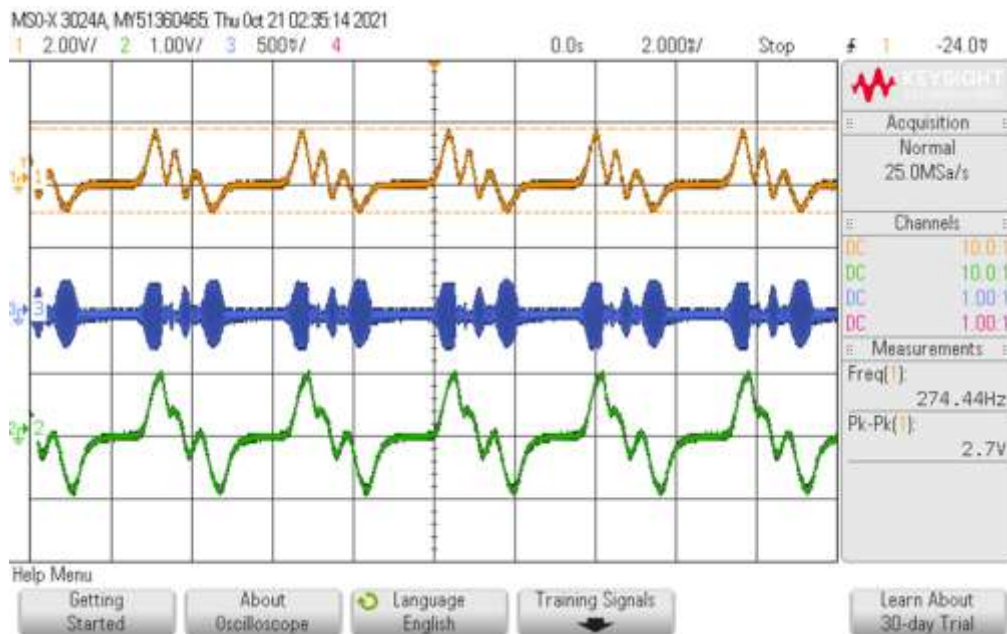


(b)

**Figure 6.10:** Test results for composite signal (a) driver circuit and (b) frequency spectrum.



(a)



(b)

**Figure 6.11:** Test results for composite signal (a) without LPF and (b) with LPF.

Fig. 6.11 shows experimental results for the composite pulse signal transmission and reception for the short-range wireless data telemetry. Test results shows that, the driver circuit is also capable to drive the RF mixer circuit and the LPF retrieve the transmitted



composite signal successfully without signal distortion. Fig. 6.11(a) shows the test results to transmit and receive composite pulse signal for analog pulse based compressed data volume. The orange, blue, and green traces indicate the transmitted composite pulse signal, frequency up-converter signal at 500 MHz in transmitter, and frequency down-converted signal at the receiver, respectively. In Fig. 6.11(b) the green trace depicts the LPF output that retrieve the transmitted signal successfully after removing the high frequency noise.

### 6.5 Prototype Test Platform

A prototype high data density wireless test platform is realized by integrating the discrete parts, including the microcontroller board, RF driver circuit, and RF chain block in the Tx section. Similarly, the RF chain and LPF module are integrated into Rx section to develop the test platform. Fig. 6.12 shows the prototype test platform development using the customize RF modules for AOP-based high-density wireless data telemetry. In Fig. 6.12 the right side represents the Tx and the most left is the Rx.

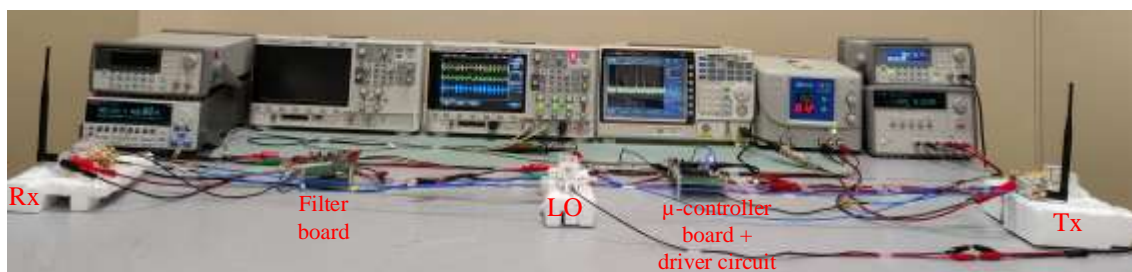


**Figure 6.12:** Prototype test platform development using customize RF modules.

In the Tx section, the pulse-based data encoding algorithm is implemented into MKR1010 board. The RF mixer translated the low-frequency analog pulse signal to high-frequency at 500 MHz using a sinusoidal carrier signal. Then the PA is used to increase the output of the RF mixer before transmitting it through the RF antenna. The transmitted

composite pulse signal is received by Rx antenna and passed through the RF-chain for amplification, frequency down-conversion, and recovered the baseband signal. Finally, the correlator receiver decodes the individual pulses sequentially from the received signal.

### ***6.5.1 Test Results for Multi-bit Encoding***

The 3-bit encoding scheme is considered in this demonstration and evaluated the performance through prototype test platform to validate the PI encoding. Fig. 6.13 shows the test results of the proposed PI scheme at 500 MHz frequency band. The green, yellow, and blue traces show the multi-bit data encoded analog pulse train, received signal, and carrier modulated signal at 500 MHz. The transmitted bitstream is first divided into 300 bits per block for 100 pulses to simplify the encoding scheme. Then, the 300 bits data frame is encoded by the memory storage AOPs as described in *chapter 03*. In front of each data encoded 100 pulse frame, a zero-order pulse is added to simplify the time synchronization complexity for correlator receiver. Full-length of the oscilloscope window is captured and saved the received pulse frame into a flash drive for offline signal processing. In signal processing, the first step is to find the starting point of the data encoded pulse frame through the indicator pulse detection. Then, the received pulse frame is divided into  $136 \times 100$  matrix for 100 pulses based on the sample points of the corresponding single pulse. After that, the correlation peak is applied to check the correlation sequentially with the memory-based pulse template and decode the transmitted data bits. This work used the threshold level at 0.85 to recover the received pulse signal. If the correlation peak is higher than threshold level then corresponding pulse signal is present and print the index number. Finally, the index number is converted to 3-bit data with the prior known encoding template. The correlation peak based decoding also simplifies to find the missing transmitted data bits.



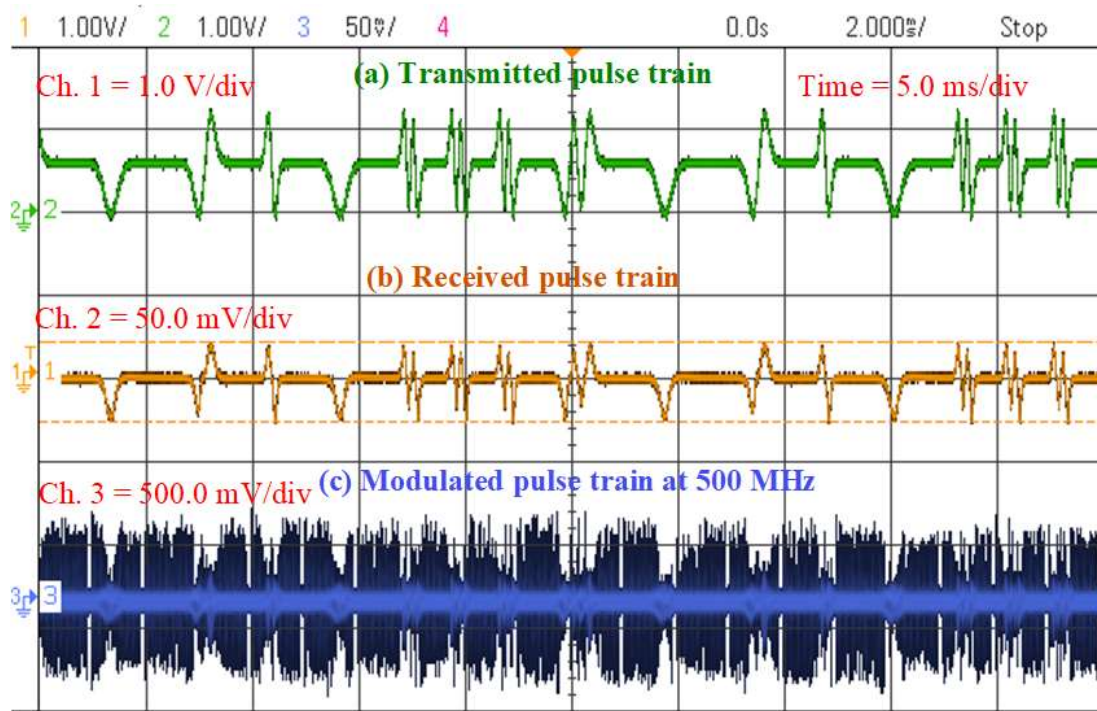
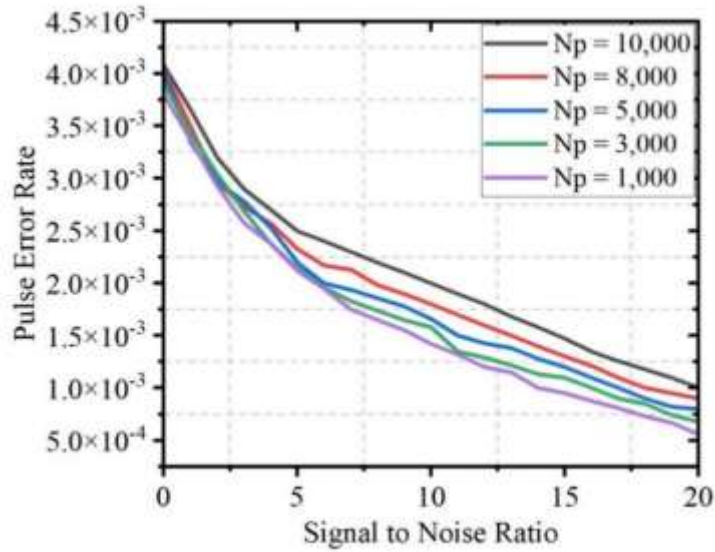


**Figure 6.13** Test results of pulse train (a) transmitted, (b) received, and (c) modulated signal at 500 MHz.

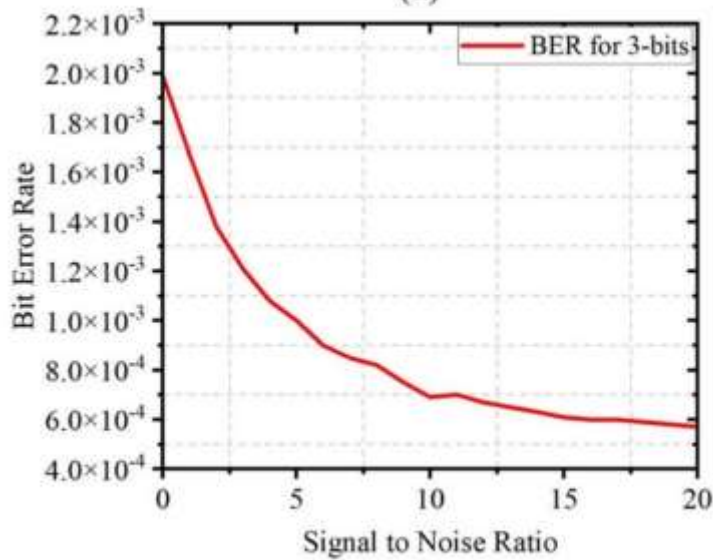
### 6.5.2 BER and PER Investigation for PI Encoding Scheme

To demonstrate the performance of the proposed techniques, the PER and BER are evaluated with different test conditions. The error rate is calculated by adding the AWGN signal with the test results and varying the SNR from 0.0 dB to 20.0 dB. Fig. 6.14(a) shows the test results of PER at different number of pulse frame transmission. Test results show that the error rate increases with increasing the frame size of the transmitted pulses, which is same as the simulation results. The BER is also investigated to validate the performance of the proposed PI encoding. Fig. 6.14(b) shows the test results of BER of the multi-bit encoding using single order AOPs. The experimental results experiences the reflections from different objects in door environment, including the electronic devices, surrounding objects, reflections from human body, channel noise, measurement noise, noise made by human and hardware circuit, etc. Therefore, the BER is little-bit higher in the test ( $7.5 \times 10^{-$

<sup>4)</sup> compared to the simulation ( $1.0 \times 10^{-4}$ ) at  $\sim 10.0$  dB SNR for 3-bit encoding, but it satisfies the lower bound for wireless data transmission. Test results shows that the single order pulse based multi-bit data transmission is suitable for short-range SE wireless telemetry.



(a)



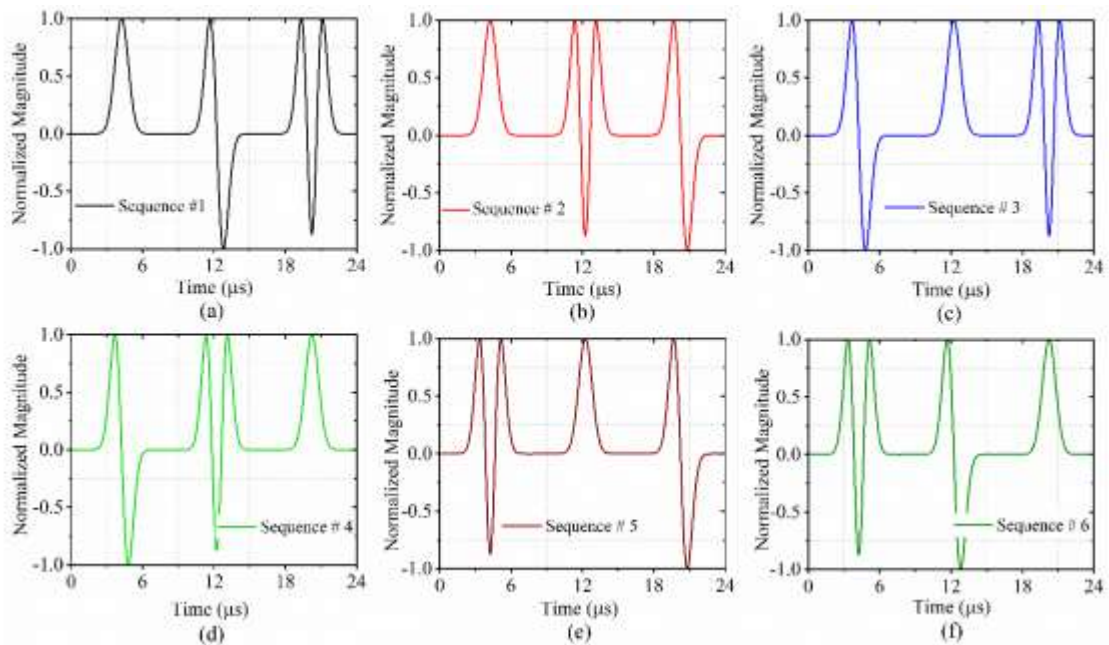
(b)

**Figure 6.14:** Test results (a) PER and (b) BER for multi-bit data transmission.

### 6.5.3 Test Results for Pulse Sequence Based Encoding

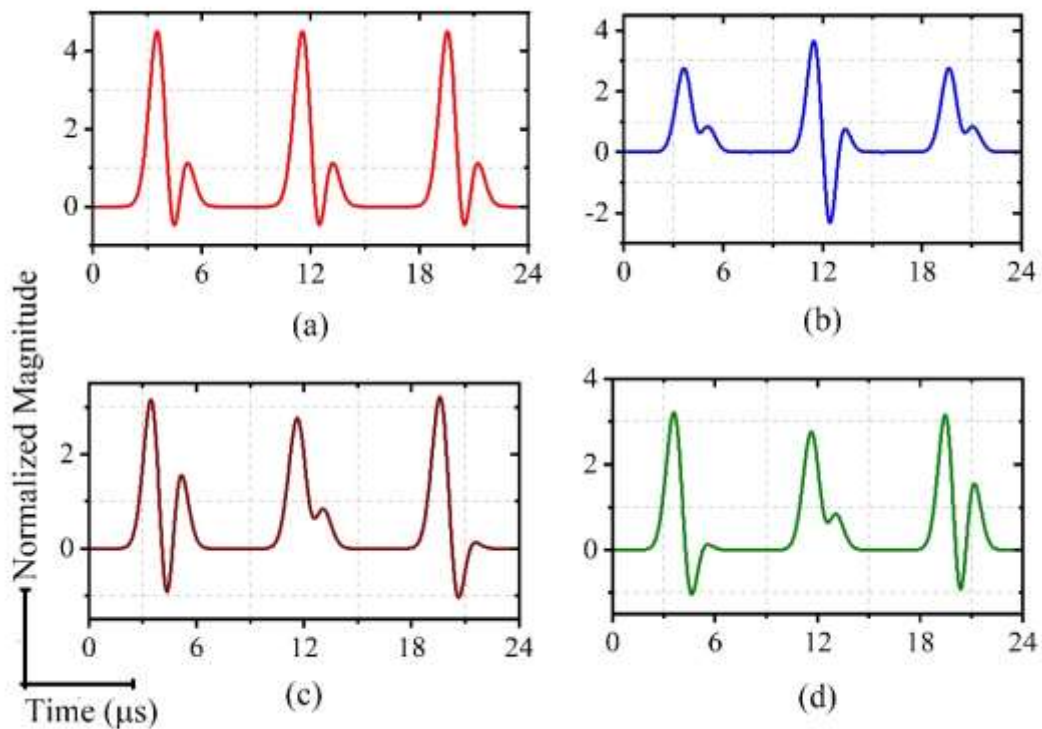
In this dissertation work, the 3-pulse system is considered to simplify the data channel encoding and validate the PS-based wireless telemetry. The PS generation

algorithm creates a total of 6 distinct PSs and each sequence comprises 3-different order pulses without any redundancy. Fig. 6.15 shows the PS generation results using multi-order AOPs. Test results shows that the width of individual pulse signal is 8.0  $\mu$ s and the total length of a PS is 24.0  $\mu$ s. The data encoding algorithm creates the UCP signal to compress the data volume. Fig. 6.16 shows the UCP signal at different test conditions. The UCP signal carries the 6-distinct channels information by sharing the same time window of 24.0  $\mu$ s and transmitted by a single carrier frequency.



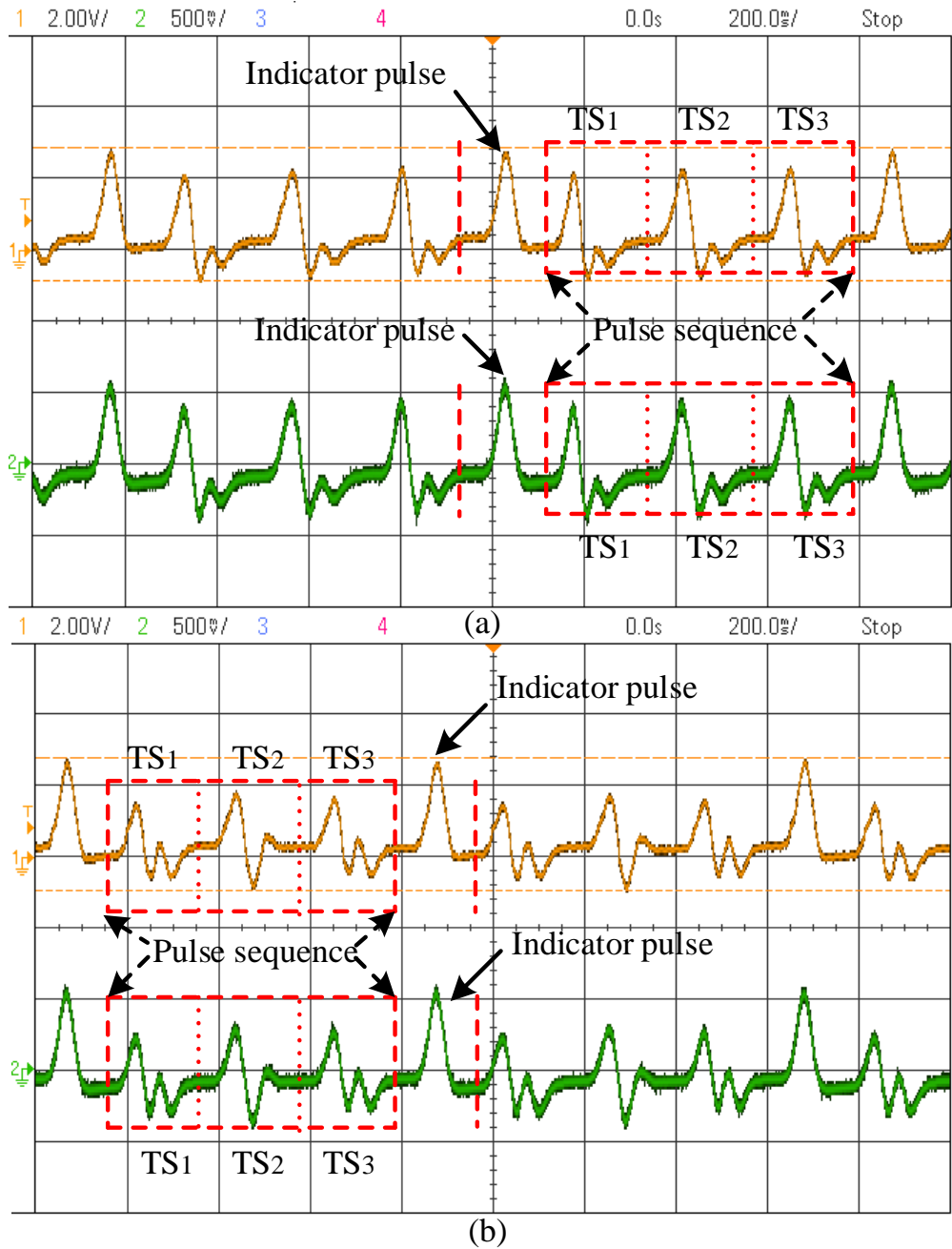
**Figure 6.15:** Test results of distinct PS generation using AOPs of 8.0  $\mu$ s width.

Fig. 6.16(a) shows the UCP signal where all the PSs presents and indicates the transmitted data bits symbolically as a compressed data volume. Fig. 6.16(b) shows channels 1, 2, 4, and 6 are existed in the UCP signal while the rest of the channels are absent. Similarly, in Fig. 6.16(c) and (d), channels 1 and 4, and 2 and 6 are missing in the UCP signal, and the rest of the PSs are present.



**Figure 6.16:** Composite UCP signal corresponding to each time slot of 8.0  $\mu$ s.

Fig. 6.17 shows the test results of PS based short-range wireless data telemetry. In Fig. 6.17(a), all the PSs are present in the transmitted UCP signal, while the PSs 3 and 5 are absent in Fig. 6.17(b). A zero-order pulse is added in front of each UCP signal as an indicator to synchronize with the template signal for correlation analysis. The CPE algorithm is applied on the composite pulses corresponding individual time slot to decode all the distinct order pulses from the received signal. The channel decoding algorithm is performed in offline using the measured hardware test data. The received UCP signal is captured by a full-length scale of Agilent Oscilloscope and stored in flash memory. In test results the green and orange trace indicate the Tx and Rx UCP signal.



**Figure 6.17:** Test results (a) all the PSs are present and (b) PS 3 and 5 are absent in the UCP signal.

Fig. 6.18 shows the performance of the CPE algorithm to decode individual pulses from the composite signal by correlation peak analysis. The pulse decoding algorithm decodes the individual pulses corresponding to each TS in parallel to verify the CPE. Fig. 6.18(a) shows the composite pulse signal corresponding to the first TS of Fig. 6.18(b). The

composite signal consisting with  $2 \times \text{MHP}_0$ ,  $\text{MHP}_1$ , and  $\text{MHP}_2$  pulse. In the computer simulation, a 10.0 dB AWGN is added with composite signal to represent communication channel noise. Figs. 6.18(b), (d), (f), and (h) depict the eliminated pulses from the composite cyclically corresponding to the maximum correlation peak. Figs. 6.18(c), (e), and (g) represent the residual signal after eliminating individual pulses cyclically. Fig. 6.18(i) shows the residual noise after eliminating all the pulses from the composite signal.

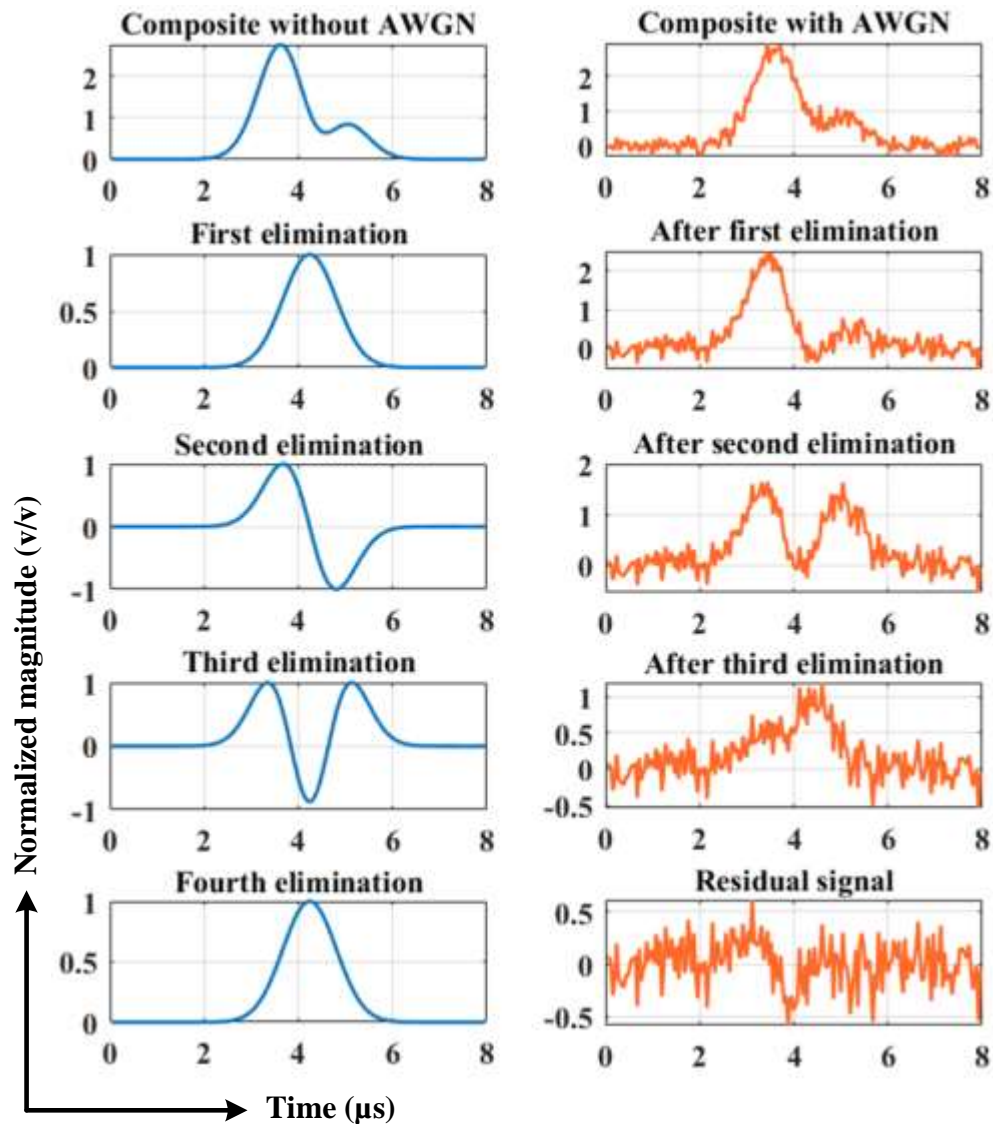


**Figure 6.18:** Test results of pulse elimination from the composite signal by CPE.



The above test verifies the performance of the CPE algorithm to decode the individual pulses successfully from the composite signal. All the channels are decoded successfully in both test results shown in Figs. 6.18(a) and (b). However, the threshold level is 0.25 compared to simulation for improper synchronization and human error.

#### ***6.5.4 Test Results for Orthogonal Pulse Sequence Based Encoding***

Fig. 6.19 shows the PS encoding template signal for OPS-based wireless data telemetry. The gold code generation scheme creates nine distinct OPSs from 6 distinct PSs generated by the permutation technique. The permutation of distinct pulse positions generates different PSs that consistently do not maintain signal orthogonality and show a non-orthogonality property. In Fig. 6.19, the first three PSs are the same as the original PSs, and the rest of the PSs are the product of gold code generation. The time domain representation of all the PSs are distinct from each other and indicates separate data channels. The OPSs also occupy the same time window and orthogonality with others.

Fig. 6.20(a) shows the simulation results of the composite signal. All the OPSs are present in their composite signal and sharing the same time window in time domain. The AWGN signal represents the channel model for computer simulation. This dissertation work also performed two different test cases to evaluate the performance and validity of OPS-based short-range wireless telemetry. Figs. 6.19(b) and (c) shows the test results for the indoor environment. The OPS is created and superimposed on top of one another. The data encoding algorithm is implemented in MKR1010 board and fed to RF chain. In Fig. 6.20, the green and orange trace shows the baseband OPS signal before passing through the RF chain and after passing through the RF chain, respectively. In Fig. 6.20(a), all the OPS are present in the composite signal, while sequences 3 and 5 are absent in Fig. 6.20(b).

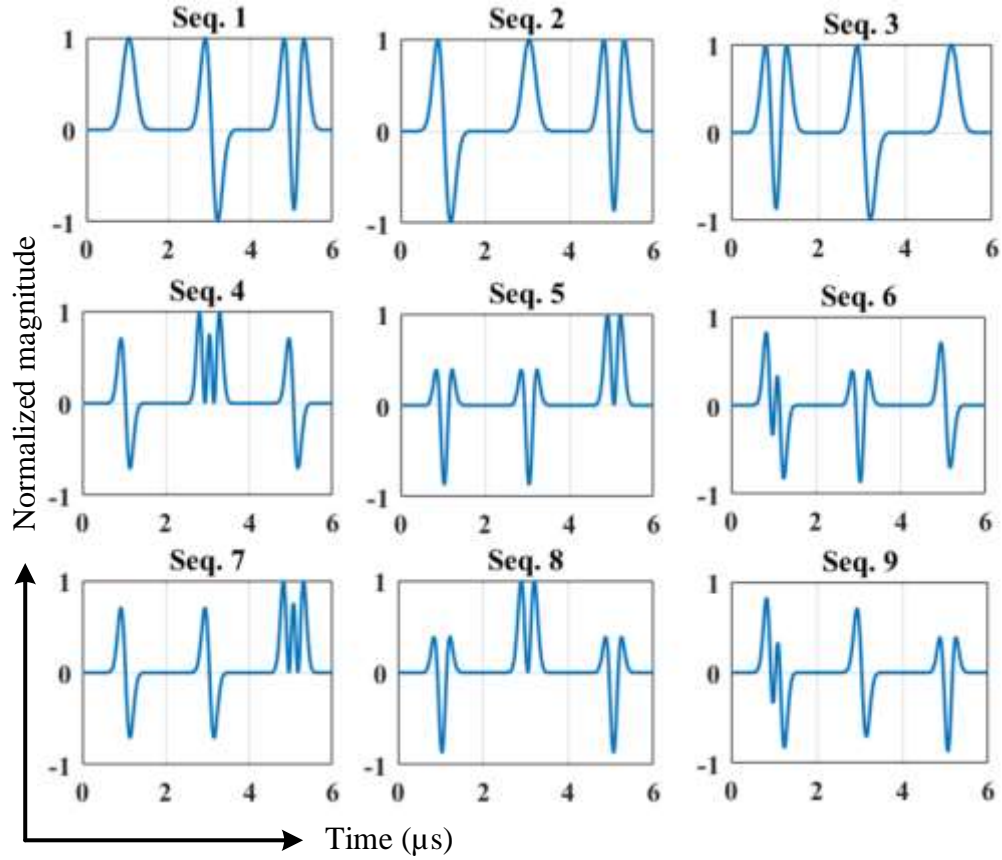


**Figure 6.19:** Template signal of distinct orthogonal pulse sequences.

Fig. 6.21(a) shows the PS decoding results from the corresponding composite signal. In MATLAB® simulation, the threshold level is selected at 0.55 to eliminate all the OPSs from the combined signal. Fig.6.21(a) depicts the eliminated PSs corresponding to each iteration. After eight iterations, all the PSs were eliminated, and the correlation peak arrived below the predefined threshold level (Table 6.3). Fig. 6.21(b) shows the residual signal after eliminating the entire PS in each iteration based on the highest correlation peak.

**Table 6.3:** Correlation peak table for entire OPSs eliminated from composite signal.

Ite. #	1	2	3	4	5	6	7	8	9
Seq.1	0.6034	0.5721	0.5401	0.5244	<b>0.5948</b>	0.4155	0.4840	0.5879	-0.4659
Seq.2	0.6898	0.6760	<b>0.6598</b>	0.4190	0.4611	0.4982	0.3535	0.3719	-0.3000
Seq.3	0.4938	0.5150	0.4886	0.6236	0.5818	0.1102	<b>0.6055</b>	0.1877	-0.1692
Seq.4	0.4190	0.4475	0.4698	0.3963	0.4708	<b>0.6783</b>	0.5072	0.2683	0.22340
Seq.5	0.5172	0.5563	0.5708	<b>0.6524</b>	0.4578	0.2968	0.4895	0.4010	0.09186



Seq.6	0.4312	0.4087	0.4421	0.4682	0.4718	0.5108	0.4086	0.3966	<b>0.47823</b>
Seq.7	0.7065	<b>0.7133</b>	0.5912	0.5197	0.5168	0.2738	0.4536	0.2368	-0.2803
Seq.8	0.6165	0.5240	0.6187	0.5634	0.5270	0.6021	0.5291	<b>0.6019</b>	-0.0923
Seq.9	<b>0.7194</b>	0.6280	0.6216	0.5456	0.5899	0.3117	0.3607	0.3324	-0.4620

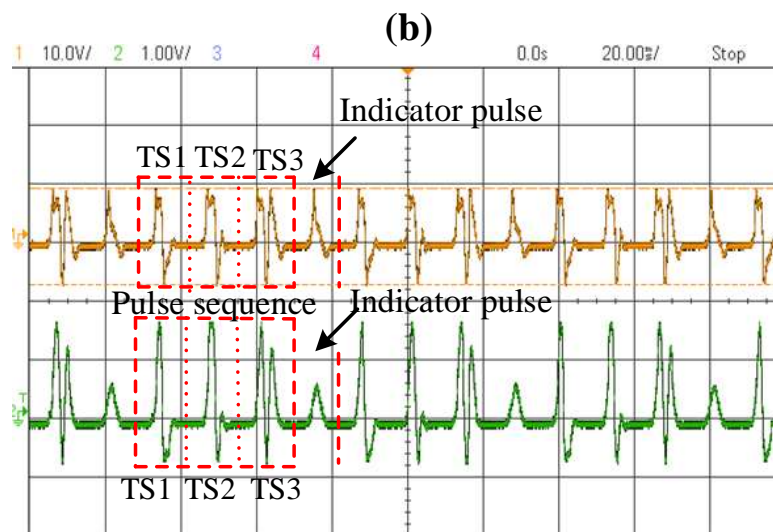
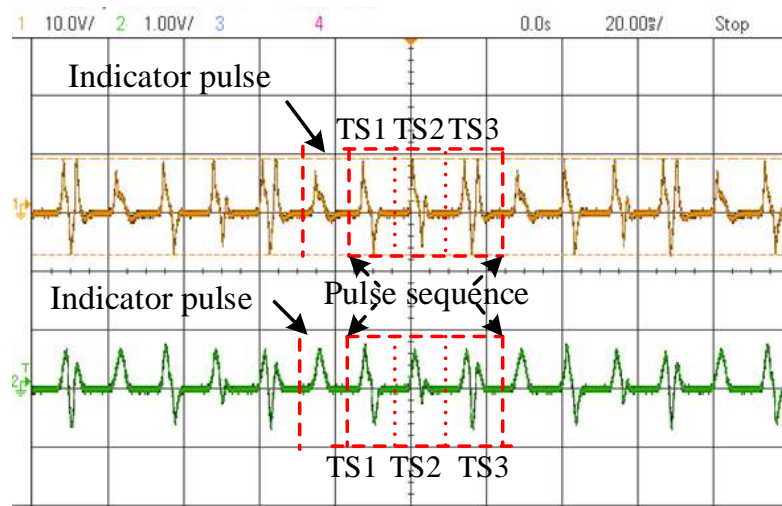
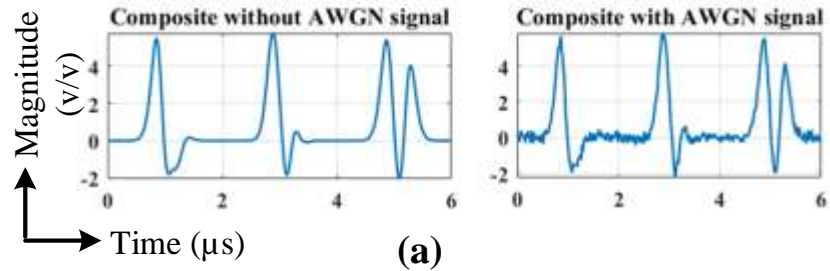


**Figure 6.20:** Composite signal for OPSs (a) simulation results, (b) experimental results, where all the sequences are present, and (c) 3 and 5 PSs are absent.

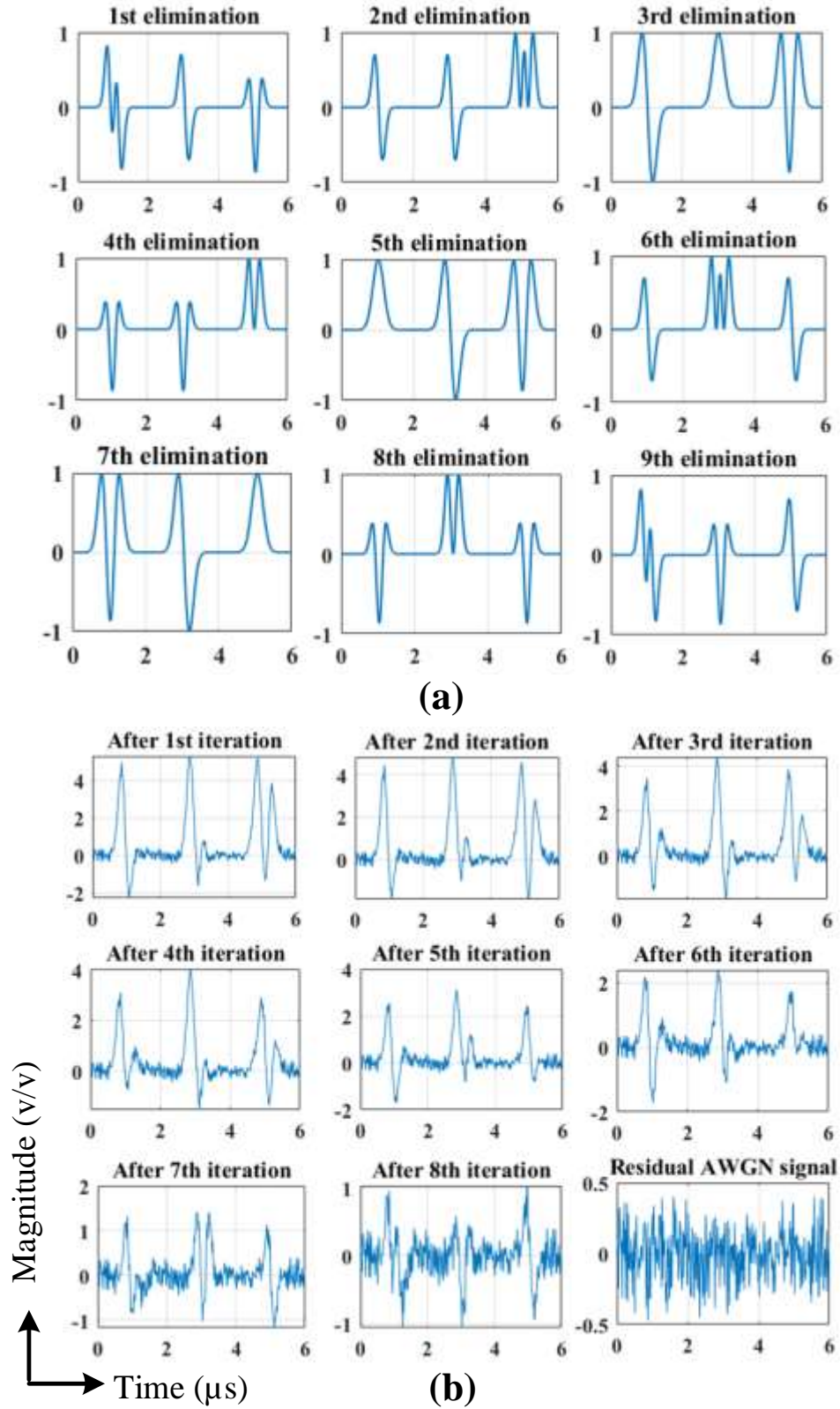


**Figure 6.21:** Test results for data decompression scheme (a) eliminated OPSs in each iteration and (b) residual composite signal after eliminating OPSs sequentially.

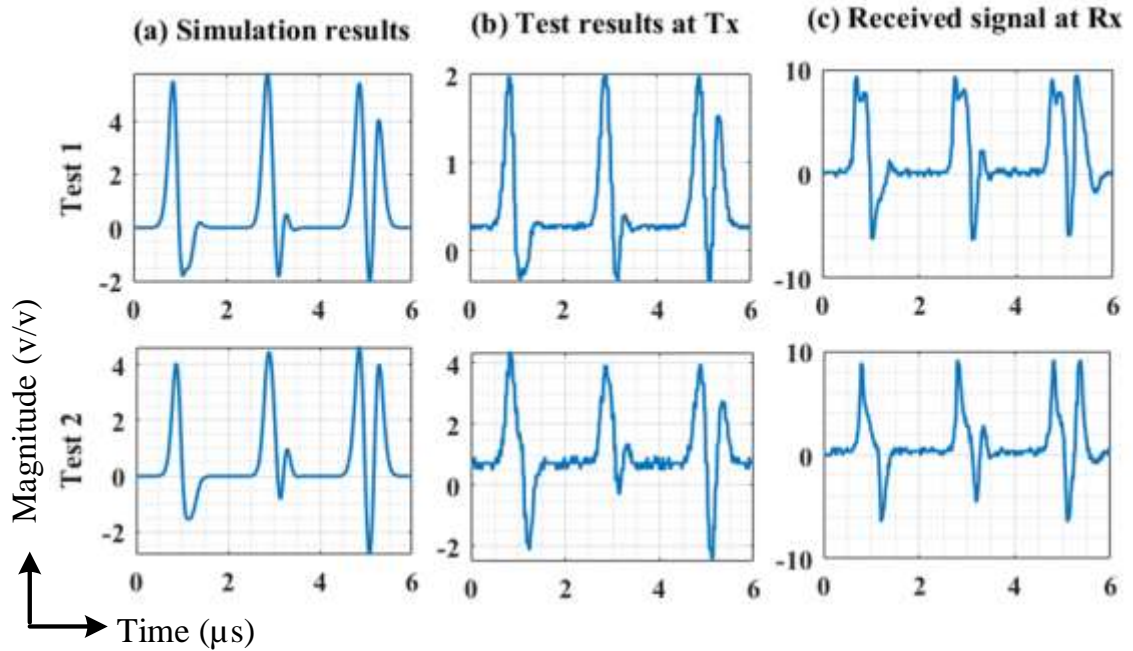
In the first iteration, the correlation peak table shows that the seq. 9 has the height peak with the composite signal. The seq. 9 is eliminated based on the correlation peak. Fig. 6.21(b), the first signal (1,1) positions show the residual signal after eliminating seq. 9, and (3,3) position shows the noise signal. The correlation peak of the residual signal shows below the threshold level at 0.55.

Fig. 6.22 shows the test results at two different cases. In the 2×3 subplot, the row represents the test conditions. Column 'a', 'b,' and 'c' shows the composite signals in MATLAB simulation and experimental results at Tx and Rx end. In the first test, all the OPSs are present in their composite signal, whereas, in the second test, sequences 3 and 5 are absent. The received signal is distorted due to the impacts of indoor communication channels on the AOPs for wireless telemetry.

Table 6.4 shows the test validation of orthogonal PS based data compression and decompression scheme. In this table the symbols E, S, P, and A indicate the experiment number, sequence number, presence, and absence, respectively. The data compression composite signals are shown in Figs. 6.20(b) and (c) and Fig. 6.22, corresponding to the experiment 1 and 2, respectively. The correlator based channel decoding scheme successfully decodes all the PSs from the composite signal by correlation peak checking. Similarly, in the second experiment, the decoding results shows that channel 3 and 6 are absent in the channel encoded composite signal.

**Table 6.4:** Test validation of orthogonal pulse sequence based wireless telemetry.

E #	OPS based channel encoding									Correlator based channel decoding								
	S <sub>1</sub>	S <sub>2</sub>	S <sub>3</sub>	S <sub>4</sub>	S <sub>5</sub>	S <sub>6</sub>	S <sub>7</sub>	S <sub>8</sub>	S <sub>9</sub>	S <sub>1</sub>	S <sub>2</sub>	S <sub>3</sub>	S <sub>4</sub>	S <sub>5</sub>	S <sub>6</sub>	S <sub>7</sub>	S <sub>8</sub>	S <sub>9</sub>
E1	P	P	P	P	P	P	P	P	P	1	1	1	1	1	1	1	1	1
E2	P	P	A	P	P	A	P	P	P	1	1	0	1	1	0	1	1	1
E = Experiment			S = Orthogonal sequence						P or 1 = Presence			A or 0 = Absence						



**Figure 6.22:** Test results at two test conditions, where column represent (a) MATLAB<sup>®</sup> simulation, experimental results (b) transmitted signal before carrier multiplication, and (c) received signal at baseband frequency after carrier removing.

## 6.6 Conclusion

This chapter presents the prototype development and implementation of an analog pulse-based high-volume data encoding and decoding schemes for wireless telemetry. The commercially available customized RF modules are used to configure the transceiver architecture. The low-power analog electronics-based RF-mixer driver and LPF circuit are designed and implemented to drive the mixer module and retrieve the baseband AOP signal. Different encoding schemes are also implemented in the Arduino board and fed the analog signal to the RF chain for rapid prototyping. This work also performed offline signal processing using the collected test data to find the missing bits data transmission accuracy in terms of BER and PER. Test results show that the orthogonal pulse-based wireless telemetry is compatible with the existing communication architecture and network

protocol, feasible for data transmission, and capable to carries multi-bit data by orthogonal pulses. It also shows the proposed scheme is suitable and applicable for SE IoT networks.

## CHAPTER 7

### CONCLUSION AND FUTURE WORKS

#### 7.1 Introduction

In this dissertation, two innovative pulse-based data encoding schemes are explored based on orthogonal pulses for efficient wireless telemetry. A prototype test platform is also developed to validate the wireless telemetry in indoor communication to meet the requirements of next-generation high-density IoT networks. The standard communication architecture and network protocol, customized RF modules, and Arduino platform are used to validate the compatibility, capability, and performance of proposed technology. In addition, the channel effect on AOPs is done to observe the impacts of different dielectric media and indoor reflections for pulse based telemetry. The research extension is also proposed to continue the orthogonal pulse technology for short-range wireless telemetry to support the proliferation of IoT networks.

#### 7.2 Summary and Potential Research Impacts

This section summarizes the entire dissertation with key findings, research innovations, and improvements of analog pulse-based encoding schemes. The proposed  $2.0 \mu\text{s}$  multi-order orthogonal pulse signal almost contains a fixed bandwidth around  $1 \pm 0.15 \text{ MHz}$  and improved the spectral efficiency 50% for 3-bit encoding. The main difference of the AOPs with the Gaussian pulse signals are the constant time window in

time domain and fixed spectrum in frequency domain regarding the changes of the pulse orders. Another significant benefits of the proposed scheme is the spectrum sharing with other pulses or applications. A single carrier frequency is good enough to transmit the UCP signal because all the individual pulses and the OPSs are orthogonal to each other. **In chapter 01** introduces the brief history of IoT markets and standard data telemetry for IoT networks. It also presented a short literature review based on the data encoding and modulation schemes. In addition, it established a concrete research motivation and solution methods based on the resource limitations of IoT devices, spectrum scarcity to support new devices, the necessity of spectrum sharing, and meeting the demands of next-generation technology for efficient wireless telemetry. **Chapter 02** described the orthogonal pulse set generator model based on a MHP, signal properties analysis, and data compression schemes to solve some of the existing problems, including high-volume data transmission using the limited spectrum, supports resource-constraint IoT devices, improves data latency, and so forth. The requirements of distinct pulses and their higher-order generation difficulties are also solved by considering different time shift factors and their signal orthogonality. The pulse generator model is developed with MATLAB<sup>®</sup> Simulink and the signal processing are performed by MATLAB<sup>®</sup> coding.

**Second**, this dissertation work explores the innovative data encoding schemes using distinct order AOPs to support large-volume data by orthogonal pulses. In the first scheme, the  $k$ -bit data encodes by a single AOP signal with index randomization to increase the data security. The PI encoding scheme compressed the data volume by  $k$ -times without computational complexity compared to the other existing PIM schemes. It also simplifies the existing data encoding and decoding scheme to transmit the same number of data bits

by a single pulse compared to the more than single HG pulse system [42]. Simulation results show it improved data rate  $k$ -times directly supporting  $2^k \times k$  number of bits by a specific  $2^k$  number of orthogonal pulses. In the second scheme, a sequence of analog pulses are used to encode distinct data channels and support numerous channels by sharing the same frequency spectrum. The permutation technique creates distinct PSs, and their UCP signal indicates the compressed data volume. The simulation results show the performance of the PS generation, data channel encoding, decoding, and missing bits finding algorithms. The PS scheme increased data volume  $(n-1)!$  times more by supporting  $n!$  distinct channels using  $n$  number of different orthogonal pulses. The OPS generation scheme also simplifies the PS decoding and missing data finding using CPE algorithm. **Chapters 03** and **chapter 04** discussed the algorithm design and implementation in detail and discuss the improvements by analyzing simulation results. The proposed analog pulse-based telemetry is scalable by adopting any number of pulse systems as per requirements for SE high-volume wireless data transmission.

**Third**, the PI randomization technique also increases security by randomizing the data encoding template. The index randomization creates the pulse blinding to the attacker and increases the ambiguous among them because they can't identify which  $k$ -bits data belong to in which pulse signal. Similarly, PI randomization also increases the data security by encoding the channel randomly in PS scheme, where a specific PS doesn't always represents the same data channel. Thus, the attackers always try to match the randomized pulse pattern through a brute force attack. The security strength depends on the margin of security exhaustive key search for decipher the encoded data bits according to Table 3.1. In Table 3.1 shows, the security strength is directly proportional to the level of data bits



encoding and the number of pulse system for PS scheme. The PI randomization increases the security by creating a new random sequence after a threshold time,  $T_h$  sec. Therefore, the PI randomization technique not only increases the data volume but also adds a low-level physical layer security.

**Fourth**, chapter 05 explores the detailed investigation of channel effects on AOPs and object sensing for indoor environment. Different case studies and channel obstructions are used to observe the impact of dielectric materials on AOP propagation through wireless media. A straightforward time-frequency signal processing scheme is developed to compute the simulated numerical output results for monitoring the channel impacts. The network parameter  $S_{21}$  is measured using the VNA at different test conditions for LOS communications at various locations, including room-to-room, room-to-corridor, and so forth. The numerically simulated output shows the actual scenario of the AOP signal when propagating through the wireless communication channel. It also shows the channel properties' for the physical signal distortion, pulse spreading, time delay, and extra dip at the beginning and end of the pulses. The test results help to design the decoding algorithm, signal restoration, and select the threshold level for correlation peak analysis at the receiver. It also helps to choose the pulse order that maintains signal orthogonality with their composite signal and easily decodes at the receiver end. The critical finding of channel effects on AOPs also helps for object sensing, detection, and ranging applications.

**Finally**, a prototype test platform is developed with mixer driver and LPF circuit design and implementation, microcontroller programming, and signal characterization to validate the orthogonal pulse-based short-range wireless data telemetry for SE applications. The commercially available customize FPGA-based transceiver board is

incompatible with analog pulse communication. Therefore, this dissertation work configures the transceiver architecture using commercially available RF modules. It also implemented different data encoding schemes into the microcontroller board using the memory-storing pulse information. Test data is collected by oscilloscope memory and then applied offline signal processing to find the missing data bits or channels. Test results also show that the proposed data telemetry is compatible with the standard communication architecture. Table 7.1 shows the comparison results with the existing works in terms of channel numbers, data rate improvements, and computational complexity. The existing works in ref. [34, 35, 37] involves with sophisticated signal processing with FFT and IFFT computation. The main benefits of the proposed orthogonal pulse-based scheme is different than the IFFT-based Walsh-Hadamard orthogonal code generation for wireless data communication [79]. The proposed works also differs from the existing pulse-based wireless telemetry in terms of data rate and channel numbers improvements. It can support any bit ( $k$ -bit) encoding using a single order pulse signal and supports numerous data channels, i.e.,  $n!$ -numbers for the  $n$ -pulse system. Simulation results also indicates the BER in proposed schemes are lower,  $1.0 \times 10^{-4}$  around 11 dB than the pulse pattern based channel encoding [41] and PIM [42]. Therefore, orthogonal pulse-based wireless telemetry will pave the way for a new SE platform to meet the demands of next-generation IoT networks.

**Table 7.1:** Comparison results with the existing works.

	[42]	[41]	[37]	[34]	[35]	<b>k-bits</b>	<b>PS scheme</b>
Data rate	$\times$	$(n-1)$	$D+1$	$\times$	$n$	$k$	$(n-1)!$
Channel #	$\times$	$n(n-1)$	$\times$	$\times$	$\times$	single	$n!$
Pulse #	$>1$	$n$	$D$	$\times$	$n$	$2^k$	$n$
BER at	$8.5 \times 10^{-3}$	$1.0 \times 10^{-4}$	$1.0 \times 10^{-3}$	$9.0 \times 10^{-2}$	$7.0 \times 10^{-4}$	$1.0 \times 10^{-4}$	$1.0 \times 10^{-4}$
SNR (dB)	40	13.6	6.5	10	10	11	13

The proposed analog pulse-based data telemetry has several benefits including the following advantages-

- (i) The PI encoding scheme encodes  $k$ -bit data and compresses the data volume without standard compression algorithm or computational complexity.
- (ii) The PS scheme supports  $n!$  distinct data channels and compresses data volume by  $(n-I)!$  times directly by sharing the same frequency spectrum.
- (iii) The proposed orthogonal pulse-based schemes are applicable both for NB and UWB applications by generating the narrow-width pulse set using the pulse generator.
- (iv) The PI randomization technique adds an extra data security layer without any encryption or decryption algorithms at the physical layer implementation.
- (v) The memory-based pulse information also simplifies the encoding scheme at the transmitter and is applicable at sensor hub for MISO applications using a single carrier.
- (vi) The proposed encoding schemes are scalable for any number of bits or channels according to the requirements and supports the rapid growth of IoT networks.
- (vii) The orthogonal pulses are also applicable for object sensing, detection, ranging applications based on the physical signature of the received composite signals.

### **7.3 Future Works**

This dissertation highlights the preliminary exploration of orthogonal pulse based wireless data telemetry for high-density IoT networks. It also proposes the extension of the presented work in future to solve the critical findings and meet the upcoming challenges of IoT networks. The following points can summarize and consider as the future work to extend the current dissertation work.

1. Time synchronization is a critical issue to decode the individual pulses from composite signal using correlator receiver for analog communication. This dissertation work used the manual computation to find the starting point for checking correlation with template signal by offline signal processing. The zero order AOP signal is used as an indicator pulse for time synchronization. The PLL Oscillator module can be used in future to lock the received signal with the template for proper time synchronization. The different time synchronization schemes could be investigated and implemented for finding the optimal solution for proper time synchronization.

2. Pulse sequence based data channel sensing and proper utilization would be another research extension of the proposed analog pulse-based wireless data telemetry. In this dissertation, the preliminary simulation work has been done for data channel sensing to optimize the existing frequency spectrum for proper utilization. Several spectrum sensing techniques can also be investigated and implemented as further extension of PS based channel encoding scheme for finding the unused spectrum and reused for secondary applications to optimize the resources.

3. Higher level data compression technique can be investigated using the AOPs. New and innovative encoding and data compression algorithm will be developed based on the current multi-bit data encoding schemes. The signal reconstruction scheme can be developed to improve the decoding algorithm and optimize the threshold level selection for decoding individual pulses from the received composite signal.

4. The customize transceiver architecture can be designed and implemented for rapid prototyping using the commercially available off-the-shelf IC and RF components in future. The new design should be in compact size, flexible, and portable for sensor node

applications. This research will include the RF PCB design, antenna design, driver circuit, time synchronization, hardware security, and algorithm improvement.

5. In future, the entire PS information can be stored in flash memory instead of the individual pulses to simplify the arduino coding and minimize the memory space in resource limited microcontroller IC. The down sampling technique can be utilized to solve the memory issue and store the entire PS information in memory storage device.

6. The detail channel effect investigation can be done by designing and developing mathematical model considering reflection, multi-path interference, and external noise for line-of-sight communications in indoor and outdoor applications.

## LIST OF REFERENCES

- [1] B. Jovanovic, 2022, "Internet of Things Statistics for 2022- Taking Things Apart", accessed on Sep, 19, 2022, <https://dataprot.net/statistics/iot-statistics/>.
- [2] J. Wang, H. Roy, S. Alam, T. Rao, S. Ahshrup, and W. McCluskey, 2021, "5G Accelerates Economic Growth" accessed on September 20, 2022, <https://www.accenture.com/us-en/insights/high-tech/5g-economic-impact>.
- [3] K. L. Lueth, 2020, State of the IoT 2020: 12 billion IoT connections, surpassing non-IoT for the first time, accessed on September 20, 2022, <https://iot-analytics.com/state-of-the-iot-2020-12-billion-iot-connections-surpassing-non-iot-for-the-first-time/>.
- [4] B. Debasis and J. Sen. Internet of Things: Applications and Challenges in Technology and Standardization, *Wireless Personal Communications*, vol. 58(1), pp. 49–69, 2011.
- [5] M. Jo, T. Maksymyuk, R. L. Batista, T. F. Maciel, A. L. F. d. Almeida, and M. Klymash. A survey of converging solutions for heterogeneous mobile networks, *IEEE Wireless Communications*, vol. 21(6), pp. 54–62, 2016.
- [6] H. M. Jawad, R. Nordin, S. K. Gharghan, A. M. Jawad, and M. Ismail. EnergyEfficient Wireless Sensor Networks for Precision Agriculture: A Review, *Sensors (Basel, Switzerland)*, vol. 17(8), pp.1781-1798, 2017.
- [7] A. A. Brincat et al., "The Internet of Things for Intelligent Transportation Systems in Real Smart Cities Scenarios," *IEEE 5th World Forum on Internet of Things (WF-IoT)*, 2019, pp. 128-132.
- [8] E. Sisinni et al., "Industrial Internet of Things: Challenges, Opportunities, and Directions," *IEEE Transactions on Industrial Informatics*, vol. 14(11), pp. 4724-4734, Nov. 2018.
- [9] V. Sivaraman et al., "Smart IoT Devices in the Home: Security and Privacy Implications," *IEEE Technology and Society Magazine*, vol. 37(2), pp. 71-79, June 2018.
- [10] M. S. Farooq, S. Riaz, A. Abid, K. Abid and M. A. Naeem, "A Survey on the Role of IoT in Agriculture for the Implementation of Smart Farming," *in IEEE Access*, vol. 7, pp. 156237-156271, 2019.

- [11] T. Yucek and H. Arslam, "A Survey of Spectrum Sensing Algorithms for Cognitive Radio Applications," *IEEE Commun. Surv. Tutorials*, vol. 11(1), pp. 116–130, 2009.
- [12] EMERGEN Research, 2020, Industrial IoT Market By Component, End User (Healthcare, Agriculture, Manufacturing and Transport) Forecast to 2027, accessed on September 21, 2022, <https://www.emergenresearch.com/industry-report/industrial-iot-market> (emergenresearch.com).
- [13] N. Javaid, A. Sher, H. Nasir and N. Guizani, "Intelligence in IoT-Based 5G Networks: Opportunities and Challenges," in *IEEE Communications Magazine*, vol. 56(10), pp. 94-100, October 2018.
- [14] F. Peper et al., "High-Density Resource-Restricted Pulse-Based IoT Networks," in *IEEE Transactions on Green Communications and Networking*, vol. 5(4), pp. 1856-1868, Dec. 2021.
- [15] A. K. Gupta and R. Johari, "IoT based Electrical Device Surveillance and Control System," *2019 4th International Conference on Internet of Things: Smart Innovation and Usages (IoT-SIU)*, Ghaziabad, India, 2019, pp. 1-5.
- [16] L. Feltrin et al., "Narrowband IoT: A Survey on Downlink and Uplink Perspectives," in *IEEE Wireless Communications*, vol. 26(1), pp. 78-86, February 2019.
- [17] F. J. Dian and R. Vahidnia, "NB-IoT Preamble Signal: A Survey," *2021 IEEE 7th World Forum on Internet of Things (WF-IoT)*, New Orleans, LA, USA, 2021, pp. 107-112.
- [18] E. M. Migabo, K. D. Djouani and A. M. Kurien, "The Narrowband Internet of Things Resources Management Performance State of Art, Challenges, and Opportunities," in *IEEE Access*, vol. 8, pp. 97658-97675, 2020.
- [19] W. Ayoub, et al., "Internet of Mobile Things: Overview of LoRaWAN, DASH7, and NB-IoT in LPWANs Standards and Supported Mobility," in *IEEE Communications Surveys and Tutorials*, vol. 21(2), pp. 1561-1581, Second quarter, 2019.
- [20] S. Parvez, P. K. Singya and V. Bhatia, "On ASER Analysis of Energy Efficient Modulation Schemes for a Device-to-Device MIMO Relay Network," in *IEEE Access*, vol. 8, pp. 2499-2512, 2020.
- [21] A. Narbudowicz, A. Zandamela, N. Marchetti and M. J. Ammann, "Energy-Efficient Dynamic Directional Modulation with Electrically Small Antennas," in *IEEE Antennas and Wireless Propagation Letters*, vol. 21(4), pp. 681-684, April 2022.

- [22] J. Chen, S. Li, J. Tao, S. Fu and G. E. Sobelman, "Wireless Beam Modulation: An Energy- and Spectrum-Efficient Communication Technology for Future Massive IoT Systems," in *IEEE Wireless Communications*, vol. 27(5), pp. 60-66, October 2020.
- [23] A. Al-Dweik, S. Younis, A. Hazmi, C. Tsimenidis, and B. Sharif, "Efficient OFDM Symbol Timing Estimator Using Power Difference Measurements", in *IEEE Transactions on Vehicular Technology*, vol. 61(2), pp. 509-520, Feb. 2012.
- [24] X. Cheng, M. Zhang, M. Wen and L. Yang, "Index Modulation for 5G: Striving to Do More with Less," *IEEE Wireless Communications*, vol. 25(2), pp. 126-132, April 2018.
- [25] T. AthisayaAnushya et al., "Dual Mode Dual Index Orthogonal Frequency Division Multiplexing Index Modulation," *International Conference on Emerging Trends in Information Technology and Engineering*, Vellore, India, 2020, pp. 1-5.
- [26] F. Cogen, E. Aydin, N. Kabaoglu, E. Basar and H. Ilhan, "Generalized Code Index Modulation and Spatial Modulation for High Rate and Energy-Efficient MIMO Systems on Rayleigh Block-Fading Channel," *IEEE Systems Journal*, vol. 15(1), pp. 538-545, March 2021.
- [27] G. Kaddoum, M. F. A. Ahmed and Y. Nijssure, "Code Index Modulation: A High Data Rate and Energy Efficient Communication System," *IEEE Communications Letters*, vol. 19(2), pp. 175-178, Feb. 2015.
- [28] I. -W. Lai et al., "Spatial Permutation Modulation for Multiple-Input Multiple-Output (MIMO) Systems," in *IEEE Access*, vol. 7, pp. 68206-68218, May 2019.
- [29] K. Zhang, H. Hai, M. Wen, X. -Q. Jiang and R. Qiu, "Generalized Space-Code Index Modulation for High Rate and Energy-Efficient MIMO Transmission," in *IEEE Transactions on Vehicular Technology*, vol. 70(12), pp. 12812-12820, Dec. 2021.
- [30] M. Wang, Z. Chen and Z. Chen, "Energy-Efficient Index Modulation With In-Phase/Quadrature Format in the Generalized Fading Channel," in *IEEE Access*, vol. 9, pp. 117938-117948, August 2021.
- [31] R. F. Siregar, N. Rajatheva and M. Latva-aho, "Permutation Channel Modulation: New Index Modulation Mechanism for MIMO," in *2021 IEEE 93rd Vehicular Technology Conference*, Helsinki, Finland, 2021, pp. 1-6.
- [32] M. Saad et al., "A Novel Index Modulation Dimension Based on Filter Domain: Filter Shapes Index Modulation," *IEEE Transactions on Communications*, vol. 69(3), pp. 1445-1461, March 2021.



- [33] L. Yin and H. Zhu, "UWB pulse design using the approximate prolate spheroidal wave functions," *IEEE International Symposium on Microwave, Antenna, Propagation and EMC Technologies for Wireless Communications*, Beijing, China, 08-12 August, 2005, pp. 450-453.
- [34] S. Aldirmaz, A. Serbes, and L. Durak-Ata, "Spectrally Efficient OFDMA Lattice Structure via Toroidal Waveforms on the Time-Frequency Plane", *EURASIP J. Adv. Signal Process*, vol. 2010(13), March 2010.
- [35] S. Senay, L. Durak and L. F. Chaparro, "A time-frequency division multiplexing communications system with hexagonal lattice structure," *17<sup>th</sup> European Signal Processing Conference*, Glsgow, UK, 2009, pp. 1186-1189.
- [36] H. Taki et al., "On Optimizing the Performance of Impulse Radio Pulse Position Modulation Based on UWB Gaussian Pulse Derivatives," *Fourth International Conference on Advances in Computational Tools for Engineering Applications*, Beirut, Lebanon, 3-5 July, 2019, pp. 1-5.
- [37] E. Çatak and L. Durak-Ata, "An efficient transceiver for superimposed orthogonal waveforms with polynomials," *IEEE International Black Sea Conference on Communications and Networking*, Istanbul, Turkey, 5-8 June, 2017, pp. 1-5.
- [38] S. Praseuth, D. Lakanchanh, K. Luangxaysana and S. Promwong, "Measurement and Modeling of WUWB Impulse Radio Transmission with Indoor Environment," *Global Wireless Summit*, pp. 231-235, Nov. 2018.
- [39] F. Inanlou, M. Kiani, and M. Ghovanloo, "A novel pulse-based modulation technique for wideband low power communication with neuroprosthetic devices," *Annual International Conference of the IEEE Engineering in Medicine and Biology*, Buenos Aires, Argentina, 2010, pp. 5326-5329.
- [40] A. Das and D. Kundu, "Pulse shape modulation-generation and detection strategies," *IEEE 1st International Conference on Power Electronics, Intelligent Control and Energy Systems*, Delhi, India, 2017, pp. 1-4.
- [41] K. P. Pradhan, Y. G. Li, A. K. M. Arifuzzman, M. R. Haider, "Modified Hermite Pulse-Based Wideband Communication for High-Speed Data Transfer in Wireless Sensor Applications". *J. Low Power Electron.* vol.7(4), pp. 30- 45, Appl. 2017.
- [42] S. Aldirmaz-Colak, E. Aydin, Y. Celik, Y. Acar and E. Basar, "Pulse Index Modulation," *IEEE Communications Letters*, vol. 25(7), pp. 2309-2313, July 2021.
- [43] L. B. Michael, M. Ghavami, and R. Kohno, Multiple pulse generator for ultra-wideband communication using Hermite polynomial based orthogonal pulses. in *2002 IEEE Conference on Ultra-Wideband Systems and Technologies*, Baltimore, MD, USA, 2002, pages 47–51.

- [44] Xu, Ke. "UWB Signal Generation and Modulation Based on Photonic Approaches" *In UWB Technology and its Applications*, edited by Dusan Kocur. London: Intech Open, 2018.
- [45] Y. Wang and L. Zhou. Performance evaluation in the presence of timing jitter using a novel pulse design based on Hermite functions for UWB communications, in *2008 Asia-Pacific Microwave Conference*, Hong kong, China, 2009, pages 1–4.
- [46] Xiaomin Chen and S. Kiaei, Monocycle shapes for ultra-wideband system, in *2002 IEEE International Symposium on Circuits and Systems*, Proceedings, Phoenix-Scottsdale, AZ, USA, 2002, pages I–5.
- [47] A. B. Parr, B. L. Cho, and Z. Ding. A new UWB pulse generator for FCC spectral masks, in *The 57<sup>th</sup> IEEE Semiannual Vehicular Technology Conference, 2003. VTC 2003-Spring*, vol. 3, pp. 1664–1666, April 2003.
- [48] N. C. Beaulieu and B. Hu. A novel pulse design algorithm for ultra-wideband communications, *IEEE Global Telecommunications Conference, GLOBECOM '04*, vol. 5(1), pp: 3220–3224, 2004.
- [49] Lu Yin and Zhu Hongbo. UWB pulse design using the approximate prolate spheroidal wave functions. In *2005 IEEE International Symposium on Microwave, Antenna, Propagation and EMC Technologies for Wireless Communications*, vol. 1, pp. 450–453, August 2005.
- [50] Xianren Wu, Zhi Tian, T. N. Davidson, and G. B. Giannakis. Optimal waveform design for UWB radios. *IEEE Transactions on Signal Processing*, vol. 54(6), pp. 2009–2021, June 2006.
- [51] T. Matsumoto, H. Ochiai, and R. Kohno, "Super-orthogonal convolutional coding with orthogonal pulse waveform for UWB communications," in *2004 International Workshop on Ultra-Wideband Systems Joint with Conference on Ultra-Wideband Systems and Technologies. Joint UWBST IWUWBS 2004*, Kyoto, Japan, 2004, pp. 202–206.
- [52] M. Ouertani, H. Besbes, and A. Bouallégué, "Bi-orthogonal pulse design based on Hermite functions for UWB communications," in *2009 3rd International Conference on Signals, Circuits and Systems (SCS)*, Medenine, Tunisi, 2009, pp. 1–4.
- [53] K. Fan, S. Zhang, and X. Liu, "A UWB Pulse Shapes Modulation Scheme Based on Modified Hermite Polynomials," in *2008 4th International Conference on Wireless Communications, Networking and Mobile Computing*, Dalian, China, 2008, pp. 1–4.

- [54] M. Ouertani, H. Besbes, and A. Bouallègue, "Modified Hermite functions for designing new optimal UWB pulse-shapers," in *2005 13<sup>th</sup> European Signal Processing Conference*, Antalya, Turkey, 2005, pp. 1–4.
- [55] Park, Y.; Wentzloff, D.D, "All-digital synthesizable UWB transmitter architectures," in *Proceedings of the 2008. IEEE International Conference on Ultra-Wideband*, Hannover, Germany, September 2008, pp. 10-12.
- [56] Tantiparimongkol, L.; Phasukkit, P. Experiment of UWB Pulse Generator using FPGA based on Delay Line-Based Pulse Generation for Radar Application. *In Proceedings of the 2018 International Symposium on Multimedia and Communication Technology (ISMATC)*, Tottori, Japan, August 2018, pp. 29–31.
- [57] Tantiparimongkol, L.; Phasukkit, P. Designing of UWB Pulse Generation in FPGA Based on Delay Line Method for Human Range Through the Wall Detecting Application. *In 2019 16th International Conference on Electrical Engineering/Electronics, Computer, Telecommunications and Information Technology*, Pattaya, Thailand, July 2019, pp. 10–13.
- [58] L. Tantiparimongkol and P. Phasukkit, "IR-UWB Pulse Generation Using FPGA Scheme for through Obstacle Human Detection," *Sensors, MDPI* 2020, vol. 20(13), pp. 3750-70.
- [59] Y. Li, et al., "An efficient orthogonal pulse set generator for high-speed sub-GHz UWB communications," *IEEE International Symposium on Circuits and Systems (ISCAS)*, Melbourne, VIC, Australia, June 2014, pp. 1913-1916.
- [60] I. Mahbub and S. K. Islam, "A low power pulse position modulation based ultra-wideband transmitter for implantable sensors," *IEEE International Symposium on Medical Measurements and Applications*, Benevento, Italy, 15-18 May, 2016, pp. 1-5.
- [61] S. Jabbar et al., "Efficient strategy for throughput improvement in wireless sensor networks," *Sensors*, vol. 15(2), pp. 2473–2495, Feb. 2015.
- [62] R. A. Vatti and A. N. Gaikwad, "Throughput Improvement of High Density Wireless Personal Area Networks," *International Conference on Computational Intelligence and Networks*, Bhopal, India, Nov. 14-16, 2014, pp. 506-509.
- [63] E. Reusens et al., "Characterization of On-Body Communication Channel and Energy Efficient Topology Design for Wireless Body Area Networks," *in IEEE Transactions on Information Technology in Biomedicine*, vol. 13(6), pp. 933-945, November 2009.
- [64] J. F. Coll, J. Chilo and B. Slimane, "Radio-Frequency Electromagnetic Characterization in Factory Infrastructures," *in IEEE Transactions on Electromagnetic Compatibility*, vol. 54(3), pp. 708-711, June 2012.

- [65] L. Pometcu et al., "An Indoor Channel Model for High Data-Rate Communications D-Band," in *IEEE Access*, vol.8, pp. 9420-9433, Dec. 2020.
- [66] E. Adams et al., "Broadband Characterisation of Interior Materials and Surface Scattering using Terahertz Time-Domain Spectroscopy," *2021 14th UK-Europe-China Workshop on Millimetre-Waves and Terahertz Technologies (UCMMT)*, Lancaster, United Kingdom, 2021, pp. 1-3.
- [67] M. Hosseini, M. Assefzadeh, S. Razavian, Y. Mehta and A. Babakhani, "Terahertz Channel Characterization using a Silicon-based Picosecond Pulse Source," *IEEE Radio and Wireless Symposium*, San Antonio, TX, 2020, pp. 76-79.
- [68] R. U. Tariq, M. Ye and Y. He, "Development of Single Measurement Setup to Test S-Parameters and Distortions of Microwave Devices," *2020 IEEE Asia-Pacific Microwave Conference (APMC)*, Hong Kong, 2020, pp. 567-569.
- [69] H. Huang, et. al., "Introducing S-parameters for ultrasound-based structural health monitoring", in *IEEE Transactions on Ultrasonics, Ferroelectrics, and Frequency Control*, vol. 61(11), pp.1856-1863, Nov. 2014.
- [70] M. Poturalski, M. Flury, P. Papadimitratos, J. P. Hubaux, and J. Y. L. Boudec, "The cicada attack: Degradation and denial of service in ranging," in *2010 IEEE International Conference on Ultra-Wideband*, Nanjing, China, September 20-23, 2010, pp. 1-4.
- [71] J. Clulow, G. P. Hancke, M. G. Kuhn, and T. Moore, "So near and yet so far: Distance-bounding attacks in wireless networks," in *Proceedings of the Third European Conference on Security and Privacy in Ad-Hoc and Sensor Networks, ser. ESAS'06. Springer*, vol. 4357, 2006, pp. 83-97.
- [72] N. O. Tippenhauer, H. Luecken, M. Kuhn, and S. Capkun, "UWB rapid-bit-exchange system for distance bounding," in *Proceedings of the 8<sup>th</sup> ACM Conference on Security and Privacy in Wireless and Mobile Networks, ser. WiSec '15. ACM*, article no. 2, pp. 1-12, June 2015.
- [73] M. Singh, P. Leu, and S. Capkun, "UWB with Pulse Reordering: Securing Ranging against Relay and Physical-Layer Attacks", *Proceedings 2019 Network and Distributed System Security Symposium*, January 2019, doi:10.14722/ndss.2019.23109
- [74] V. Umadevi and P. Easwaran, "A study on Rake Receivers," *2017 IEEE International Conference on Electrical, Instrumentation and Communication Engineering (ICEICE)*, Karur, 2017, pp. 1-5.
- [75] Mirahmadi, M.; Al-Dweik, A.; Shami, A. BER Reduction of OFDM Based Broadband Communication Systems over Multipath Channels with Impulsive Noise. *IEEE Trans. Commun.* 2013, 61, 4602-4615.

APPENDIX A  
LIST OF PUBLICATIONS

## List of Publications

### Book Chapter

- [1] **Md. Kamal Hossain** and Mohammad R. Haider, "Electromagnetic Fields and Radiations," *Biological Effects of Nonionizing Radiation*, Bantam publisher April 30<sup>th</sup> (2022).

### Journal Articles

- [2] Lu, R, **Hossain, M. K.**, Alexander, JI, Massoud, Y, Haider, MR., "An efficient DC-DC converter for inductive power transfer in low-power sensor applications," *Int J Circ Theory Appl.*, vol. 50(8), pp. 2887-2899, Apr. 2022.
- [3] R. Lu, AKM Arifuzzman, **Md. Kamal Hossain**, S. Gardner, S. A. Eliza, J. I. D. Alexander, Y. Massoud, and M. R. Haider, "A Low-Power Sensitive Integrated Sensor System for Thermal Flow Monitoring," in *IEEE Transactions on Very Large Scale Integration (VLSI) Systems*, vol. 27(2), pp. 2949-2953, Dec. 2019.
- [4] **Md. Kamal Hossain**, Muhammad Masud Rana, and Mohammad R. Haider," Spectrum-Efficient Analog Pulse Index Modulation for High-Volume Wireless Data Telemetry", *IEEE Internet of Things Journal*, Submitted, Manuscript id: **IoT-24002-2022**, Accepted, May-2022, August 2022.
- [5] **Md. Kamal Hossain** and Mohammad R. Haider," A Spectrum-Efficient Analog Pulse Sequence Based Encoding for IoT Applications," *IEEE Internet of Things Journal*, Submitted, Manuscript id: **IoT-25751-2022**, 19-Sep-2022.
- [6] **Md. Kamal Hossain** and Mohammad R. Haider, "Indoor Channel Effect Investigation for Analog Pulse-Based IoT Communication", *International Journal of Wireless Information Networks*, Manuscript id: **IJWI-S-21-00125** 2021, rev. 1 submitted, May-2022.
- [7] **Md. Kamal Hossain**, Farah Ferdous, Md. Kawsar Bepary, Md. Imtiaz Rashid, Md. Tauhidur Rahman, and Mohammad R. Haider, "Secure Data Transmission in IoT Devices Using Randomized Pulse-Based Data Modulation", *International Journal of Wireless Personal Communication*, Manuscript id: **WIRE-D-21-01583**, submitted, June-2021.

### Conference Proceedings

- [8] **Md. Kamal Hossain** and M. R. Haider, "A Multi-bit Data Modulation Using Orthogonal Pulses for High-Density Data Transmission," *2021 IEEE International*

*Midwest Symposium on Circuits and Systems (MWSCAS)*, Lansing, MI, USA, 2021, pp. 599-602.

- [9] **Md. Kamal Hossain** and M. R. Haider, "Analog Pulse-Based Channel Sensing for Spectrum Efficient Wireless Data Transmission," *2021 IEEE International Midwest Symposium on Circuits and Systems (MWSCAS)*, Lansing, MI, USA, 2021, pp. 929-932.
- [10] **Md. Kamal Hossain** and M. R. Haider, "Analog Pulse Based Data Transmission for Internet-of-Things Applications," *2020 11th International Conference on Electrical and Computer Engineering (ICECE)*, Dhaka, Bangladesh, 2020, pp. 53-56.
- [11] **Md. Kamal Hossain** and M. R. Haider, "S-Parameters Based Channel Characterization Using Ultra-Wideband Pulse Signal," *2020 11th International Conference on Electrical and Computer Engineering (ICECE)*, Dhaka, Bangladesh, 2020, pp. 81-84.
- [12] **Md. Kamal Hossain** and M. R. Haider, "Channel Decoding Using Cyclic Elimination Algorithm for Pulse Based UWB Transceiver," *2020 11th International Conference on Electrical and Computer Engineering (ICECE)*, Dhaka, Bangladesh, 2020, pp. 85-88.
- [13] **Md. Kamal Hossain**, M.I. Rashid, M. R. Haider, and M.T. Rahman, "Randomized Pulse-Based Encoding for Secure Wireless Data Communications", *2020 IEEE 63rd International Midwest Symposium on Circuits and Systems*, Springfield, MA, USA, 2020, pp. 289-292.
- [14] **Md. Kamal Hossain**, Y. Massoud, and M. R. Haider, "A Spectrum-Efficient Data Modulation Scheme for Internet-of-Things Applications," *2020 IEEE 63rd International Midwest Symposium on Circuits and Systems*, Springfield, MA, USA, 2020, pp. 770-773.

APPENDIX B  
CORRELATION PEAK TABLE



## Correlation Peak Table

Table B1: Correlation peak table for different pulse-sequences with others.

	S <sub>1</sub>	S <sub>2</sub>	S <sub>3</sub>	S <sub>4</sub>	S <sub>5</sub>	S <sub>6</sub>	S <sub>7</sub>	S <sub>8</sub>	S <sub>9</sub>	S <sub>10</sub>	S <sub>11</sub>	S <sub>12</sub>	S <sub>13</sub>	S <sub>14</sub>	S <sub>15</sub>	S <sub>16</sub>	S <sub>17</sub>	S <sub>18</sub>	S <sub>19</sub>	S <sub>20</sub>	S <sub>21</sub>	S <sub>22</sub>	S <sub>23</sub>	S <sub>24</sub>
S <sub>1</sub>	1.00	0.40	0.45	0.14	0.43	0.14	0.55	-0.04	0.26	-0.04	0.24	-0.04	0.26	-0.04	0.52	0.21	-0.04	-0.04	-0.04	0.24	0.21	0.50	-0.04	-0.04
S <sub>2</sub>	0.40	1.00	0.14	0.45	0.14	0.43	-0.04	0.55	-0.04	0.26	-0.04	0.24	-0.04	0.26	0.21	0.52	-0.04	-0.04	0.24	-0.04	0.50	0.21	-0.04	-0.04
S <sub>3</sub>	0.45	0.14	1.00	0.43	0.14	0.40	0.26	-0.04	0.55	0.24	-0.04	-0.04	0.52	-0.04	0.26	-0.04	0.21	-0.04	0.21	-0.04	-0.04	-0.04	0.50	0.24
S <sub>4</sub>	0.14	0.45	0.43	1.00	0.40	0.47	-0.04	0.26	0.24	0.55	-0.04	-0.04	-0.04	0.52	-0.04	0.26	-0.04	0.21	-0.04	0.21	-0.04	-0.04	0.24	0.50
S <sub>5</sub>	0.43	0.14	0.14	0.40	1.00	0.45	0.24	-0.04	-0.04	-0.04	0.55	0.26	-0.04	0.21	-0.04	-0.04	0.26	0.52	-0.04	0.50	-0.04	0.24	-0.04	0.21
S <sub>6</sub>	0.14	0.43	0.40	0.14	0.45	1.00	-0.04	0.24	-0.04	-0.04	0.26	0.55	0.21	-0.04	-0.04	-0.04	0.52	0.26	0.50	-0.04	0.24	-0.04	0.21	-0.04
S <sub>7</sub>	0.55	-0.04	0.26	-0.04	0.24	-0.04	1.00	0.40	0.52	0.21	0.50	0.21	0.45	0.14	0.26	-0.04	-0.04	-0.04	0.14	0.43	-0.04	0.24	-0.04	-0.04
S <sub>8</sub>	-0.04	0.55	-0.04	0.26	-0.04	0.24	0.40	1.00	0.21	0.52	0.21	0.50	0.14	0.45	-0.04	0.26	-0.04	-0.04	0.43	0.14	0.24	-0.04	-0.04	-0.04
S <sub>9</sub>	0.26	-0.04	0.55	0.24	-0.04	-0.04	0.52	0.21	1.00	0.50	0.21	0.40	0.26	-0.04	0.45	-0.04	-0.04	0.14	-0.04	-0.04	0.14	-0.04	0.24	0.43
S <sub>10</sub>	-0.04	0.26	0.24	0.55	-0.04	-0.04	0.21	0.52	0.50	1.00	0.40	0.21	-0.04	0.26	-0.04	0.45	0.14	-0.04	-0.04	-0.04	-0.04	0.14	0.43	0.24
S <sub>11</sub>	0.24	-0.04	-0.04	-0.04	0.55	0.26	0.50	0.21	0.21	0.40	1.00	0.52	-0.04	-0.04	-0.04	0.14	0.45	0.26	-0.04	0.24	-0.04	0.43	0.14	0.04
S <sub>12</sub>	-0.04	0.24	-0.04	-0.04	0.26	0.55	0.21	0.53	0.40	0.21	0.52	1.00	-0.04	-0.04	0.14	-0.04	0.26	0.45	0.24	-0.04	0.43	-0.04	-0.04	0.14
S <sub>13</sub>	0.26	-0.04	0.52	-0.04	-0.04	0.21	0.45	0.14	0.26	-0.04	-0.04	-0.04	1.00	0.43	0.55	0.24	0.50	0.24	0.40	0.14	-0.04	-0.04	0.21	-0.04
S <sub>14</sub>	-0.04	0.26	-0.04	0.52	0.21	-0.04	0.14	0.45	-0.04	0.26	-0.04	-0.04	0.43	1.00	0.24	0.55	0.24	0.50	0.14	0.40	-0.04	-0.04	-0.04	0.21
S <sub>15</sub>	0.52	0.21	0.26	-0.04	-0.04	-0.04	0.21	-0.04	0.45	-0.04	-0.04	0.14	0.55	0.24	1.00	0.50	0.24	0.43	-0.04	-0.04	0.40	0.21	-0.04	0.14
S <sub>16</sub>	0.21	0.52	-0.04	0.26	-0.04	-0.04	-0.04	0.26	-0.04	0.45	0.14	-0.04	0.24	0.55	0.50	1.00	0.43	0.24	-0.04	-0.04	0.21	0.40	0.14	-0.04
S <sub>17</sub>	-0.04	-0.04	0.21	-0.04	0.26	0.52	-0.04	-0.04	-0.04	0.14	0.45	0.26	0.50	0.24	0.24	0.43	1.00	0.55	0.21	-0.04	-0.04	0.14	0.40	-0.04
S <sub>18</sub>	-0.04	-0.04	-0.04	0.21	0.52	0.26	-0.04	-0.04	0.14	-0.04	0.26	0.45	0.24	0.50	0.43	0.24	0.55	1.00	-0.04	0.21	0.14	-0.04	-0.04	0.40
S <sub>19</sub>	-0.04	0.24	0.21	-0.04	-0.04	0.50	0.14	0.43	-0.04	-0.04	-0.04	0.24	0.40	0.14	-0.04	-0.04	0.21	-0.04	1.00	0.45	0.55	0.26	0.52	0.26
S <sub>20</sub>	0.24	-0.04	-0.04	0.21	0.50	-0.04	0.43	0.14	-0.04	-0.04	0.24	0.04	0.14	0.40	-0.04	-0.04	-0.04	0.21	0.45	1.00	0.26	0.55	0.26	0.52
S <sub>21</sub>	0.21	0.50	-0.04	-0.04	-0.04	0.24	-0.04	0.24	0.14	-0.04	-0.04	0.43	-0.04	-0.04	0.40	0.21	-0.04	0.14	0.55	0.26	1.00	0.52	0.26	0.45
S <sub>22</sub>	0.50	0.21	-0.04	-0.04	0.24	-0.04	0.24	-0.04	-0.04	0.14	0.43	-0.04	-0.04	-0.04	0.21	0.40	0.14	-0.04	0.26	0.55	0.52	1.00	0.45	0.26
S <sub>23</sub>	-0.04	-0.04	0.50	0.24	-0.04	0.21	-0.04	-0.04	0.24	0.43	0.14	-0.04	0.21	-0.04	-0.04	0.14	0.40	-0.04	0.52	0.26	0.26	0.45	1.00	0.55
S <sub>24</sub>	-0.04	-0.04	0.24	0.50	0.21	-0.04	-0.04	-0.04	0.43	0.24	-0.04	0.14	-0.04	0.21	0.14	-0.04	-0.04	0.40	0.26	0.52	0.45	0.26	0.55	1.00

\*\* S indicates the pulse sequence

Table B2: Correlation peak table for individual orthogonal pulse-sequences with others.

	GS <sub>1</sub>	GS <sub>2</sub>	GS <sub>3</sub>	GS <sub>4</sub>	GS <sub>5</sub>	GS <sub>6</sub>	GS <sub>7</sub>	GS <sub>8</sub>	GS <sub>9</sub>	GS <sub>10</sub>	GS <sub>11</sub>	GS <sub>12</sub>	GS <sub>13</sub>	GS <sub>14</sub>	GS <sub>15</sub>	GS <sub>16</sub>	GS <sub>17</sub>	GS <sub>18</sub>	GS <sub>19</sub>	GS <sub>20</sub>	GS <sub>21</sub>	GS <sub>22</sub>	GS <sub>23</sub>	GS <sub>24</sub>
GS <sub>1</sub>	1.00	0.59	0.27	0.66	0.67	0.59	0.27	0.48	0.48	0.32	0.48	0.46	0.47	0.32	0.58	0.47	0.25	0.46	0.43	0.23	0.23	0.23	0.12	0.33
GS <sub>2</sub>	0.59	1.00	0.50	0.48	0.59	1.00	0.50	0.64	0.50	0.25	0.64	0.47	0.64	0.25	0.47	0.64	0.26	0.48	0.48	0.64	0.48	0.64	0.12	0.24
GS <sub>3</sub>	0.27	0.50	1.00	0.27	0.48	0.50	0.65	0.50	0.46	0.25	0.50	0.48	0.25	0.39	0.32	0.25	0.31	0.32	0.17	0.14	0.21	0.14	0.13	0.13
GS <sub>4</sub>	0.66	0.48	0.27	1.00	0.46	0.48	0.27	0.59	0.32	0.48	0.59	0.67	0.47	0.48	0.46	0.47	0.22	0.58	0.67	0.12	0.25	0.12	0.33	0.12
GS <sub>5</sub>	0.67	0.59	0.48	0.46	1.00	0.59	0.48	0.47	0.27	0.32	0.47	0.58	0.48	0.32	0.46	0.48	0.37	0.66	0.23	0.24	0.43	0.24	0.25	0.67
GS <sub>6</sub>	0.59	1.00	0.50	0.48	0.59	1.00	0.50	0.64	0.50	0.25	0.64	0.47	0.64	0.25	0.47	0.64	0.26	0.48	0.48	0.64	0.48	0.64	0.12	0.24
GS <sub>7</sub>	0.27	0.50	0.65	0.27	0.48	0.50	1.00	0.50	0.25	0.46	0.50	0.48	0.25	0.25	0.32	0.25	0.19	0.32	0.17	0.14	0.21	0.14	0.13	0.13
GS <sub>8</sub>	0.48	0.64	0.50	0.59	0.47	0.64	0.50	1.00	0.25	0.50	1.00	0.59	0.64	0.50	0.48	0.64	0.17	0.47	0.24	0.28	0.12	0.28	0.24	0.12
GS <sub>9</sub>	0.48	0.50	0.46	0.32	0.27	0.50	0.25	0.25	1.00	0.39	0.25	0.32	0.50	0.25	0.48	0.50	0.47	0.27	0.21	0.39	0.17	0.39	0.21	0.17
GS <sub>10</sub>	0.32	0.25	0.25	0.48	0.32	0.25	0.46	0.50	0.39	1.00	0.50	0.27	0.50	0.65	0.27	0.50	0.23	0.48	0.13	0.14	0.13	0.14	0.17	0.21
GS <sub>11</sub>	0.48	0.64	0.50	0.59	0.47	0.64	0.50	1.00	0.25	0.50	1.00	0.59	0.64	0.50	0.48	0.64	0.17	0.47	0.24	0.28	0.12	0.28	0.24	0.12
GS <sub>12</sub>	0.46	0.47	0.48	0.67	0.58	0.47	0.48	0.59	0.32	0.27	0.59	1.00	0.48	0.27	0.66	0.48	0.22	0.46	0.33	0.12	0.12	0.12	0.67	0.25
GS <sub>13</sub>	0.47	0.64	0.25	0.47	0.48	0.64	0.25	0.64	0.50	0.50	0.64	0.48	1.00	0.50	0.59	1.00	0.26	0.59	0.12	0.64	0.24	0.64	0.48	0.48
GS <sub>14</sub>	0.32	0.25	0.39	0.48	0.32	0.25	0.25	0.50	0.25	0.65	0.50	0.27	0.50	1.00	0.27	0.50	0.42	0.48	0.13	0.14	0.13	0.14	0.17	0.21
GS <sub>15</sub>	0.58	0.47	0.32	0.46	0.46	0.47	0.32	0.48	0.48	0.27	0.48	0.66	0.59	0.27	1.00	0.59	0.25	0.47	0.12	0.23	0.33	0.23	0.43	0.23
GS <sub>16</sub>	0.47	0.64	0.25	0.47	0.48	0.64	0.25	0.64	0.50	0.50	0.64	0.48	1.00	0.50	0.59	1.00	0.26	0.59	0.12	0.64	0.24	0.64	0.48	0.48
GS <sub>17</sub>	0.25	0.26	0.31	0.22	0.37	0.26	0.19	0.17	0.47	0.23	0.17	0.22	0.26	0.42	0.25	0.26	1.00	0.37	0.12	0.16	0.27	0.16	0.12	0.27
GS <sub>18</sub>	0.46	0.48	0.32	0.58	0.66	0.48	0.32	0.47	0.27	0.48	0.47	0.46	0.59	0.48	0.67	0.59	0.37	1.00	0.25	0.24	0.67	0.24	0.23	0.43
GS <sub>19</sub>	0.43	0.48	0.17	0.67	0.23	0.48	0.17	0.24	0.21	0.13	0.24	0.33	0.12	0.13	0.12	0.12	0.12	0.25	1.00	0.47	0.58	0.47	0.31	0.22
GS <sub>20</sub>	0.23	0.64	0.14	0.12	0.24	0.64	0.14	0.28	0.39	0.14	0.28	0.12	0.64	0.14	0.23	0.64	0.16	0.24	0.47	1.00	0.59	1.00	0.47	0.59
GS <sub>21</sub>	0.23	0.48	0.21	0.25	0.43	0.48	0.21	0.12	0.17	0.13	0.12	0.12	0.24	0.13	0.33	0.24	0.27	0.67	0.58	0.59	1.00	0.59	0.23	0.54
GS <sub>22</sub>	0.23	0.64	0.14	0.12	0.24	0.64	0.14	0.28	0.39	0.14	0.28	0.12	0.64	0.14	0.23	0.64	0.16	0.24	0.47	1.00	0.59	1.00	0.47	0.59
GS <sub>23</sub>	0.12	0.12	0.13	0.33	0.25	0.12	0.13	0.24	0.21	0.17	0.24	0.67	0.48	0.17	0.43	0.48	0.12	0.23	0.31	0.47	0.22	0.47	1.00	0.58
GS <sub>24</sub>	0.33	0.34	0.13	0.12	0.67	0.24	0.13	0.12	0.17	0.21	0.12	0.25	0.48	0.21	0.23	0.48	0.27	0.43	0.22	0.59	0.54	0.59	0.58	1.00

\*\* GS stand for gold sequenc which is equivalet for orthogonal pulse sequence in this dissertation.

## APPENDIX C

### PSEUDO CODE FOR ALGORITHM DESIGN

## Pseudo Code for Algorithm Design

---

### Algorithm C<sub>1</sub>: K-bit Data Encoding Algorithm

---

**Input** Data store (A, D) » Where A- array for AOP set storage, D- Digital bitstream

1. Initialize number of pulses, length of data bits, array B, array V,  $x = 0$ ,  $m = 0$
  2. Read the pulse information from SD card and store in microcontroller flash memory
  3. Read the digital bitstream and store in microcontroller flash memory
  4. Divide the digital bitstream into k-bit using splitter
  5. **for**  $i = 1$  to number of pulses **do**
  6.   **for**  $j = 1$  to length of k-bit **do**
  7.      $B[j] = D[j+x]$                                // Split the digital bitstream into k-bit data
  8.     **for**  $p = 1$  to length of k-bit **do**
  9.          $V[j] =$  Convert the  $B[j]$  array value binary number to decimal number
  10.     **end for**
  11.      $x \leftarrow x + k$
  12.   **end for**
  13. **end for**
  - // Implement the OOK modulation scheme
  14. **for**  $q = 1$  to length of pulse **do**
  15.   **if**  $V[j] = 0$  **then**
  16.     Select the corresponding pulse according to the encoding template
  17.   **end if**
  18.   Repeat for rest of the  $V[j]$  for pulse selection
  19. **end for**
  20. Implement counter and add sync pulse at the beginning of encoded pulse train
-

---

**Algorithm C2: Pulse Sequence Generation Algorithm**

---

**Input** Data store  $(A, D)$  » Where A- array for AOP set, D- Number set of (1, 2, 3)

1. Initialize length of PS N, length of analog pulse L, permutation array PA, Size of PA, Row and Col, Variable  $m = 0$  , Empty array Z for PS storage
  2. Calculate the permutation array, PA of the given set D
  3. **for**  $i = 1$  to Row **do**
  4.   **for**  $j = 1$  to Col **do**
  5.     **if**  $PA(i, j) = 1$  **then**
  6.       **for**  $k = 1$  to L **do**
  7.         Calculate PS and store in array,  $Z(k+m, i)$ ;
  8.       **end for**
  9.     **end if**
  10.   Repeat for  $PA(i, j) = 2$
  11.   Repeat for  $PA(i, j) = 3$
  12.    $m \leftarrow m + 1$
  13.   **end for**
  14. **end for**
  15. Print PS array Z
  16.  $Z_1$  to  $Z_i$  indicates distinct PSs and encodes sensors information bits, each PS represents an individual data channel
  17. **for**  $q = 1$  to Row **do**
  18.   **for**  $r = 1$  to length of bitstream **do**
  19.     Apply OOK channel encoding
  20.     Repeats for other channels
  21.   **end for**
  22.   Superimpose all the data encoded channel  $Z_1$  to  $Z_i$
  23. **end for**
-

---

**Algorithm C3: Cyclic Pulse Elimination Algorithm**

---

**Input** Data store (B) . Where B - array for AOP storage as template pulse (TP)

1: Initialize variable  $\text{numi} = 3$ ,  $\text{th} = 0$ ,  $r = n$ ,  $\text{id} = 0$ , where  $n$  is the number of distinct analog pulse, and empty array Ximg for storing eliminated pulses, empty array Ka to store the pulse index (PI)

2: Divided the entire UCP signal into several  $n$  small sub-block corresponding to each time slot  $T_s$

3: **while** meet a certain condition,  $r > 1$  **do**

4: Declaration  $\text{index}(i) = 0$ , Here  $i$  is 1 to  $n$

5: **for**  $k = 1$  to the number of pulse  $n$  **do**

6: Correlation peak checking with TP

7: **if**  $\text{Corr}(k) > \text{th}$  **then**

8: Set  $\text{index}(k) = 1$

9: **end if**

10: **end for**

11: **if** check the condition,  $\text{sum}(\text{index}) = 0$  **then**

12: Set the value  $r = 0$

13: **else**

14: Find the maximum correlation peak

15:  $\text{id} \leftarrow \text{id} + 1$

16: Store the index corres. to highest peak,  $\text{Ka}(\text{id}) = I$

17:  $\text{num}(I) \leftarrow \text{num}(I) + 1$

18: Composite signal  $\leftarrow$  Composite signal - TP signal

19:  $\text{Ximg}(\text{id}) \leftarrow$  composite signal

20:  $\text{Xe}(\text{id}) \leftarrow$  eliminated pulse

21: **end if**

22: **end while**

23: Repeat for  $T_s$  ( $i$ )

24: Print the eliminated PI storage array, Ka

---

---

**Algorithm C4: Pulse Index Pattern Regeneration Algorithm**

---

**Input** Data store (Ka) . Where Ka - array for eliminated PI storage from CPE decoding

1: Define empty column vector  $col(n)$ ,  $n \times n$  empty matrix  $T$ , and  $n \times n$  zero matrix  $A$ , where  $n$  is the number of pulses in a PS

2: Initialize variable  $r = 0$ ,  $th1 = 0$ , and empty array  $X$  for storing the pulse index pattern

3: Calculate  $T$  matrix whose elements are the sum of the repetition of distinct index corresponding to each  $T_s$

4: **for**  $i = 1$  to the maximum value of elements of  $T$  **do**

5:   **for**  $k = 1$  to the number of pulse  $n$  **do**

6:      $x = \text{find the elements of } T > th1$

7:     Replace the rows of zero matrix  $A$  by  $x$

8:      $T(:, k) \leftarrow T(:, k) - 1$

9:      $col(1+r:3+r, k) = A(:, k)$

10:   **end for**

11:    $r \leftarrow r + 3$

12: **end for**

13: Print column vector,  $col = col(:, k)$ , here  $k = 1$  to  $n$

14: **for**  $i = 1$  to length of column vector **do**

15:   **if**  $col1(i) \neq 0$  **then**

16:      $d \leftarrow col1(i)$

17:     **for**  $j = 1$  to length of column vector **do**

18:       **if**  $col2(j) \neq 0$  and  $d \neq col2(j)$  **then**

19:          $e \leftarrow col2(j)$

20:          $col2(j) \leftarrow 0$

21:         **for**  $k = 1$  to length of column vector **do**

22:           **if**  $col3(k) \neq 0$  and  $d \& e \neq col3(k)$  **then**

23:              $f \leftarrow col3(k)$

24:              $Z(i, :) \leftarrow d, e, f$

25:             break

26:         **end if**

27:           **end for**

28:           break

29:           **end if**

30:           **end for**

31:           **end if**

32: **end for**

33: Print the regenerated PI pattern, Z and match with the prior known template to find the missing channel

---